

MICROFICHE

DEVELOPMENT OF A STRETCHED-MEMBRANE DISH

Phase II, Task 2. Topical Report

Solar Kinetics, Inc.

SAND90-7036

RECORD COPY *a.*
REFERENCE COPY

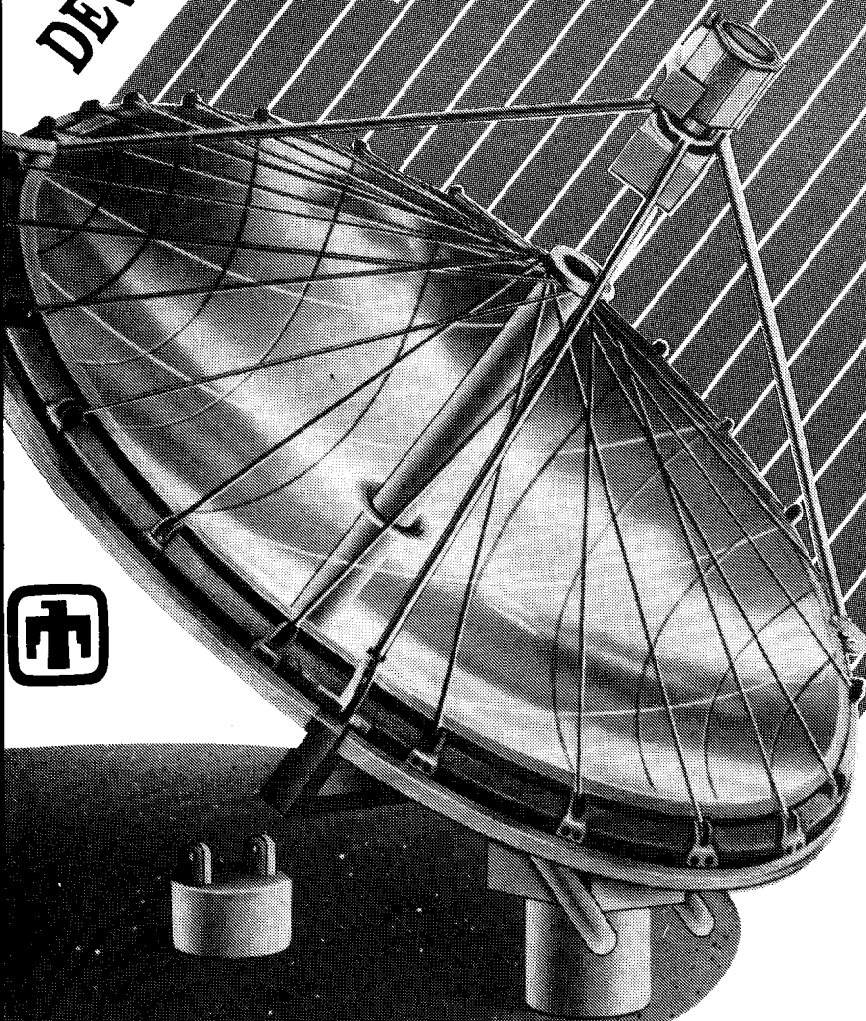
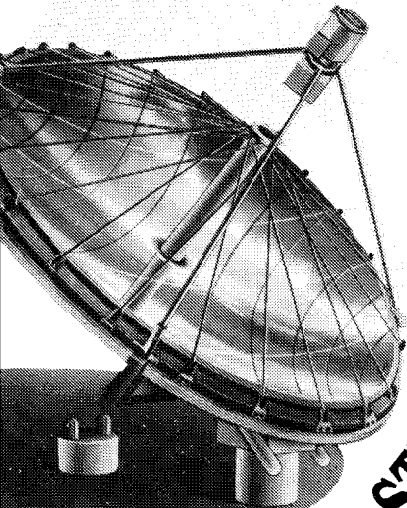
SNLA LIBRARY



SAND90-7036
0001
UNCLASSIFIED

07/91
95P

STAC



95P

Issued by Sandia National Laboratories, operated for the United States Department of Energy by Sandia Corporation.

NOTICE: This report was prepared as an account of work sponsored by an agency of the United States Government. Neither the United States Government nor any agency thereof, nor any of their employees, nor any of their contractors, subcontractors, or their employees, makes any warranty, express or implied, or assumes any legal liability or responsibility for the accuracy, completeness, or usefulness of any information, apparatus, product, or process disclosed, or represents that its use would not infringe privately owned rights. Reference herein to any specific commercial product, process, or service by trade name, trademark, manufacturer, or otherwise, does not necessarily constitute or imply its endorsement, recommendation, or favoring by the United States Government, any agency thereof or any of their contractors or subcontractors. The views and opinions expressed herein do not necessarily state or reflect those of the United States Government, any agency thereof or any of their contractors or subcontractors.

Printed in the United States of America
Available from
National Technical Information Service
U.S. Department of Commerce
5285 Port Royal Road
Springfield, VA 22161

NTIS price codes
Printed copy: A05
Microfiche copy: A01

SAND90-7036
Unlimited Release
Printed July 1991

DEVELOPMENT OF A STRETCHED-MEMBRANE DISH

Phase II, Task 2, Topical Report

Solar Kinetics, Inc.
10635 King William Drive
Dallas, TX 75220

Sandia Contract: 55-2495

ABSTRACT

Solar Kinetics, Inc., successfully designed and constructed the optical element of a 7-meter diameter stretched-membrane dish as Task 2 of the second phase of a contract directed by Sandia National Laboratories. Earlier work on this project defined the configuration of the optical element and demonstrated the membrane-forming process on 1.4- and 3.7-meter diameter membranes. In Task 2, the membrane-forming process was successfully scaled to 7-meters in diameter, and an innovative hub-and-spoke structure optical element was fabricated. The slope error, as measured with Solar Kinetics' laser-ray-trace system, was within 3.6 mrad of a perfect parabola.

Four major technical issues were successfully addressed in this work:

1. The technique of large-scale membrane forming was shown to be predictable, accurate, and repeatable. Three 7-meter membranes were formed without any contoured tooling.
2. A tensioned hub-and-spoke structure was demonstrated to be practical to fabricate. This innovative structure, like a bicycle wheel, was shown to be very stiff. Optical effects from ring distortion were not apparent.
3. The use of field-replaceable, unattached polymer reflective membrane was demonstrated. This approach allows for the practical field replacement of the reflective membrane when it has degraded due to weathering.
4. A technique was developed and demonstrated to ship the formed membranes from the factory to the dish-installation site. This allows the critical forming of the membrane to be performed in a controlled factory environment, and the membrane then to be shipped using standard-dimension shipping containers. This development further reduces manufacturing and installation costs of the completed dish.

This effort indicates that the stretched-membrane dish concept is a promising approach for solar concentration. The prototype optical element is a significant step in the development of the complete, full-sized dish.

CONTENTS

	<u>Page</u>
List of Figures	vii
List of Tables	xi
1.0 INTRODUCTION	1
2.0 STRUCTURAL ANALYSIS AND SIZING OF THE OPTICAL ELEMENT	5
2.1 Definition of Loads	5
2.2 Definition of Rear Structure	7
2.3 Ring Sizing	12
2.4 Hub Sizing	17
2.5 Sizing of Power Conversion Assembly Support	18
3.0 MEMBRANE FORMING AND OPTICAL ANALYSIS	23
3.1 Membrane Strain	23
3.2 Analytical Modeling of Membrane Forming	23
3.3 Membrane Slope Measurement Techniques	25
3.4 Membrane Forming and Optical Shape	26
3.4.1 Effects of Stabilization Pressure	29
3.4.2 Detailed Measurement	30
3.4.3 Effects of Seams	31
3.4.4 Effects Of Receiver Loads	33
4.0 7-M OPTICAL ELEMENT PROTOTYPE FABRICATION	35
4.1 Tooling and Master Assembly Procedure	36
4.1.1 Forming Tooling	36
4.1.2 Field Assembly Tooling	39
4.2 Membranes	39
4.2.1 Metal Membrane	41
4.2.2 Reflective Polymer Membrane	42
4.2.3 Rear Membrane	46
4.3 Ring and Membrane Attachments	46
4.4 Hub and Spokes	50
4.5 Filter Assembly	53
4.6 Vacuum Controls	54
4.7 Power Conversion Assembly Support Arrangement	56
4.8 Drive Attachments	56
4.9 Site Assembly	58
5.0 MEMBRANE ROLLING AND TRANSPORTATION	65
5.1 Introduction	65
5.2 Experimentation	66
5.3 Implementation at 7-M Diameter Optical Element	70
5.4 Future Work	72
6.0 SUMMARY	73
7.0 REFERENCES	75
APPENDIX A	77
APPENDIX B	79

List of Figures

<u>Figure</u>	<u>Description</u>	<u>Page</u>
1.1	Component Description of Optical Element.	2
2.1	Wind Pressure Distribution Assumption.	6
2.2	Spoke Pattern.	8
2.3	Spoke Deflection and Load Relation.	9
2.4	Spoke and Rear Membrane Deflection.	9
2.5	Survival Ring Stress.	13
2.6	Model Description of Ring as Shown from the Front When Facing the Horizon.	14
2.7	Sources of Ring Stress.	14
2.8	Ring and Hub Rotation Due to Stabilization Pressure.	16
2.9	Operational Ring Distortion.	17
2.10	Hub Stress as Function of Distance Between Hub Support and Flange.	20
2.11	Power Conversion Assembly Support Configuration.	20
3.1	Measured Membrane Strain Parallel to Seams.	24
3.2	Comparison of Measured Membrane Strain Parallel and Perpendicular to Seams.	24
3.3	Sensitivity of Reported Slope Error to Number of Measured Data Points.	26
3.4	Slope Accuracy Improvements with Tuning.	27
3.5	Membrane Slope Error Showing Unaffected Area.	29
3.6	Effects of Stabilization Pressure on Membrane Contour.	30
3.7	Membrane Contour Results for Third and Final Membrane as Supported in the Assembled Optical Element.	31
3.8	Optical Effects of Metal Seams.	32
3.9	Optical Effects of Metal and Polymer Seams.	32
4.1	Membrane Forming Tooling Ring. Upper View - Overview of Ring with Segments and Access Door Shown. Lower View - Cross Section of Tooling Showing Major Components to Support Ring and Seal Tooling.	37
4.2	Set Up for Formed Membrane Rolling.	38
4.3	Optical Element Assembly Tooling Utilizing Heliostat Membrane Tensioning Ring Support Pylon.	40
4.4	Metal Membrane Welded Seam Detail.	41
4.5	Metal Membrane Center Reinforcing Ring Weld Details.	43
4.6	Diagrams of Seam Configurations Tested for Use in Reflective Polymer Membrane Fabrication.	45
4.7	Cross Section of Dish Ring Showing Rear Membrane Clamping Arrangement.	47

4.8	Cross Section of Dish Ring Positioned in Tooling for Forming Operation. Also Shown are Metal Membrane, Membrane. Tensioning Weight, and Tooling Sealing Plate.	48
4.9	Cross Section of Formed Membrane Departure Bar on Optical Element Ring Showing Final Assembly Membrane Clamping Arrangement.	49
4.10	Detailed Cross Section of Rear Spoke Spring Assembly.	50
4.11	Diagram of Hub Flange with Inner Spoke End Connection Details Shown.	52
4.12	Cross Section of Dish Ring Showing Details of Outer Spoke End Attachment Bracket.	52
4.13	Cross Section of Assembled Dish Showing Vacuum Source Connection, Internal Filter Assembly, Membranes, and Polymer Membrane Central Bellows Seal.	53
4.14	Schematic Diagram of Control System for Membrane Stabilization.	54
4.15	Detail of Reflective Polymer Membrane Central Seal.	55
4.16	Exploded View Showing Components of the Rear Central Hub Drive Attachment.	57
4.17	Cross Section of Dish Ring Showing Original and Modified Ring to Drive Adapter Attachment Components.	57
4.18	7-M Tooling Ring with Formed Membrane in Place.	59
4.19	7-M Formed Membrane Being Rolled onto a Contoured Mandrel.	60
4.20	Final Assembly of Dish Ring Being Checked for Planarity and Concentricity with Dial Indicators Mounted on a Revolving Sweep Arm.	60
4.21	Assembled Dish Ring Supported in Field Tooling and Ready for Membrane Unrolling.	61
4.22	7-M Membrane Being Unrolled onto Dish Ring During Final Field Assembly.	61
4.23	7-M Membrane Unrolled onto Dish Ring during Final Field Assembly.	62
4.24	Rear Flange, Hub, Rear Spokes, and Internal Filter Assembly During Final Field Assembly. Rear Membrane is not Yet Installed at This Time.	62
4.25	Completed 7-M Optical Element Supported from Upper Half of Field Tooling.	63
4.26	7-M Optical Element Mounted to Drive Adapter at SNLA.	64
4.27	Completed 7-M Optical Element Mounted on Drive Adapter at SNLA.	64
5.1	Schematic Diagram of Parabolic Membrane Rolling Procedure.	66
5.2	Contoured Mandrel Fabrication Details.	68
5.3	Set-up for Formed Membrane Rolling.	68
5.4	7-M Formed Membrane Unrolled onto Final Optical Element Ring Prior to Field Assembly.	69

5.5	Plot of Radial Slope Error on First 7-M Membrane Before and After Membrane was Rolled onto Contoured Mandrel.	71
-----	---	----

List of Tables

<u>Table</u>	<u>Title</u>	<u>Page</u>
2.1	Operational and Survival Cases for FE Analysis.	13
2.2	Description of Cases for PCA Support Analysis.	21
3.1	Optical Quality of Each Membrane.	28

1.0 INTRODUCTION

The costs of parabolic dish solar collectors have been steadily reduced as new technologies have been applied. The stretched-membrane concept has been proposed as a further step in cost reductions.

Toward this end, Sandia National Laboratories, Albuquerque, (SNLA) contracted with Solar Kinetics, Inc. (SKI) in 1986 to begin evaluation of issues relevant to forming parabolic membranes and to develop conceptual designs for a complete stretched-membrane concentrating collector. The free-forming process of membrane fabrication was demonstrated with 3.7-m diameter membranes in Phase I (1). The process was refined and its repeatability was demonstrated in the first task of Phase II (2). The successful scaling of this process to 7-m diameter and the demonstration of a prototype optical element is the subject of this report.

Four major technical issues were successfully addressed in this work:

1. The technique of large scale membrane forming was shown to be predictable, accurate, and repeatable. Three 7-m membranes were formed without any contoured tooling. The readily controlled forming process used a combination of uniform (vacuum) and nonuniform (water) pressures.
2. A tensioned hub-and-spoke structure was demonstrated to be practical to fabricate. This innovative structure, like a bicycle wheel, was shown to be very stiff. Optical effects from ring distortion were not apparent.
3. The use of a field replaceable, unattached polymer reflective membrane was demonstrated. This approach allows for the practical field replacement of the reflective membrane when it has degraded due to weathering.
4. A technique was developed and demonstrated to ship the formed membranes from the factory to the dish installation site. This allows the critical forming of the membrane to be performed in a controlled factory environment, and the membrane then shipped using standard dimension shipping containers. This development further reduces manufacturing and installation costs of the completed dish.

The prototype optical element is nominally 7 m in diameter, and its design is based on the proposed 14-m commercial design from Phase I. The prototype size was selected to provide fabrication experience representative of a commercial dish while minimizing cost risks. The previous work also defined the use of stainless steel membranes with a f/D of 0.6, use of spoke supported rear membranes, and support of the optical element by two points on the ring and at the rear of the central hub. These design decisions were not revisited.

The structural members of the optical element are similar to a bicycle wheel; a ring supported from a hub by spokes as shown in Figure 1.1. The parabolic membrane is stretched across one side of the peripheral ring. The hub passes through the center of the membrane. Another membrane is draped over the outside of the rear set of spokes. This permits a slight negative pressure to be drawn in the space behind the formed membrane to stabilize it against wind and gravity loads. The negative pressure also serves to draw a reflective polymer membrane down on the front of the formed metal membrane. A tripod arrangement standing on the front of the ring supports the power conversion assembly (PCA) at the focal position of the concentrator.

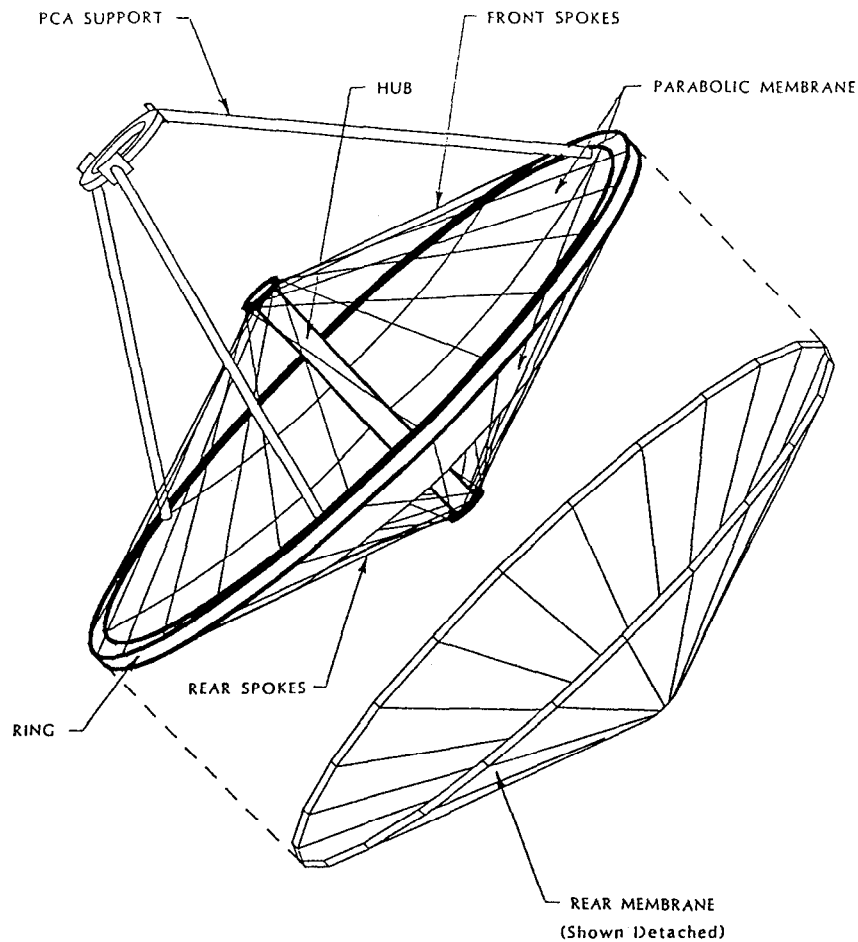


Figure 1.1 Component Description of Optical Element.

The ring, hub, and associated hardware is primarily carbon steel. The spokes are alloy steel, and the formed metal membrane is stainless steel. The rear membrane is a polymer composite cloth.

The reflective membrane is made from 2-mil aluminized polyester. This area of the project requires further development. A commercially available solar reflective film that we intended to use did not have acceptable mechanical properties. The alternative material used on the prototype will probably not serve as a good long-term reflective film. Alternative materials need to be researched or developed, although such an investigation was beyond the scope of the current work.

Initial testing of the membrane contour was performed on three 7-m membranes while they were still in the tooling and on one fully assembled optical element. Testing included characterization of the membrane's shape (in terms of slope error) on an average basis and in small areas of specific interest such as near the seams in the membrane material.

2.0 STRUCTURAL ANALYSIS AND SIZING OF THE OPTICAL ELEMENT

The major structural components of the optical element were analyzed and sized to prevent both structural failure and excessive deformation that could result in optical distortion. This effort was limited to the components themselves and did not include consideration of optical element geometry and configuration. Rather, the 14-m commercial element designed in Phase I of this effort was used as a basis (1).

The challenges of implementing stretched membranes in dishes are large. To minimize program risks and to ensure that vital issues pertaining to the membrane were demonstrated, a conservative philosophy was adopted for sizing the structural members. From this demonstration, we could proceed in the next tasks to optimize the structural members and scale to a more commercially marketable size.

This section of the report first documents the environmental loads on the optical element and then discusses the design of each of the major components. Wind tunnel analysis of this unique structure was not done; rather, applicable data were extracted from the literature. The rear structure (consisting of the rear spokes and the rear membrane) was sized to withstand the pressure of stabilization and wind without imparting excessive loads into the ring or allowing the rear membrane to touch the front one. The ring was then sized to carry the loads from the spokes. The hub, drive adaptor, and support for the power conversion assembly were all sized in a similar fashion.

2.1 DEFINITION OF LOADS

Loads from wind and gravity were determined for use in the structural analysis. Dish orientations that induced the worst loading were evaluated.

The survival wind speeds were defined as a gust to 90 mph with the optical element in a stow orientation (facing the zenith) and a gust to 50 mph with the optical element at any orientation. The peak operational wind load was defined as a gust to 27 mph. These wind speeds were selected to be consistent with those used for design of heliostats (3).

These wind speeds were resolved into loads using wind tunnel data developed by Colorado State University under contract with Solar Energy Research Institute (4). The model used for the wind tunnel tests had a similar focal length-to-diameter ratio (f/D), but a significantly different contour of the rear surface. The drag loads for the vertical survival cases were increased by the ratio of the projected relative areas of the desired dish and the tested geometry to account for differences in the projected areas. It was assumed that the differences in the flow properties across the surface of the optical element were insignificant. The pressure was assumed to act on the ring through the front membrane with the resulting ring normal load having a pill box distribution as shown in Figure 2.1. The magnitude of the normal loads was defined to match the

normal and moment loads determined from wind tunnel data. Also included is the accompanying radial load on the ring associated with the angle of departure of the membrane. Artificial, but small, distributed loads were added in the plane of the ring to maintain the in-plane force balance.

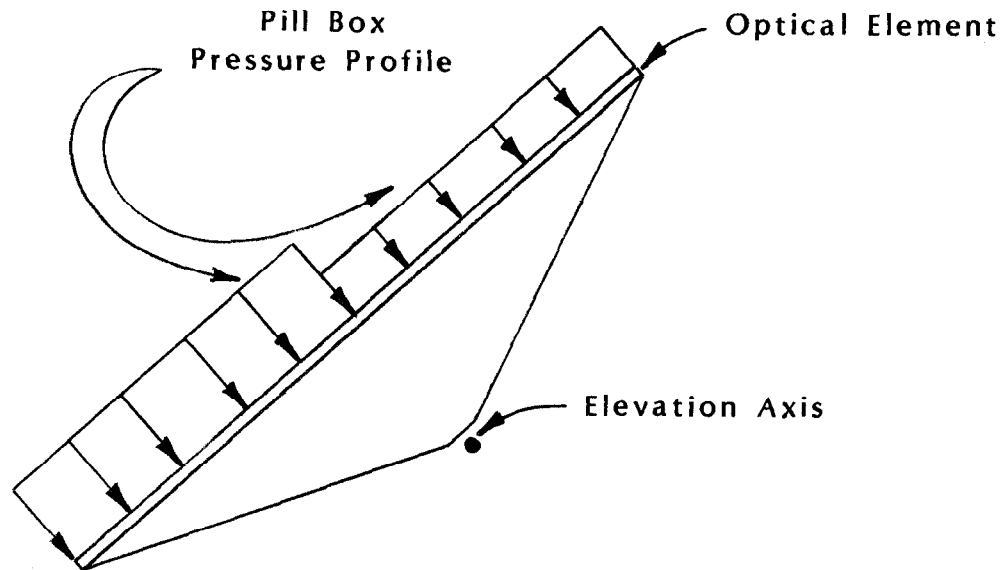


Figure 2.1 Wind Pressure Distribution Assumption

The power conversion assembly weight was assumed to be 500 pounds with a center of gravity located 24 inches above the focal point along the axis of the dish. These values are consistent with SNL's cold water calorimeter.

The stabilization pressure induces a significant load on the optical element. The magnitude of the stabilization pressure used for design is that predicted to be required to pull the polymer membrane against the metal membrane. The following relation was developed based on anticipated strain of the polymer:

$$P_{ST} = KE \frac{0.014}{1 - \nu^2} \frac{2t \sin(22.6^\circ)}{r}$$

E represents the modulus of elasticity of the polymer (500,000 psi used for polyester), t is polymer thickness, ν is Poisson's ratio, and r is dish radius. K is an empirically derived constant to account for the metal membrane carrying some of the pressure that would otherwise act solely on the polymer. The value for K was defined to be 1.44 based on a test with a 3.7 m diameter membrane. It was assumed that the polymer membrane's initial shape was conic with a depth of 80% of the center deflection of the metal membrane. This relation accurately predicted the pressure required for the 7-m

membrane (within 5%); although, the initial depth of the 7-m polymer membrane may have been as low as 75%. The polymer membrane material used for the 7-m dish was the same as that used for the 3.7-m test, so the effect of the modulus and thickness were not confirmed.

The original polymer membrane configuration assumed a laminate of ECP-305 and 0.002 inch thick PET (polyester). The dish was sized for this membrane, which would require stabilization pressure of 0.32 psi.

2.2 DEFINITION OF REAR STRUCTURE

A load from the stabilization pressure is imparted to the plastic and metal membranes on the front of the dish and the rear membrane and spokes on the back. The front membranes transfer this load to the ring through membrane tension. The magnitude and direction of this load are defined by the geometry of the membrane at the point of attachment to the ring. Computation of the loads from the rear structure is more complex because the load paths are dependant on structural stiffness and because of the number of undefined design variables (such as spoke diameter, initial tension, etc.). The design variables were isolated and defined where possible. Trade-offs on the remaining variables were then made.

The overall geometry of the optical element (relative length of hub to the diameter of the ring) and number of spokes were taken from the 14-m diameter commercial design (1). Twenty-four spokes are used on each side of the dish in a mirror-image arrangement. The spoke pattern is similar to that used on many bicycle wheels in that the spokes attach to the hub along a tangent to the hub perimeter, as shown in Figure 2.2. This pattern greatly reduces the magnitude of moments induced into the hub by nonuniform loads on the ring. Adjacent spokes at the ring attach to opposite sides of the hub (as shown by spokes A and B in Figure 2.2), thereby canceling the tendency to induce a moment.

The spoke pattern also adds torsional stiffness to the optical element. Torsional stiffness is important so that the wind does not excite the structure's natural frequency. Torsional stiffness also limits dish rotation from torsional loads. The torsional natural frequency was calculated using lumped parameter modeling. The stiffness of the rear spokes was neglected because their deflection makes them relatively "soft." It was found that the stiffness of the front spokes and hub acting in series was sufficient to avoid excitation by wind fluctuations. The natural frequency was calculated to be 3.1 Hz. (Rotation from 91,000 in.-lbs of torque would cause a rotation of 3.6 mrad.) These results were later supported by finite element modeling. A torsional load was applied to a finite element model of the optical element. The resulting wind-up of the optical element was within 10% of that predicted earlier. Sixty-five percent of the wind-up occurred in the hub itself with the remainder in the ring relative to the hub. This demonstrates the high torsional stiffness of the spokes. Informal tests of the 7-m prototype also supported these results. The optical element was torsionally oscillated by hand. The frequency of the free vibration was judged to be close to 3 Hz.

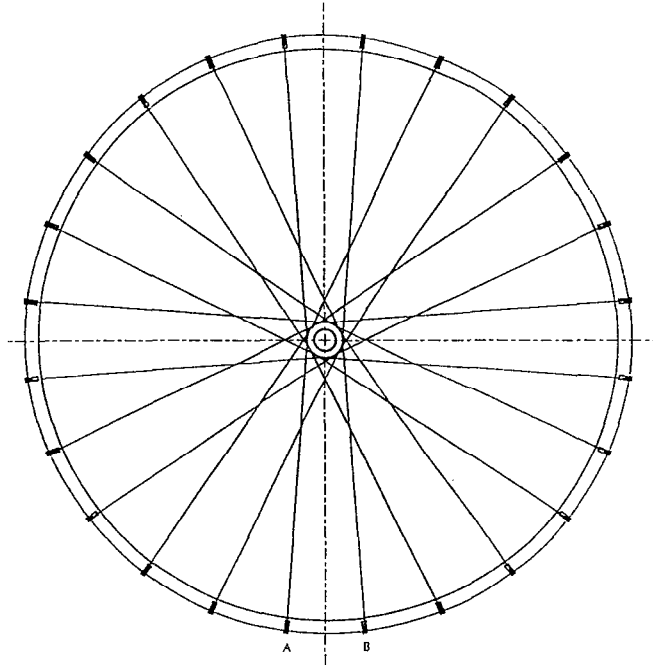


Figure 2.2 Spoke Pattern.

The stabilization pressure causes the rear spokes to deflect. Large spoke deflections are not desired because of the need to avoid contact between the front and rear membranes. However, large deflections of the spokes allow them to carry the pressure load more efficiently, which reduces the load on the ring. Figure 2.3 shows the unique correlation between spoke deflection and load on the ring. Note that this relation is independent of spoke properties and initial spoke tension. This relation allows the definition of spoke deflection and load without regard to other issues.

Figure 2.4 shows spoke deflection relative to the ring and front membrane. As is shown in the figure, the attachment point for the spoke to the ring must be offset from the ring to avoid contact between the two membranes. The disadvantage to the offset is that it adds weight to the ring assembly and increases the moment arm for the spoke load acting on the ring. This, in turn, results in an increase in ring stresses and deflections. A spoke deflection of 3.7 inches with a corresponding load of 4200 pounds was selected as a somewhat arbitrary compromise to avoid both large offsets and large spoke loads.

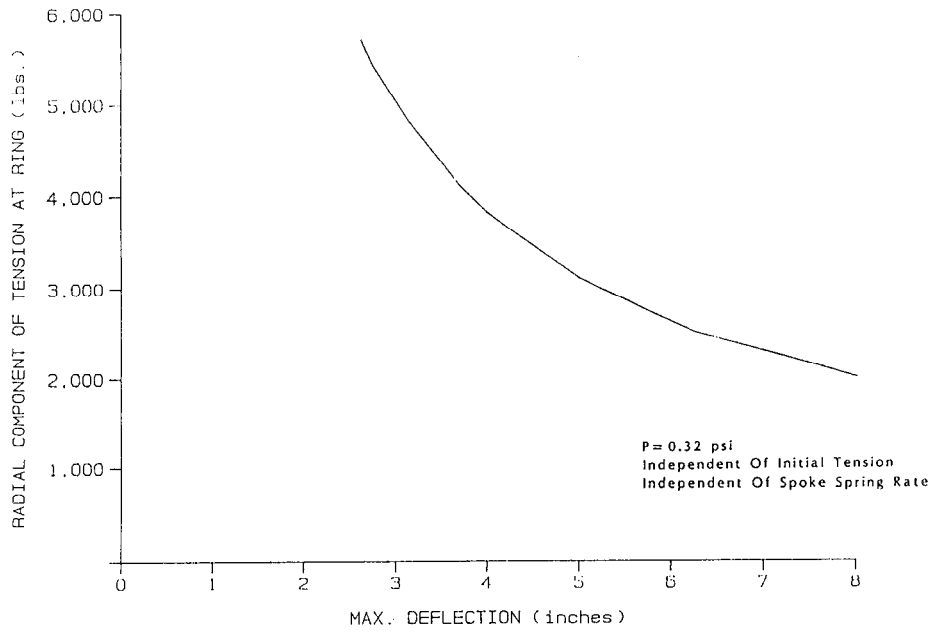


Figure 2.3 Spoke Deflection and Load Relation.

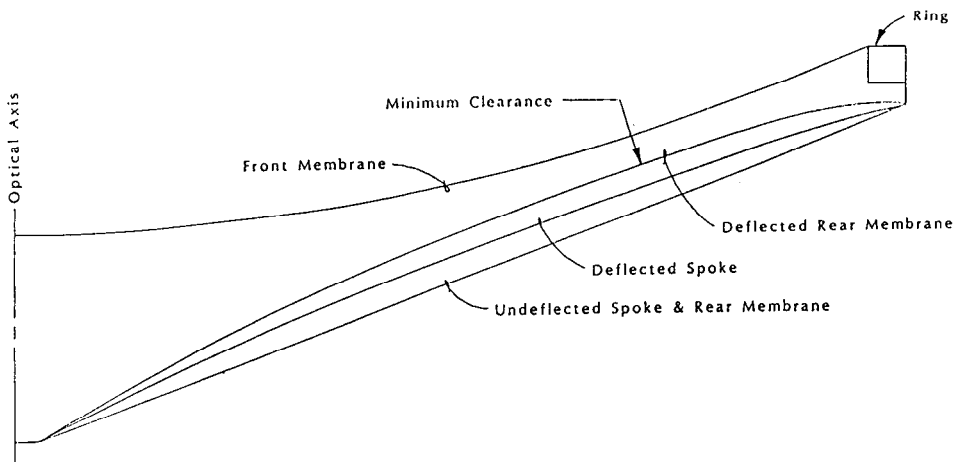


Figure 2.4 Spoke and Rear Membrane Deflection.

A budget for the deflections of the rear membrane and spokes was then defined. The point of closest contact between the front and rear membranes is 110 inches from the dish axis as measured along the spoke. The following predicted spoke and membrane deflections are reported for this location:

Spoke Sag	
Ideal, Spoke only	3.2 (inches)
With Ring Roll and Shrinkage	1.0
High Stab. Pres.	0.4
Membrane Sag Between Spokes	
Ideal, Membrane only	1.2
With Slack	1.8
Creep	<u>0.5</u>
Total	8.1

An offset of three inches was selected to avoid membrane contact. The initial gap under no load is 10.2 inches. The remaining gap during operation could be 2.1 inches.

Calculation of spoke deflection was based on a modified version of a closed form solution for spokes under a triangularly distributed load developed by SERI (5). It was assumed that all of the membrane load was carried to the adjacent spokes and none was carried directly into the ring by the membrane. The results from the spoke model were later compared to a finite element model of the membrane and spokes and also to the 7-m prototype. In both cases, the results were within 3% of one another. The model assumed an infinitely rigid ring. An independent allowance of one inch spoke deflection was made to account for the effect of ring roll and shrinkage. An additional allowance was provided for the stabilization pressure to increase to 0.40 psi. This is due to the uncertainty at that time of the predicted stabilization pressure.

The budget for membrane sag was based on finite element analysis of triangular membrane sections that have rigid boundaries (no spokes). Later comparison with a finite element model of both the membrane and spokes showed satisfactory results. We first predicted 1.2 inches of deflection, and more complete modeling predicted 1.5 inches. Both models assumed a stabilization pressure of 0.32 psi with the membrane having no initial slack. The magnitude of initial slack was difficult to predict. An engineering judgement was made that the rear membrane would not be more than 2% oversized. This would contribute another 1.8 inches of deflection. Membrane sag on the 7-m prototype was measured to be 1.2 inches. Since the stabilization pressure was significantly lower than that used for the analysis (0.14 vs. 0.32 psi) no hard conclusions can be made to the accuracy of the predictions.

The next step in the spoke analysis was to define the spoke properties and conditions that would allow the selected deflection under the defined stabilization pressure. Several approaches were considered:

1. Solid steel spokes were considered as a baseline. To achieve the required deflection, the spoke had to be structurally soft. To achieve this, the steel spoke had to have a small cross-sectional area (.065 in²). The spoke stress under ideal conditions would be 66,000 psi. Cross-section area reduction and stress concentrations at the threaded ends of the spokes would raise the actual stress value. We were uncertain as to how well we could control the initial spoke tension and how evenly the membrane load would be carried by the spokes. Yield strength for typical high strength steels that have good ductility range from 110,000 to 130,000 psi. With these factors in mind, solid steel spokes were rejected based on stress.
2. Materials having lower structural stiffness were also considered. The stiffness of wire rope is dependant on time; therefore, it was rejected. Aluminum spokes were also rejected because of the difficulty in achieving sufficiently high strengths. Stress for an ideal aluminum spoke would be 23,000 psi. The same issues of stress concentration and uncertainty would apply to aluminum, as well as steel spokes. Yield strength for typical ductile aluminums range from 40,000 to 50,000 psi.
3. An alternative to selecting a soft material would have been to initially install the spokes slack so that they would deflect the required distance under stabilization pressure. This concept would result in unacceptable impact loading and structural instabilities when no stabilization pressure is applied.
4. The selected approach was to use solid steel spokes with a spring mounted in series with the spoke. These springs provided the structural softness required to allow the spokes to deflect properly. A mechanical stop was incorporated in the spring mechanism so that the spring was not active when stabilization pressure was on and the spoke was at full deflection. In this manner, the spoke and spring assembly reacted as a solid rod during normal operation of the optical element.

The required properties of this assembly were defined to accomplish this without yielding or over stressing any material. A spring rate of 9700 lbs/in. was selected with 0.050 inches of free travel (from preload state to mechanical stop). The spoke diameter was set at 0.5 inches and a 4130 alloy, carbon steel with a Rockwell C hardness of 26 to 32 was selected as the spoke material. Ideal spoke stress is expected to be 22,000 psi. Material yield strength is 110,000 psi.

The minimum initial spoke tension was determined by the condition that avoids unloading of spokes in the most adverse wind conditions. Analysis showed that the structure will be insensitive to initial tension as long as unloading is avoided. A safe initial tension of 1000 pounds per spoke was defined.

2.3 RING SIZING

The ring was sized to withstand the imposed loads without yielding. Distortion and local stability were not limiting factors. The major ring loads are axial compression and bending about both axes. A carbon steel tube with a rectangular cross section was used as a starting point for this ring based on work done in Task 1 of this contract (2). Analysis and manufacturing constraints were used to size the tubing as will be discussed in this section.

The ring is made from straight structural square tubing bent to the radius of the dish. Web distortion during the rolling process limits how thin the tube walls can be. After discussions with experienced tube benders, it was decided that the walls would be no less than 0.312 inches thick. This constraint limited the structural efficiency of the ring. Large thin walled sections, with minimum wall thickness governed only by local stability constraints, are inherently better at carrying bending loads because of the high ratio of moment of inertia-to-weight. The manufacturing limit on wall thickness will likely be a constraint for larger dishes, but its effect on ring weight is expected to be small. Larger dishes will have a better balance of the forces that cause moments in the ring, thus, reducing the magnitude of bending loads. The highest load will be axial compression, for which moment of inertia is not important.

Finite element analysis was used for most of the structural computations. The model consisted of the entire ring, front spokes, hub, springs for rear spokes, and two support brackets from the ring to ground. Initial spoke tension was induced by an artificial change in spoke temperature. Wind and pressure loads were applied as discussed in the previous section. The PCA support was not modeled. Rather, it was simulated with artificial loads on the ring.

Operational and survival cases were considered (see Table 2.1). Five cases were run with a 27-mph wind. Four cases were also considered with no wind loads. Six cases were analyzed for 90-mph wind survival with the dish facing the zenith. The wind direction was assumed to vary 6 degrees with respect to the horizon and three directions with respect to the dish. No structural analysis was done for 50-mph wind with the dish in any orientation, because analysis of wind tunnel results indicate that the 90-mph stow is worse in terms of loads normal to the ring and elevation moments.

Ring stress for a survival case (case 14) is shown in Figure 2.5. Peak equivalent uniaxial stress is plotted for each ring node. Figure 2.6 describes the location of the nodes. The effect of the lower two PCA supports are evident near nodes 121 and 169. Note that the effect of the PCA supports are significant, but not dominant. More importantly, the effect covers a broad region. To reinforce the ring locally to reduce stresses would require a fairly long ring doubler. For reference, the distance between nodes was 4.3 inches with spokes every eight nodes.

**Table 2.1
Operational and Survival Cases
for FE Analysis**

<u>Case</u>	<u>Wind Speed</u>	<u>Dish Elev. Angle</u>	<u>Wind Direction</u>	<u>Angle of Attack</u>
1	0	0	N/A	N/A
2	0	25	N/A	N/A
3	0	40	N/A	N/A
4	0	90	N/A	N/A
5	27	0	Front	0
6	27	25	Front	0
7	27	40	Front	0
8	27	90	Front	0
9	27	90	Side	0
10	90	0	Side	+6
11	90	0	Front	+6
12	90	0	Rear	+6
13	90	0	Side	-6
14	90	0	Front	-6
15	90	0	Rear	-6

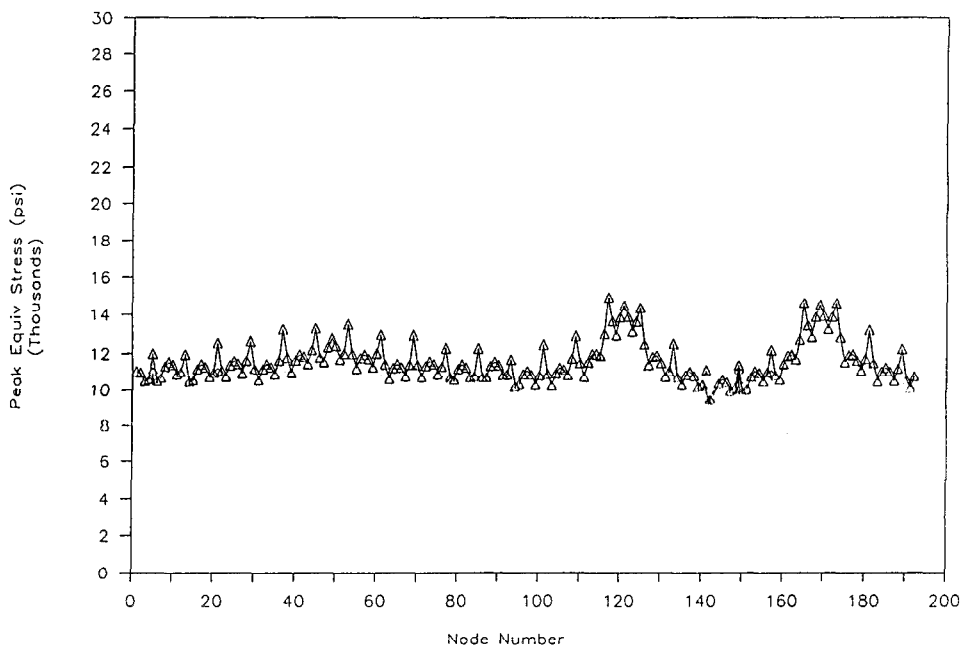


Figure 2.5 Survival Ring Stress

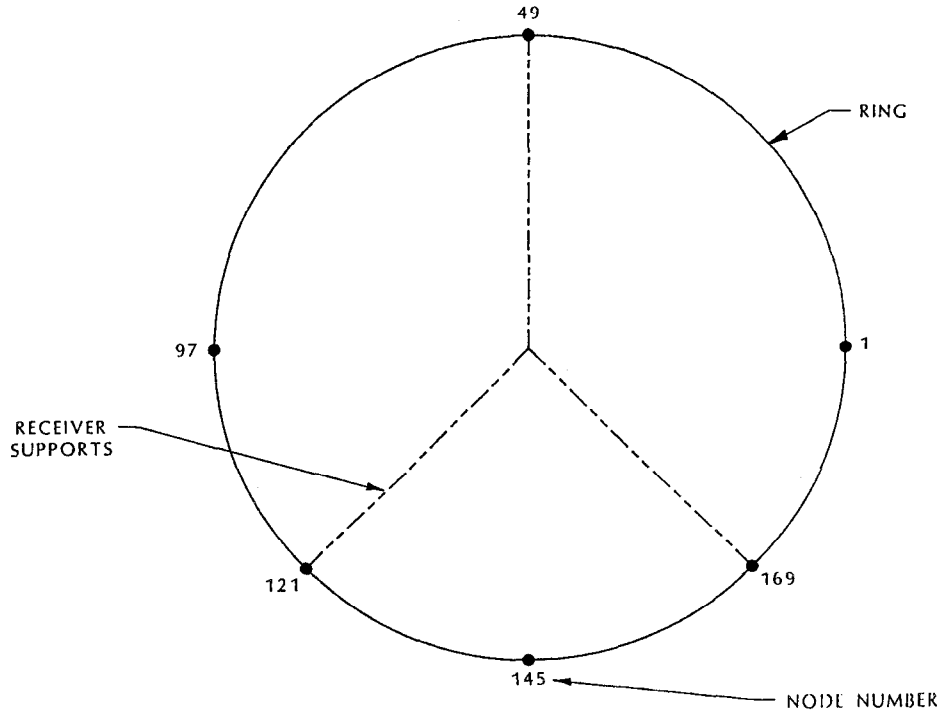


Figure 2.6 Model Description of Ring as Shown from the Front When Facing the Horizon.

The most significant source of ring load is the stabilization pressure. Figure 2.7 shows the contribution to ring stress from the various sources for case 14. At most ring locations, the stress caused by the stabilization pressure exceeds the combined stress from initial spoke tension, wind and gravity.

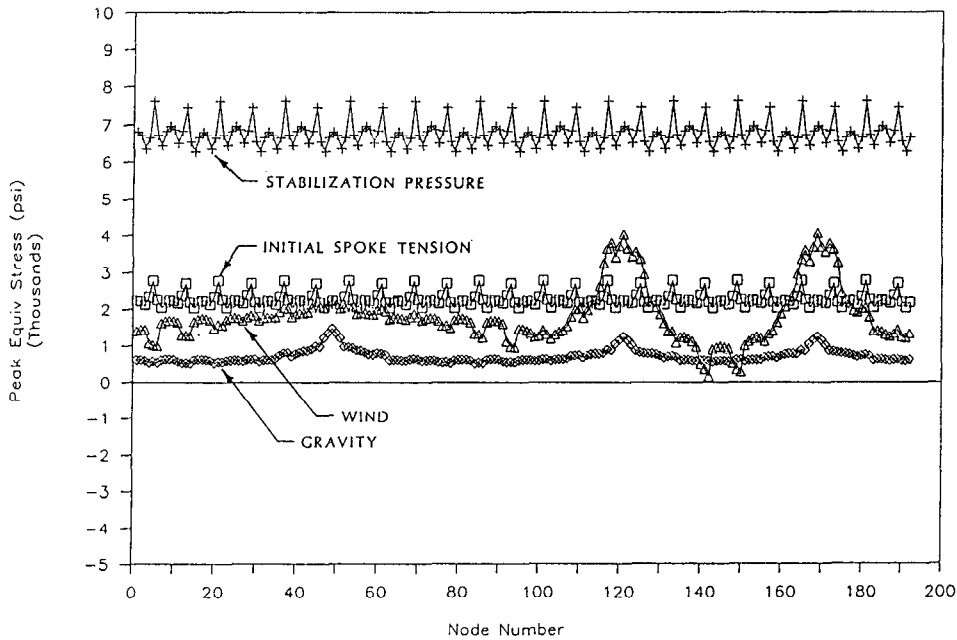


Figure 2.7 Sources of Ring Stress.

The allowable limit for stress was defined as a function of the perceived uncertainty of the load. For instance, the uncertainty of the wind load on the unique structure of the optical element is large. Therefore, the stress induced by the wind is increased by a large uncertainty factor. The uncertainty factors assigned to the loads were as follows:

Initial spoke tension	1.4
Stabilization pressure	1.75
Receiver loads	1.2
Wind loads	2.5

The stabilization pressure uncertainty factor allows for an increase of 25% (to 0.40 psi) in the stabilization pressure to ensure that the plastic membrane can be pulled down completely to the metal membrane. Uncertainty in how the pressure is translated into the ring accounts for the remainder. The maximum allowable stress for the ring material is 27,600 psi. This is the material yield strength (46,000 psi) reduced by the standard factor of 1.67 per AISC code (6). The sum of the stresses (as increased for uncertainty) equalled the maximum allowable stress for case 14. Therefore, the 6 in. by 6 in. by 0.312 in. ring passed this criterion.

Some of the large uncertainty factors used for this prototype will not be required for the design of the full sized dish. The factor applied to stabilization pressure will be significantly reduced. Experience with this prototype supported the accuracy of the method used to calculate required stabilization pressure. The uncertainty factor for initial spoke tension, however, will not decrease. Prototype experience showed a considerable difference in tension among the spokes. Spoke tension ranged from 50 to 1250 lbs with an average of 490 lbs. These values are based on nut torque measurements.

The ring was sized based on stress. Distortion during operation was reviewed to ensure adequate stiffness. Such distortion could affect the optical shape of the membrane. The most dramatic movement of the ring is caused by the application of the stabilization pressure. This pressure causes the ring to rotate about the ring supports, as shown in Figure 2.8. This movement is consistent with intuition in that stabilization pressure exerts a net downward load on the ring. This load would cause the ring to translate in that direction if not resisted by the ring supports.

The result of the ring support geometry is a rotation of the ring about the support. This rotation is large in optical terms (approximately 8 mrad), but does not compromise dish performance because the ring rotates as a whole with very little distortion. The receiver will move with the optical element since the PCA support is attached to the ring. The contribution to tracking error is believed to be small because this effect can be anticipated and compensated for with an open loop tracker (based on theoretical sun position) or completely eliminated with a closed loop tracker (based on feedback of the relative sun position).

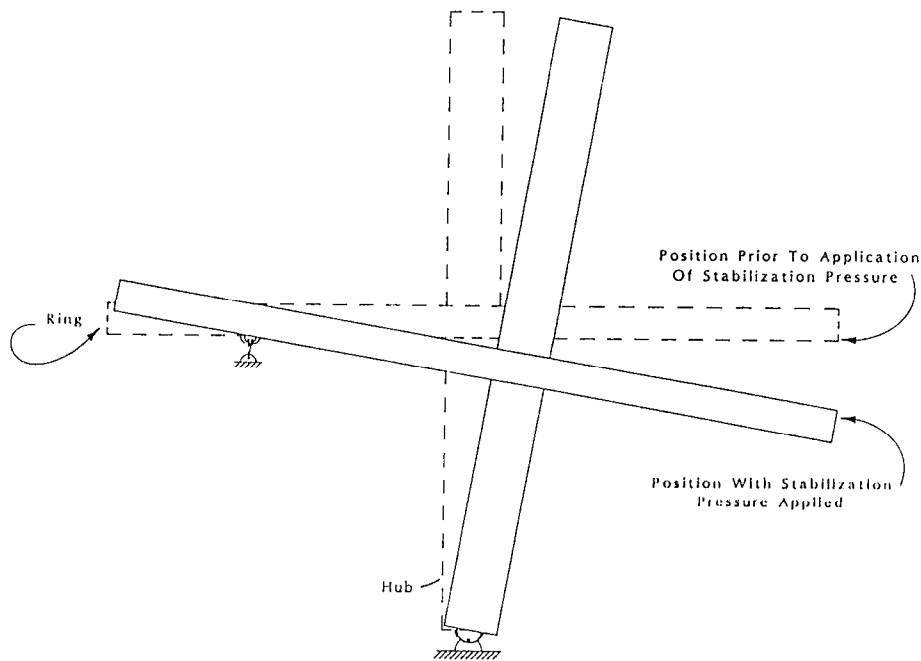


Figure 2.8 Ring and Hub Rotation Due to Stabilization Pressure.

Typical predicted ring distortion is shown in Figure 2.9. The upper line represents the radial motion of the ring at the point of contact with the membrane with positive being radially outward. The lower line represents the displacement of the ring parallel to the dish axis. This motion was referenced to the PCA to eliminate the effect of rigid body tilt. The small deflections were expected to cause only small errors. This was a judgement based on experience with stretched-membrane heliostats and work with smaller stretched-membrane dishes.

Strain gages were attached to the optical element during assembly of the prototype. Gages were mounted at two locations on the ring and on three spokes. At the ring locations, gages were mounted on all four sides of the tube in order to determine the effects of bending moments in both planes. Strain was measured with the dish at an elevation angle of 0 and 90, with and without simulated receiver loads, and as a function of stabilization pressure. The results are repeatable as a function of strain levels; there was no evidence of ratcheting or hysteresis associated with stabilization pressure. Each of the three measured spokes showed substantially different tension levels, all less than predicted with stabilization applied. Bending stresses in the ring were within 1000 psi (< 30%) of predictions at one location, but more than 2400 psi different at the other location. Compressive stresses in the ring were measured to be 3200 and 3500 psi, respectively, while analysis predicted 5900 psi. This difference appears to be consistent with the lower loads measured in the spokes. The impact of the receiver loads was consistent with expectations in that it was small in relation to the other ring stresses. However, the wide scatter of the data makes quantitative comparison of small values

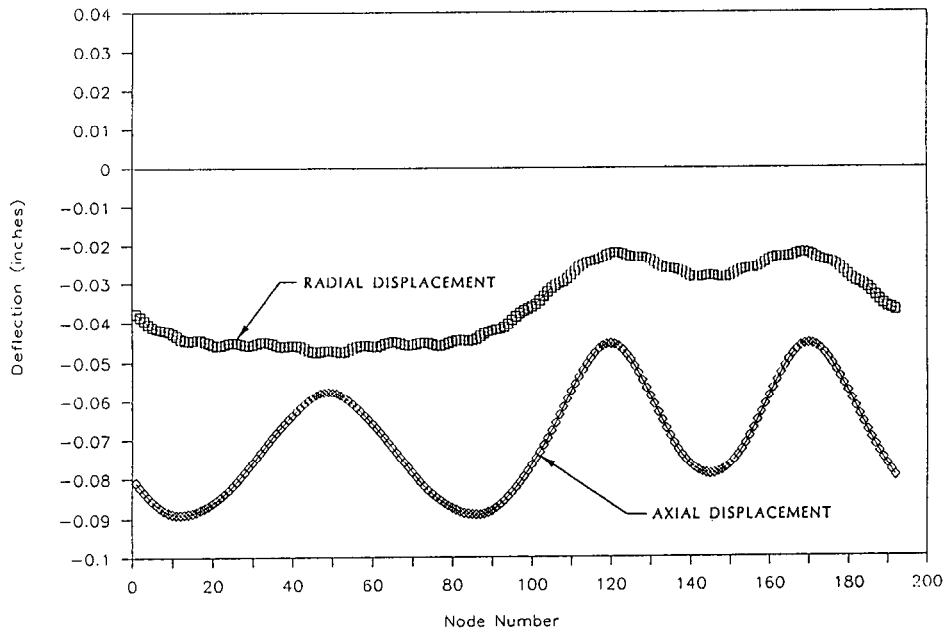


Figure 2.9 Operational Ring Distortion.

uncertain. The limited review of the strain data is inconclusive. The large scatter in a set of only a few data points makes interpretation difficult.

2.4 HUB SIZING

The hub consists of a structural steel circular tube with a flange on each end. Loads enter the hub through the spokes and through the support point located at the rear flange. Axial compression, moment, and torque are induced into the hub. Axial compression is caused by the component of spoke tension that is parallel to the hub axis. Moment is induced by the unequal spoke tension acting on the hub and by the support point at the base of the hub acting through a moment arm. Torsion is induced by optical element wind-up loads being passed through the front spokes into the hub.

The selected tube had an outside diameter of 10 inches and a 0.375-inch wall thickness. Local wall stability was not a design limitation. The walls would yield before buckling from compressive or torsional loads. This was convenient because the magnitude of the torsional load was uncertain. Torsional (or windup) loads are often very small in comparison with other loads on a dish and often are close to the measurement uncertainty in wind tunnel tests (7). This load could also be sensitive to the configuration of the rear structure for which no data exist for the selected configuration. Because of this, torsion loads predicted by wind tunnel studies were increased substantially for this design. This conservatism added confidence to the design without adding weight.

The failure mode that drove the hub design was column buckling from the combined effects of axial compression and moments. Classical techniques for eccentrically loaded compressive members were used to solve this problem (8). The slenderness ratio was small, so the Euler criteria for column stability did not apply. Rather, the critical loading was defined by the parabolic approximation for short columns:

$$c_r = y_s \left[1 - \frac{(L/r)^2}{2 C_c^2} \right]$$

$$C_c^2 = \frac{2E(\pi)^2}{y_s}$$

where c_r is critical stress for a centrally loaded short column
 y_s is material yield strength
 L is column length
 r is radius of gyration
 E is material elastic modulus

Based on the allowable-stress method, the peak stress from axial compression and bending should not exceed the ratio of critical stress to factor of safety. No load uncertainty factors were used for the hub. A factor of safety on buckling of ten was used. This factor is appropriate for long slender columns, but excessively large for short columns. A more appropriate factor of safety could have reduced the hub weight by about 50%.

The sensitivity of buckling failure to bending moment made it desirable to minimize all bending moments. The rear flange of the hub also serves as the attachment point of the optical element to the drive structure. If this connection is axially displaced away from the rear flange, a moment arm is created that imparts bending to the hub. Figure 2.10 shows the stress in the hub as a function of the length of the moment arm used to attach the hub to the drive adaptor.

To minimize this loading, the center of the support point (where the hub attaches to the drive adaptor) was moved from a point a few inches behind the outer face of the rear flange to lie in the same plane as that of the attachment of the spokes to the hub.

2.5 SIZING OF POWER CONVERSION ASSEMBLY SUPPORT

The elements of the power conversion assembly (PCA) support were sized to support SNLA's cold water calorimeter. As in the other components of the optical element, no optimization was done and only static loading was considered. Dynamic loads from inertia and shock were not considered. This discussion describes the basic structure of the PCA support, the loading of the members, the solution technique, structural deflections, and member stability. The limiting design constraint was stability of the three primary struts.

The PCA support consists of three struts connecting the ring of the optical element to a smaller ring that surrounds the PCA itself, as shown in Figure 2.11. Three mounting ears protrude from this ring to the support points on the PCA. This differs from the proposed PCA support for the full-size dish. The struts for that structure will likely be guyed trusses, rather than tubular columns.

The sizing of the prototype PCA support ring was dictated by manufacturing limitations of bending tubing. A thick-wall tube was selected to avoid crushing during rolling. The commercial ring could be made from thin sheet stock. The struts are aligned so their axes will pass through the center of gravity of the PCA (in this case the SNL cold water calorimeter was used as a model) to minimize moment loads in the struts. On the other end, the struts are aligned so their axes will pass through the centerline of the optical element ring. The outer end is ball jointed to minimize torsional loading of the ring and moment loads in the struts. Round structural tubing was selected for the struts for their structural efficiency and to avoid the potential of crosswind galloping that could be caused by irregular shapes.

Survival and worst case operational loads were considered. Table 2.2 summarizes the cases that were analyzed. Three different wind directions were considered for the stow (facing zenith) orientation. Wind loads were based on the projected area of the PCA and struts assuming a drag coefficient of one. The wind load for the PCA was applied at its center of gravity. Its projected area was assumed to be that of the cold water calorimeter (780 in²). This gave a drag load of 112 lbs at 90 mph and 34 lbs at 50 mph. A PCA weight of 500 lbs was used based on the calorimeter weight. The location of the center of gravity of the PCA was varied to account for variations of the test article. The distance listed in the table is the distance from the ring plane to the center of gravity. The wind load on the struts was applied in a distributed fashion along the struts themselves, as was their weight load. Wind load on the struts was 0.58 and 0.18 lbs/in. for 90 and 50 mph wind, respectively. No wind was used for the operational deflection case because the imposed load of 0.05 lbs/in. was insignificantly small relative to the strut weight of 0.43 lbs/in. The analysis used finite element method to solve for member loads and structural deflections. The PCA support rotates and translates slightly under operational loads. The receiver plane will rotate up to 2.5 mrad. This was judged to be insignificant. The receiver plane translates up to 0.06 inches perpendicular to the optical axis and insignificantly parallel to the optical axis. This is equivalent to approximately 0.4 mrad of tracking error.

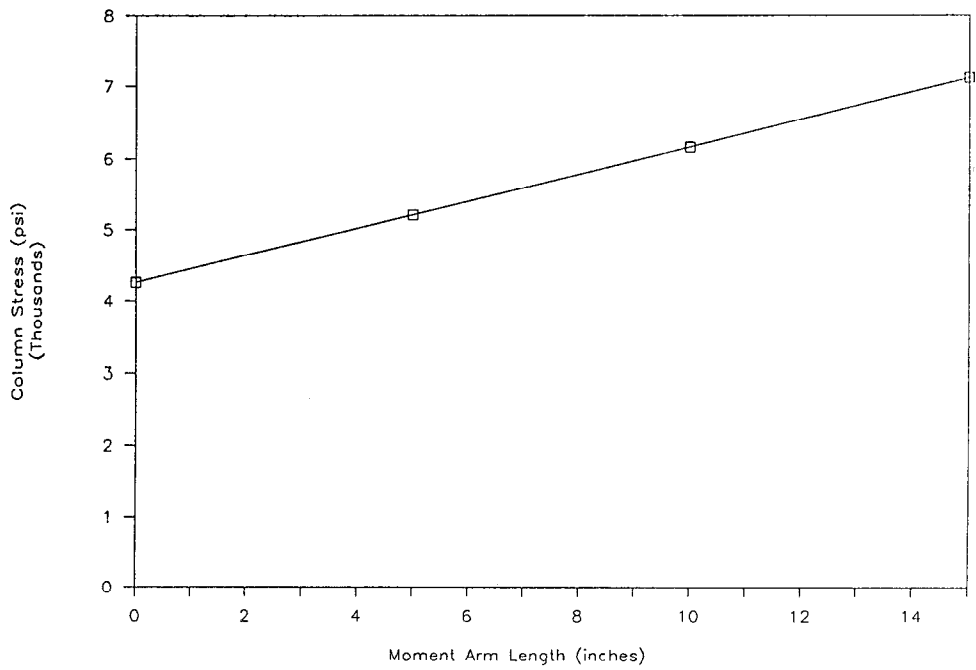


Figure 2.10 Hub Stress as Function of Distance Between Hub Support and Flange.

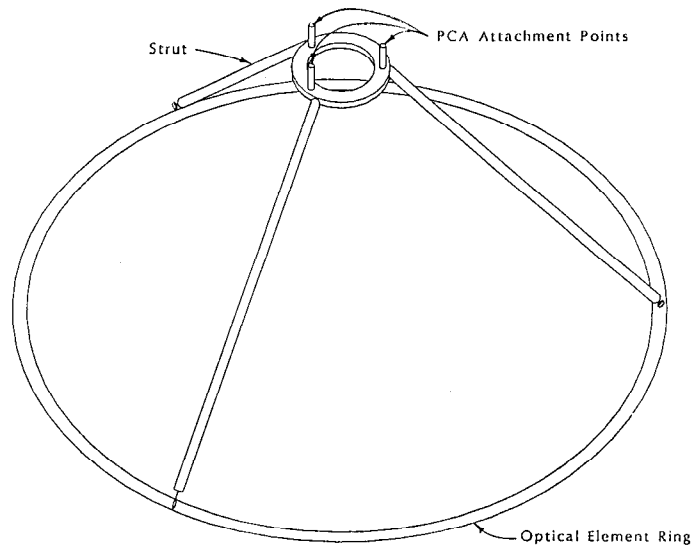


Figure 2.11 Power Conversion Assembly Support Configuration.

Table 2.2
Description of Cases for
PCA Support Analysis

<u>Case</u>	<u>Wind Speed (mph)</u>	<u>Elevation Angle (degrees)</u>	<u>Distance of CG (inches)</u>	<u>Wind Direction</u>
A	90	0	152	Front
B	90	0	152	Top
C	90	0	152	Side
D	50	33	142	Front
E	50	33	142	Side
F	50	33	152	Front
G	50	33	152	Side
H	50	33	162	Front
I	50	33	162	Side
J	0	90	142	N/A
K	0	33	142	N/A
L	0	90	152	N/A
M	0	33	152	N/A
N	0	90	162	N/A
O	0	33	162	N/A

The reactions at the ends of the struts are axial compression with a moment load imposed at the end closest to the PCA. The strut is also subjected to a distributed load from its own weight and from the wind. Strut loading was determined by finite element analysis. Classical stability analysis was applied to ensure these loads did not cause buckling. The magnitude of the stresses are small and yield is not a concern. Peak stress of 1990 psi occurred for case A. Buckling of the struts was the limiting design criteria. The struts were treated as long slender members because of their high slenderness ratio. An interactive method was used to solve for the margin of safety on buckling (8). The selected 4-inch diameter steel tube with 0.12 inch wall thickness provided a margin of safety of approximately 10. The bending effects from the transverse loads would be amplified if the margin of safety were low. The effect was judged to be small because of the high margin. Local buckling of the tube walls was also checked and found to be insignificant. The critical stress for wall buckling was above the material yield strength.

3.0 MEMBRANE FORMING AND OPTICAL ANALYSIS

The process of forming accurate metal membranes was successfully scaled and demonstrated in task 2 of this project with 7-m diameter membranes. Previous work by SKI was limited to 1.4-m and 3.7-m membranes (1,2). This section of the report contains a discussion of the strain induced in the membranes, followed by a review of the efforts to analytically model the forming process. The last two subsections deal with the forming process and the optical accuracy of the formed membranes.

3.1 MEMBRANE STRAIN

The strain induced in the metal membrane from the forming process was measured at the 3.7-m scale. The expected nonuniformity of the strain was one factor in the elimination of tempered aluminum for use as the metal membrane material (2). If the metal membrane strained uniformly, tempered aluminum could potentially survive the forming process. However, aluminum's ductility is not sufficiently high to survive the high strains expected near the membrane center.

The membrane used was 2-mil, 304 annealed stainless steel with a 3.7-m diameter. Strain gages were not used because of the high stiffness of the gages relative to the thin membrane. Rather, direct measurement of the distance between discrete marks on the membrane was used. Marks were placed every 12 inches along two radial lines to measure radial strain. A series of marks with a spacing of about 3 inches was placed on circumferential lines every 12 inches to measure circumferential strain. The distance between the marks was measured before and after forming to an f/D of 0.6.

Figure 3.1 shows the measured radial and circumferential strain along a radial line parallel to the metal seams. Murphy predicts an average radial strain of approximately 3% with a maximum at the center (9). The average strain for the measured membrane appears to be slightly less than predicted, although the highest strains clearly occur at the center. No estimates were found in literature for strain as a function of radius for an f/D of 0.6, and no further comparisons with theory were made.

Figure 3.2 is a comparison of data taken parallel and perpendicular to the seams. Little effect from the seams is noted.

3.2 ANALYTICAL MODELING OF MEMBRANE FORMING

The process of forming flat membranes into accurate paraboloids was developed experimentally by SKI before initiation of the subject work (1, 2). A combination of sand and air pressure was used on 1.4-m diameter membranes, and a combination of water and air pressure was used on 3.7-m membranes. These results were reviewed at the start of this work to develop an approximation for the scaling relation.

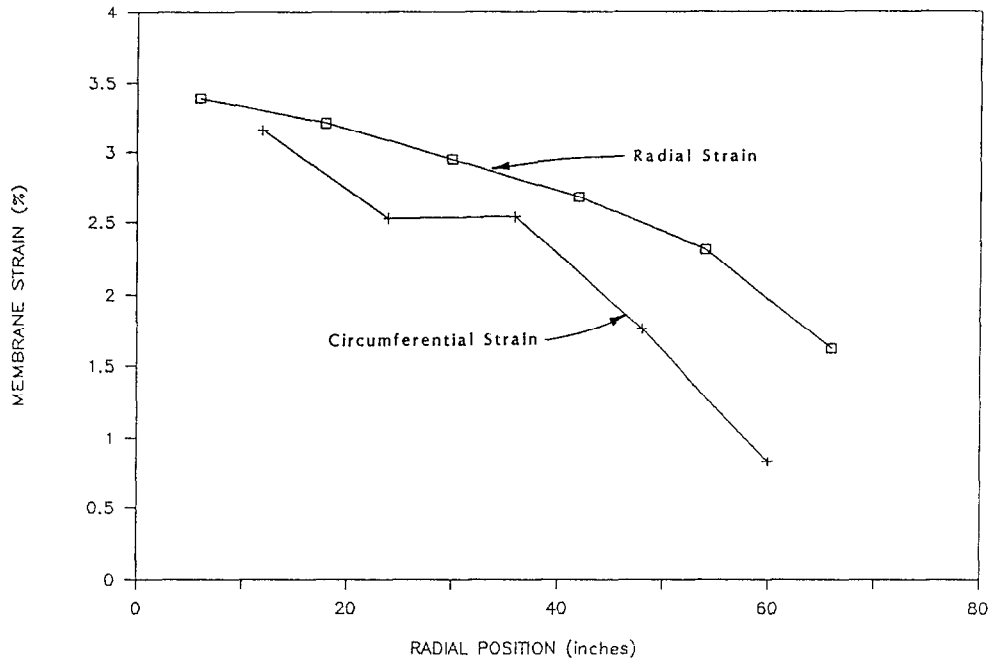


Figure 3.1 Measured Membrane Strain Parallel to Seams.

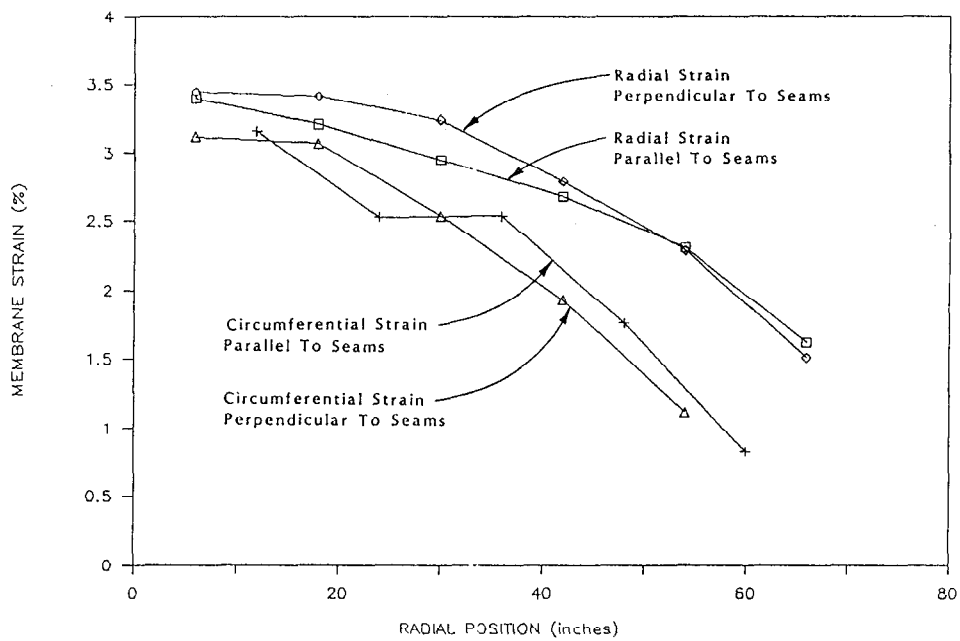


Figure 3.2 Comparison of Measured Membrane Strain Parallel and Perpendicular to Seams.

A first order relation was developed and successfully used for predicting forming of the 7-m membrane, although a more definitive analytical model was pursued initially.

The task of analytically modeling the forming process was undertaken to better define a correct set of forming variables for use on the 7-m diameter membranes. It was anticipated that this would reduce the number of experimental iterations required to obtain an acceptable membrane.

SKI contracted with the University of Nebraska to model membrane forming with nonlinear finite element techniques. Initial results using uniform pressure profiles showed promise. The model was expanded to allow the application of nonuniform pressure with a magnitude that is a function of membrane displacement and time, which is representative of the actual anticipated process. The turn-around time for these models increased to more than a week on the time-shared computer that was used. We expected that many runs would be required to debug the model because of its complexity. Because of the cost and expected schedule, this work was stopped.

Other sources for the finite element analysis were pursued to circumvent the long turn-around time. Access to faster computers at Sandia Labs was sought, but the required computer code changes made this option undesirable. Quotes were received from a private engineering firm that specializes in finite element analysis and has access to high-speed computers.

This modeling effort was canceled before completion. It was decided by SKI and the SNL technical monitor that the cost in terms of contract funds and schedule did not justify the possible benefit. The potential benefit of this work was a better estimate of the forming parameters, so that fewer membranes would need to be formed to achieve an acceptable shape. The risk of needing more forming iterations was accepted.

3.3 MEMBRANE SLOPE MEASUREMENT TECHNIQUES

Two measuring systems were used to measure the 7-m membrane. A system referred to as the "penta-prism" system was used for most of the measurements. A system called the "Video Ray Trace" (VRT) system is more thorough and accurate and was used for the final measurements. The penta-prism is used to measure membrane slope by measuring the intersection of the receiver plane and a laser beam reflected from the membrane surface. The beam strikes the membrane parallel to the optical axis of the dish. A stationary laser and a carriage-mounted penta-prism provide the incident beam. This system was developed during Phase I and is described in detail in reference 1. The system has an uncertainty of 0.6 mrad (1). The hardware was modified for 7-m membranes, and data collection was automated during this task.

The VRT system directs a thin laser beam to the reflective membrane from a fixed point located along the dish axis. This point is positioned a distance twice the focal length away from the vertex along the optical axis. The geometry defined by the incident beam and the intersection of the reflected beam and target defines the slope of the membrane at almost any point on the membrane. This system was developed as part

of Task 1 for 3.7-m membranes and was originally limited to approximately 500 data points per set (see reference 2 for a complete description). The software was modified for use on the 7-m optical element. The allowable data set size was increased to more than 5000 points. System uncertainty is less than 0.5 mrad with a repeatability of 0.1 mrad (2).

The impact of the number of data points measured with the VRT system on the results was assessed. Data from a 3.7-m membrane were used. A single, 5000-point data file was reduced in size to make ten files ranging in size from 94 to 4200 points. The removed data were selected at random. The results (see Figure 3.3) show a very small dependency on the number of data points. All values were within 0.26 mrad of the mean (area-weighted, RMS, radial slope error). The five files with 400 or more points varied only 0.01 mrad.

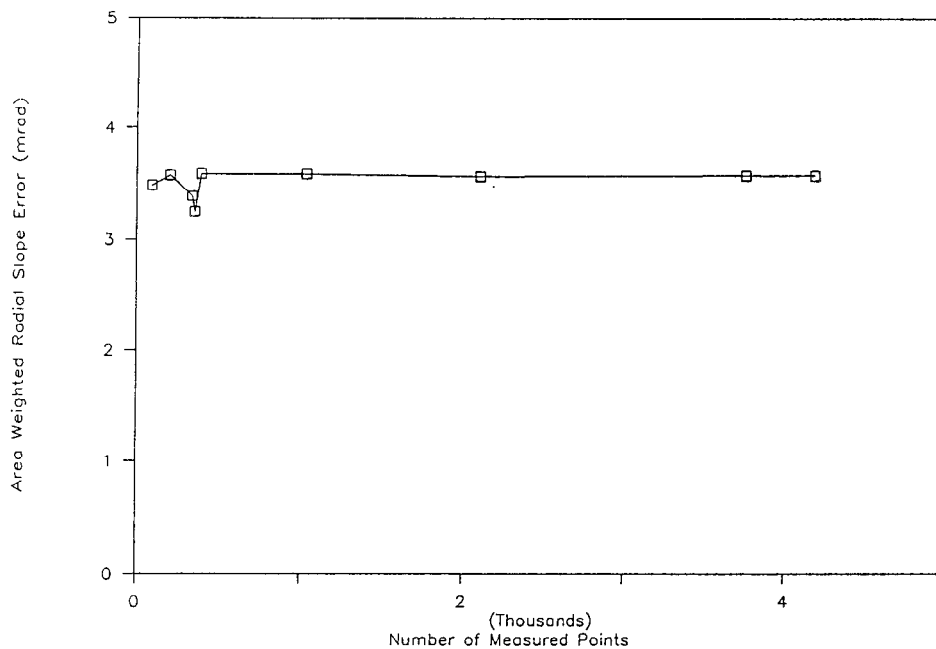


Figure 3.3 Sensitivity of Reported Slope Error to Number of Measured Data Points.

3.4 MEMBRANE FORMING AND OPTICAL SHAPE

Three 7-m diameter membranes were formed. The goal was to have the second two formed membranes available for use with the complete optical element (one as a backup) and to do most of the developmental work with the first membrane. This was accomplished. The shape of each of the three membranes was acceptable. This section describes the forming of these membranes and the optical shape that was achieved.

The forming process is divided into two distinct stages as described in reference 2. Water and air pressure are used simultaneously in stage one to form the membrane close to the final shape. The ratio of water-to-air pressure is a controlled variable. The nonuniform pressure profile provided by the correct ratio will form the membrane to a parabola. The second stage of forming uses air pressure alone to "fine tune" the membrane shape. Precise contour measurements could only be taken when no water was on the membrane. In this way, the second stage of forming (using air only) could be controlled better than the first stage, and thereby provided a more accurate shape than could be achieved with stage one forming alone.

This two-stage forming process is beneficial for prototype development. For commercial production, the repeatability of the process would allow for its refinement so that only the first stage would be required.

Figure 3.4 describes the first membrane slope as a function of radial position at several points in the forming process. This data was taken along a radial line (distance from the center is shown on the horizontal axis) with the penta-prism system. The vertical axis represents the radial component of the slope error where "slope error" is defined as the difference between the actual slope and the slope of an ideal parabola with a f/D of 0.6. The line labeled "prior to tuning" represents the shape after the first stage of forming. Improvements with each tuning step are shown by the other three lines. Note that additional tuning would start to degrade the shape by increasing the absolute error at regions near a radius of 80 and 115 inches. Tuning is stopped when the area weighted error reaches a minimum.

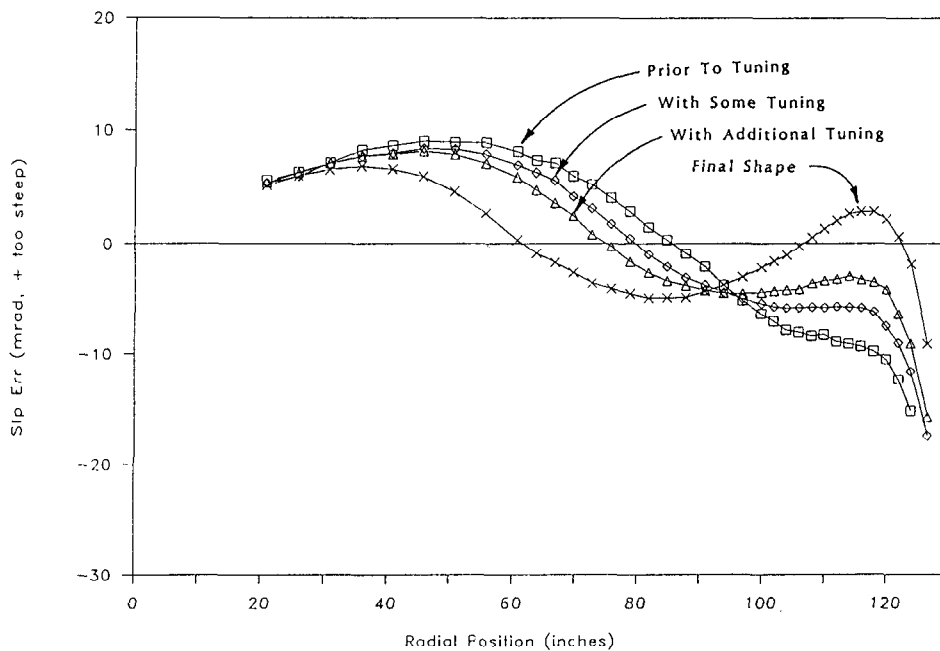


Figure 3.4 Slope Accuracy Improvements with Tuning.

Stainless steel was used as the membrane material because of results from earlier work on this project (2). This work indicated that the membrane thickness has a significant influence on the final membrane shape. Because of the lack of a proven analytical forming model, engineering judgement and first-order approximations were used to define some of the forming variables. A 4-mil thick membrane was selected, and the initial ratio of water-to-air pressure was defined. This ratio was altered during the forming process by measuring the membrane shape during the first stage of forming. These measurements were made with a set of two parallel scales mounted on guides 5.5 inches apart. The relative height of the scales indicated slope of the membrane. This system had an absolute repeatability of +/- 3 mrad and an accuracy of approximately +/- 4 mrad. Measurements were taken at ten locations along a diameter.

The accuracy of each membrane was better than 3.5 mrad as measured with the more accurate penta-prism system. Table 3.1 summarizes the results for each membrane.

Table 3.1
Optical Quality of Each Membrane

Membrane #	<u>RMS Radial Slope Error (mrad)</u>	
	After Stage 1	Final
1	7.9	3.4
2	6.3	3.3
3	5.2	3.1

The values represent the RMS of the difference between the actual slope and the slope of an ideal parabola with a f/D of 0.6. Data were taken along one radial line parallel to the seams and include only the radial component of the error. The penta-prism system was used for these measurements. The data are also area-weighted to account for the increased significance of the data close to the perimeter. The results show that forming of numerous membranes was not required to obtain good shapes, although improvements were made with each iteration. The results obtained at the end of the first stage of forming show dramatic improvement with each membrane formed. More details of membrane shape are provided later in this section.

An interesting observation can be made by referring back to Figure 3.4. Near the point 93 inches from the center, the slope error (and slope) did not change during the tuning stage. The error remained nearly constant at -4 mrad. Comparison of the three membranes, after only the first stage of forming, shows a similar effect even though slightly different air-to-water ratios were used on each. Neither the forming process of the first stage nor the tuning process of the second stage significantly affected the slope of this point. Figure 3.5 is an overlay of each of the three membranes before and after tuning, showing the nearly coincident point at a radius of 93 inches. It also can be noted that this point limits the overall accuracy of the membrane. Improvements to the region between 93 inches and the outer edge of the membrane worsen the region from about 60 inches to 93 inches.

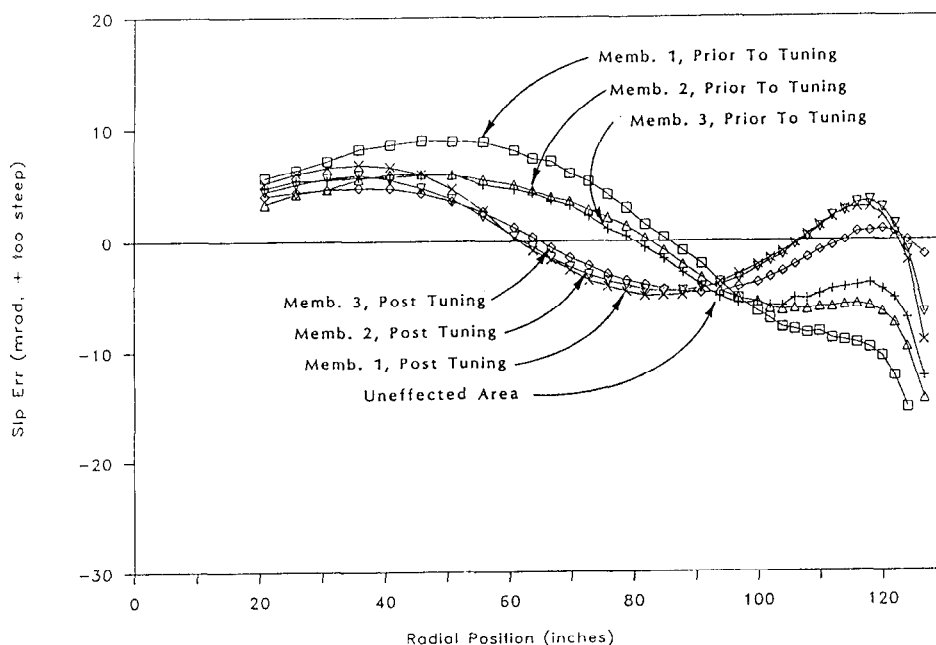


Figure 3.5 Membrane Slope Error Showing Unaffected Area.

The significance of this observation is that for a given material type and thickness, there may be a limit to the achievable accuracy without the controlled variation of other forming variables. The sensitivity of the final shape to the air/water ratio appears to be small. Material thickness is a rather simple variable to change. SKI's earlier work demonstrated the potential improvements of changing the membrane thickness (2).

Detailed measurements of the membrane were made to accurately define its shape. The VRT system was modified and used for some of the measurements. Because of height constraints on the working area where the membranes were formed, the optical element had to be tilted to point toward the horizon so it could be scanned with the VRT. This was done only on the third membrane. All earlier membranes were scanned with the penta-prism system, which is limited to scanning along radial lines. The measurements with the VRT defined the optical effect of different stabilization pressures, defined the optical accuracy based on a large data set, demonstrated the effects of the seams, and demonstrated that the receiver will not have a significant optical effect.

3.4.1 Effects of Stabilization Pressure

The effects on the shape of the metal membrane due to changing the stabilization pressure were investigated using the penta-prism system on a metal membrane without the reflective polymer membrane in place. Measurements were taken along a radial line at two different stabilization pressures. As can be seen in Figure 3.6, most of the membrane is unaffected by changes in stabilization pressure. Only at the outer edge

did the shape improve with higher pressure. The radial error was 3.3 mrad measured with a stabilization pressure of 3.5 inches of water column. The corresponding value measured with a pressure of 7 inches of water column was 3.1 mrad. This was a small but significant difference. As a result of this test, 7 inches of water column was used as the stabilization pressure for subsequent tests with the VRT.

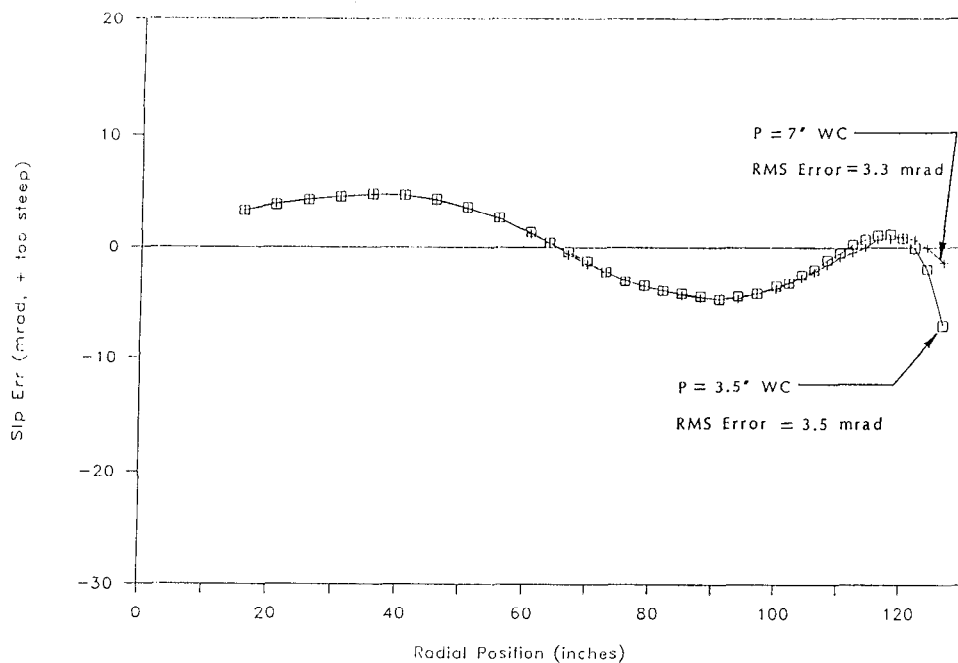


Figure 3.6 Effects of Stabilization Pressure on Membrane Contour.

3.4.2 Detailed Measurement

The third membrane was scanned with the VRT. Figure 3.7 shows the results. The data shown are the radial component of the slope error. Slope error is defined here as the difference between the actual slope and the slope of a parabola with a best fit focal length. Over 4300 data points were taken in a 3-inch grid pattern. Since some areas of the dish are not scanned, the data are area-weighted so that each unit area of the dish is equally weighted. The radial and circumferential components of the error are evaluated separately to define one RMS term for each. They are then combined in a root-sum-square fashion to obtain a single value to represent the optical quality of the entire dish.

The radial component of the error is 3.3 mrad, and the circumferential component is 1.3 mrad. These combine to give 3.6 mrad as the measured optical accuracy of the third membrane.

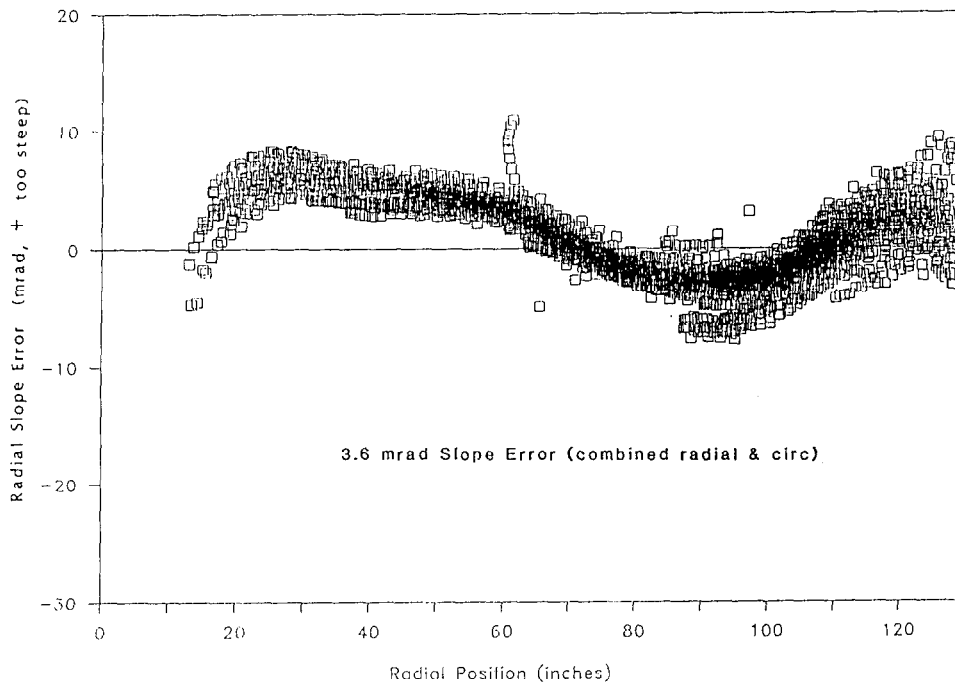


Figure 3.7 Membrane Contour Results for Third and Final Membrane as Supported in the Assembled Optical Element.

The 3.7-m membranes formed in earlier work had large slope errors very close to the perimeter. No similar effect was seen with the three 7-m membranes. For this reason, the entire membrane was assumed to be useful. That is, the reported values for the 7-m membranes represent 100% of the membrane surface area.

3.4.3 Effects of Seams

The optical effects of the seams were evaluated qualitatively by comparing radial scans taken with the penta-prism and laser system. Four sets of data were taken, two parallel and two perpendicular to the metal seams. Figure 3.8 shows the comparison between these two sets of data. The seams are clearly evident by the discontinuities in the data. The effects are similar to those seen on 3.7-m diameter membranes. The seams affect a broad area, often extending from one seam to the next. The magnitude of the effect appears to be small in relation to the error of the general dish contour. These scans were taken on the first 7-m membrane that we formed, prior to tuning. No reflective membrane was present.

A similar comparison is shown in Figure 3.9 with the polymer membrane in place. There are only four polymer seams, and they are almost coincident with the metal seams. This tends to obscure the effect that the polymer seams have on optical quality.

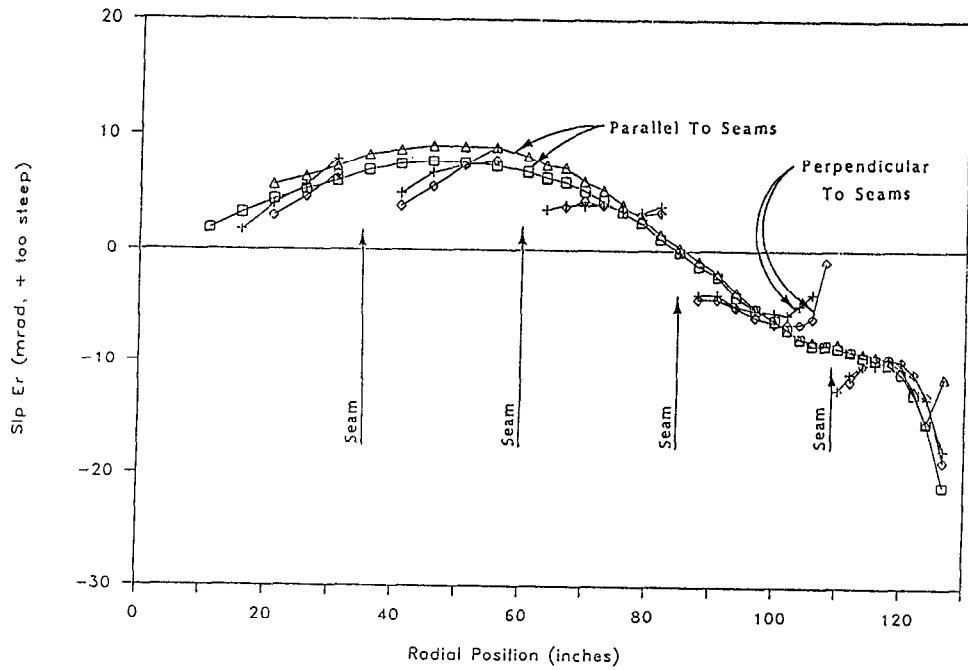


Figure 3.8 Optical Effects of Metal Seams.

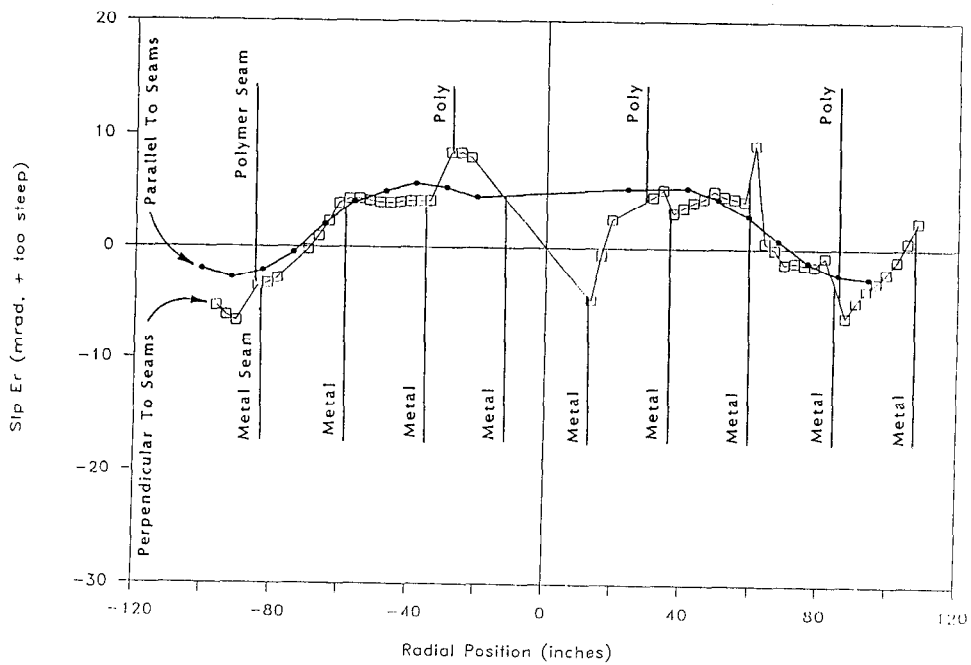


Figure 3.9 Optical Effects of Metal and Polymer Seams

3.4.4 Effects of Receiver Loads

The impact of receiver loads on the optical shape was tested by applying a simulated receiver load to the ring while the optical element was pointed toward the horizon. A VRT scan was taken before and after the application of the load. The optical accuracy of the membrane was calculated to be 3.6 mrad without the load and 3.4 mrad with the load. The difference is within the measurement uncertainty. A smaller data set (500 points) was used for the loaded case to minimize the delay created when a power failure caused a loss of data during the first attempt. The difference in the data set could account for the difference in the reported accuracy. However, the data do indicate that the receiver load does not have a significant effect on the optical accuracy of the dish.

4.0 7-M OPTICAL ELEMENT PROTOTYPE FABRICATION

Prototype fabrication involved all optical element component fabrication as well as tooling fabrication, membrane forming, followed by assembly and installation of the optical element on the drive. The entire optical element was assembled in Dallas prior to its installation in the field at Sandia in Albuquerque. Three 7-m metal membranes were formed; one for forming and handling technique development, the second for use in the field, and the third for detailed measurements in Dallas. The third membrane also served as a backup membrane for field assembly.

The major fabrication and assembly steps for the prototype 7-m optical element are as listed below:

1. Fabricate forming tool
2. Fabricate optical element components
 - a. main ring
 - b. membranes
 - stainless steel
 - reflective polymer
 - rear
 - c. membrane departure and clamp bars
 - d. hub
 - e. flanges
 - f. spokes and spoke hardware
 - spokes
 - spoke springs
 - spoke attachments brackets
 - g. vacuum controls, and
 - h. mounting hardware
3. Form stainless steel membranes
4. Measure formed membrane's shape
5. Test assemble optical element
6. Operate stabilization pressure system and measure component strains
7. Tip element and measure membrane shape
8. Disassemble optical element/ship to SNLA
9. Install assembly tooling at SNLA
10. Assemble optical element in field
11. Mount optical element on drive
12. Modify mounting hardware to accommodate drive irregularities

Work performed to accomplish each of these steps is described in this chapter.

4.1 TOOLING AND MASTER ASSEMBLY PROCEDURE

We originally intended to form the metal membranes in the field (at the dish erection site). Membrane forming requires a very large tool to resist the high membrane and vacuum loads. We built this forming tool so that we could use it both in Dallas for testing and in Albuquerque. We later developed a method for transporting formed membranes. This allowed us to leave the large, cumbersome forming tool in Dallas and use much smaller tooling for field assembly.

4.1.1 Forming Tooling

The forming tooling served as a vacuum chamber with one open end. The membrane to be formed was stretched across the open end. The forces acting on the tooling resulted from the uniform pressure differential from the vacuum inside the fixture and from the weight of the water used to form the membrane. The forming tooling design is a compromise between controlling engineering effort and ensuring a portable tooling system. The structure was conservatively sized to withstand the highest forming loads anticipated for the thickest membrane material anticipated.

The forming tooling, shown in Figure 4.1, is 25 feet in diameter and approximately 6.5 feet high. It was built in four sections that bolt together. Each section has two removable panels to allow ready access to the interior during assembly operations. A rolled 8 in. x 8 in. x 3/8 in. square tube reinforces the edges of the ring. Each section of the ring has four legs. The legs are cantilevered to the outside of the tooling to allow a bottom cover to wrap without interruption around the lower outside circumference of the tooling. A solid end spanning the bottom of the tooling ring would have been heavy and costly to fabricate from steel. Therefore, a plasticized polyester cloth membrane was used to close the bottom of the fixture. This membrane was fabricated in the shape of a dome to reduce the stress in the material when a uniform pressure was applied. The height of the dome limited the tension in the membrane. The dome height also determined the overall tooling ring height, since the apex of the bottom membrane must not interfere with the nadir of the formed stainless steel membrane above it. The bottom membrane was also reinforced with multiple radially oriented steel cables.

A series of 48 brackets around the interior wall of the tooling supported the optical element ring during membrane forming. In this way, the actual ring, which is part of the assembled dish, serves as part of the forming tooling. This assures that the diameter and planarity of the formed membrane periphery matches that of the assembled ring on which it is mounted. Tie rods link the optical element ring to the tooling ring at 24 locations to resist the tendency for the ring to reduce in diameter during forming as a result of the membrane tension acting upon it.

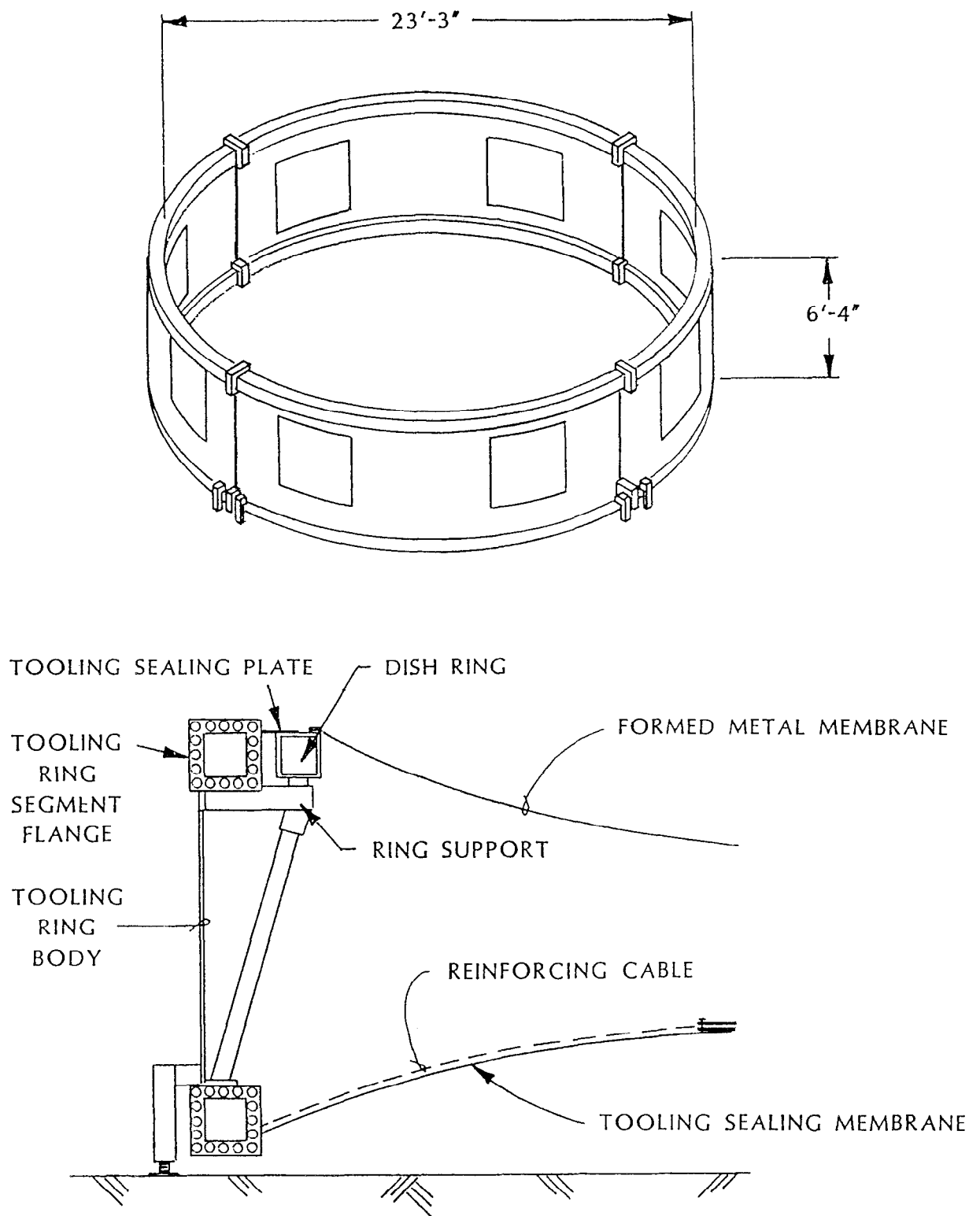


Figure 4.1 Membrane Forming Tooling Ring.
Upper View - Overview of Ring with Segments and Access Door Shown.
Lower View - Cross Section of Tooling Showing Major Components to Support Ring and Seal Tooling.

After forming and before the optical element is assembled, three brackets were bolted to the optical element ring so that it hung from the top edge of the tooling instead of being supported from below. The 48 support brackets were removed to allow the fitting of the rear membrane where it wrapped about the entire outer circumference of the optical element ring.

A pair of rails was used to support either end of a mandrel about which the membrane material was wrapped, as shown in Figure 4.2. This was used when the flat membrane was first installed on the tooling and again when the formed membrane was rolled onto the storage and shipping mandrel. The rails were simple wooden planks oriented on edge and supported on four oversized "sawhorse" legs.

The detailed procedure for using this tooling is included in appendix A.

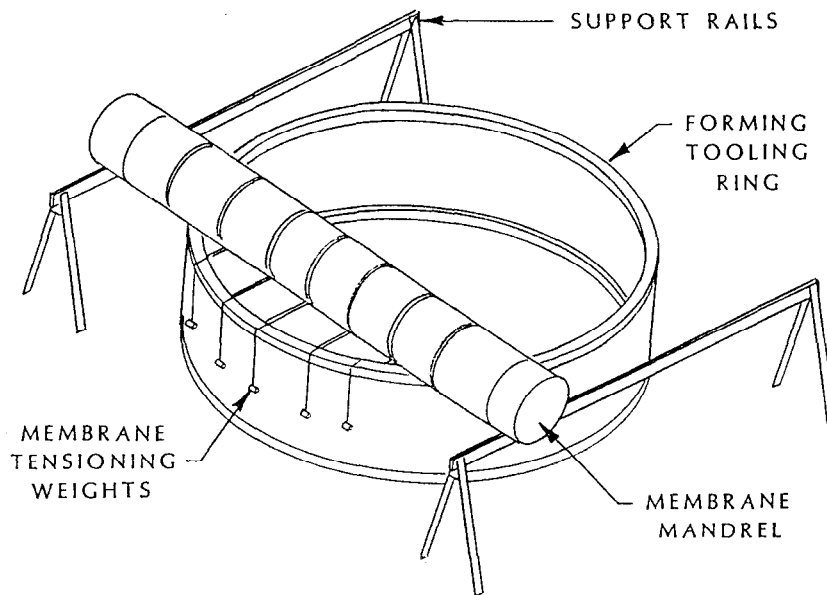


Figure 4.2 Set Up for Formed Membrane Rolling.

4.1.2 Field Assembly Tooling

The field assembly tooling served three purposes. First, it supported the two segments of the optical element from underneath while the segments were welded into a single continuous ring. The supports were adjustable in height to maintain planarity during welding. The tooling also supports the ring while the formed membrane is fixtured to it. After this operation is complete, the upper portion of the tooling supports are bolted in place. The ring is then suspended from above to permit the rear membrane to be wrapped about the entire periphery of the main ring during final assembly.

The tooling used was originally designed and built for supporting the tensioning reaction rings used during fabrication of the SKI Mark II stretched-membrane heliostat. For the dish assembly, six of the original twelve tooling pylons were used. Of these, three were anchored to the floor. Each pylon was cut to allow the upper portion to be removed, as shown in Figure 4.3, so that it would not interfere with the membrane mandrel during the formed stainless steel and the reflective polymer membrane installation. The removed upper portion was fitted with four tabs to allow later refitting over the lower portion where it was bolted back in position. The upper portion is needed for supporting the optical element later in the assembly process. The procedure for using this tooling is included in appendix B.

4.2 MEMBRANES

The prototype optical element utilizes three separate membranes of three different materials. The formed stainless steel membrane defines the shape of the reflective optical surface. It is made from .004-inch type-304 stainless steel coil stock 36-inches wide. The reflective polymer membrane is stretched over the front of the metal membrane and drawn down in contact with it by vacuum. The material is an aluminized (one side only, front surface) .002-inch polyester film. It is not expected to be a good long-life material, but was selected for these tests because it was available and inexpensive. Finally, the rear membrane is draped over the outside of the rear spokes to enclose the volume between the metal membrane and the surface described by the rear spokes to form a vacuum plenum. The material used in the back membrane is a polyester cloth impregnated with PVC to make it impervious to air. This material has a very high tensile strength, although it is not very stiff (the elastic modulus ranges from 2.6 E5 to 5.6 E5 psi). It is normally used for truck and cargo covers and for large air-supported buildings; hence, it is designed for good life under continuous stress and in exposed applications.

Several issues were addressed separately for each of the three membranes. These include material strength, material seaming procedures, attachment methods to dish structure, and weathering properties.

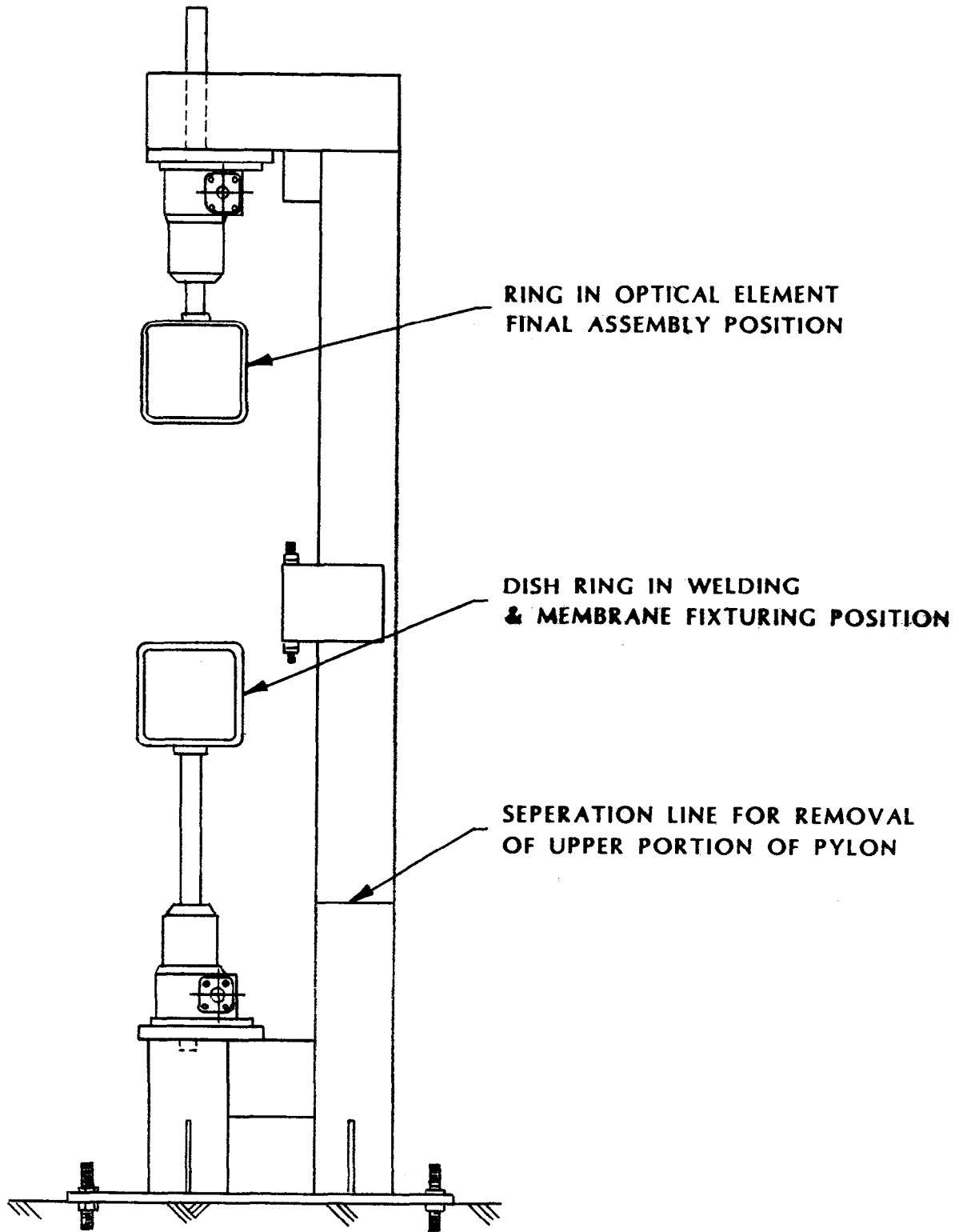


Figure 4.3 Optical Element Assembly Tooling Utilizing Heliostat Membrane Tensioning Ring Support Pylon.

4.2.1 Metal Membrane

The metal membranes were fabricated from 36-inch wide coil stock, grade B finish. A wider coil would have reduced fabrication effort, but could not be found. The seam construction had been explored in earlier work and was simply a welded overlap. Material thickness selection is discussed in Section 3.0.

Membranes were formed plastically to achieve the correct optical shape after they were seamed together. This means the seams where the panels of coil stock are joined to form the flat membrane experience tension sufficient to yield the single thickness of the membrane material. As the membrane was formed, the material near the center went through greater strain than that at the edge. Seam design was patterned after seams used in the 3.7-m membranes from earlier forming experiments, as shown in Figure 4.4. Coupons from both ends of each seam were cut and tensile tested to ensure weld quality before continuing to the next seam. The seam failure mode of properly prepared tensile samples was generally metal tensile failure of the coupon adjacent to the overlapped area.

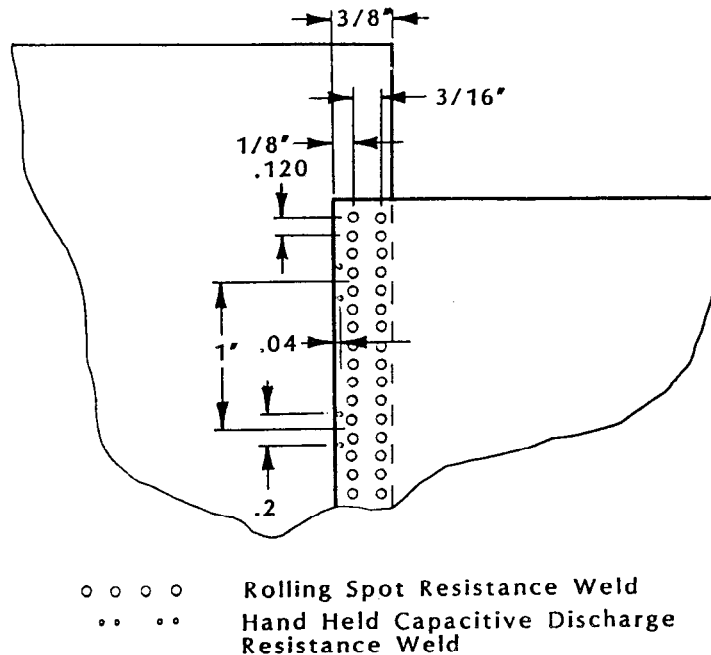


Figure 4.4 Metal Membrane Welded Seam Detail.

An additional seam area existed at the center of the metal membrane where a pair of doubler rings was attached to the formed membrane. A hole was cut in the center of the membrane for the hub. This was done after the membrane was formed. The doublers were a precaution to protect against ripping at any notches, if unanticipated handling stresses occurred. The doubler detail is shown in Figure 4.5.

4.2.2 Reflective Polymer Membrane

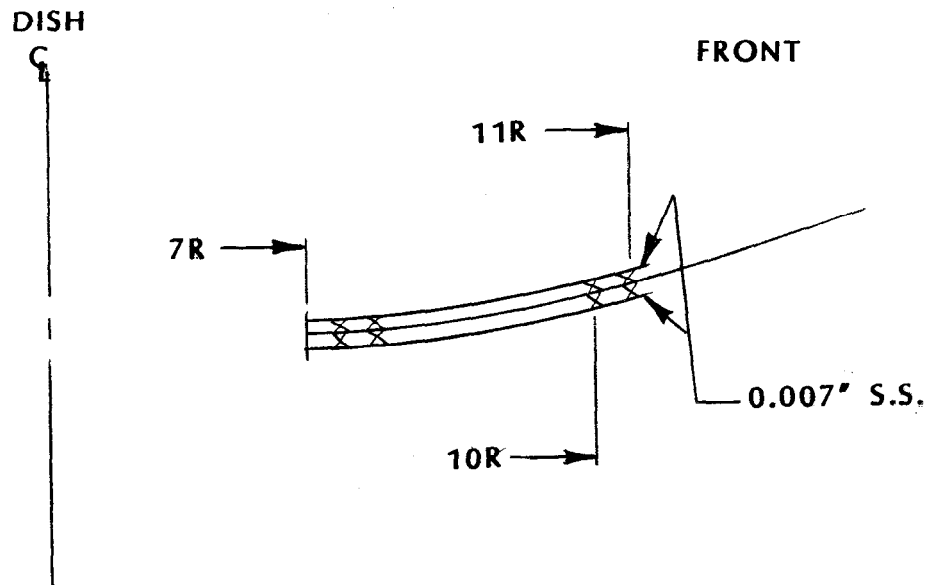
Further development of appropriate materials and designs of the reflective polymer membrane is needed. The original plan in this effort was to utilize commercially available premium grade solar reflective films. It was expected that the films might require laminating to a substrate film to achieve required mechanical properties. The difficulty in creating high strength and reliable seams in such a laminate was substantial. In fact, satisfactory results were not obtained, and in the interest of getting the optical element completed and under test, a simple aluminized polyester film was used.

The reflective film of choice was originally 3M's ECP-305, silvered acrylic. This material is not very ductile. Since a flat reflective membrane must undergo as much as eight percent strain, a method of reducing the strain for the polymer membrane was sought. The approach developed was to fabricate the polymer membrane in the shape of a cone (1). A cone requires less net change in shape, and therefore, lower stresses and strains to pull it down to conform to the parabolic metal membrane.

Seams in the polymer membrane were necessitated by the limited width of ECP-305 and available substrate films. Two types of seams occurred in this original membrane concept. The reflective film is available in a maximum width of 24 inches. Substrate film is typically 60 inches wide. Where the reflective film was laminated to the substrate, there would be longitudinal strips with no reflective film between the 24-inch strips. At the substrate edges, another seam would exist where the panels were joined together.

A problem existed in that the laminated film's total thickness and strength were reduced where there was no reflective film. Under tension, the laminate would tend to strain more in those areas to the point of failure. One solution would have been to increase the substrate strength so that this variation was insignificant. This approach drove up the tensile strength requirements of the panel-to-panel seams. The stress was the same regardless of material thickness; however, the seam loads increased with increased thickness.

Various seam designs that reinforced areas in the membrane with no reflective film were tested, as shown in Figure 4.6. Testing revealed that to achieve the level of strain required in the reflective film, very high seam strengths were required with even an insignificant substrate thickness. There were few adhesives that offered the required performance (see appendix C for adhesive data). Another problem related to adhesive selection was that the reflective film and its pressure-sensitive laminating adhesive would withstand only limited temperatures (significant adhesive softening at 130 °F, reflective film hazing at 160 °F), eliminating the use of many heat-activated adhesives.



Capacitive Discharge Resistance Welds
4 Rows Top / 4 Rows Bottom

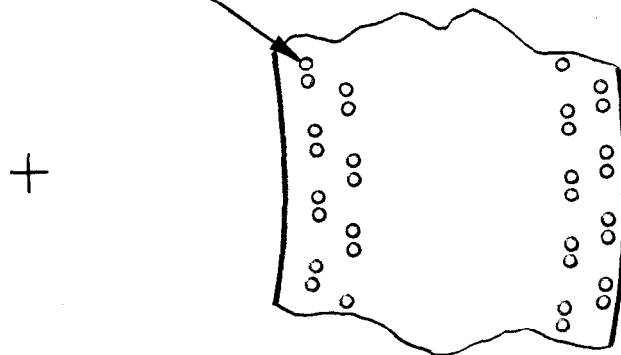


Figure 4.5 Metal Membrane Center Reinforcing Ring Weld Details.

Regardless of the adhesive used, a problem existed in all seam designs because the reinforcing strips extended under the laminated areas causing extra thickness and stiffness there. When the membranes were pulled down under vacuum, it was anticipated that these areas would initially strain less and want to chord or lift off the metal membrane. To avoid this, a tape was used that consisted of high-strength polyester fiber oriented transversely to the tape. A carrier tape held them together for handling, but had negligible longitudinal strength. The fibers would lend their strength to resist loads across the reinforced areas, but would not increase strength parallel to the seam. The fibers would simply separate as the carrier tape material yielded in that direction.

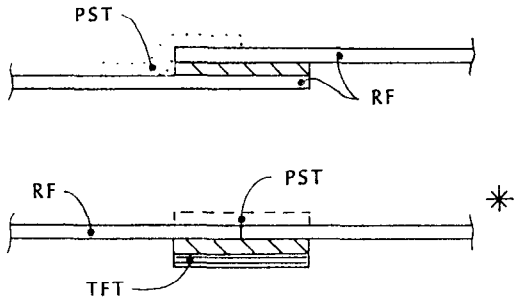
Another factor considered was that as membrane thickness was increased, the level of stabilization vacuum required to pull it down to the metal membrane also increased. The maximum stabilization vacuum available was limited by the allowable stress levels in the optical element components. This value was 7 inches water column.

Testing revealed that the silvered acrylic film was too notch sensitive and operating too close to its ultimate stress to make it structurally reliable. This could be meliorated by increasing the depth of the cone to which the polymer membrane was fabricated. It was not known how well a cone with a depth almost equal to the formed metal parabola depth would pull down against the metal membrane. There was a possibility that the center area would pull down first, obstructing the evacuation of air between the membranes further toward the dish edge. A more satisfactory solution would be the use of a reflective film that had a lower modulus and greater ductility. Further development in this area was not pursued to avoid delays in testing.

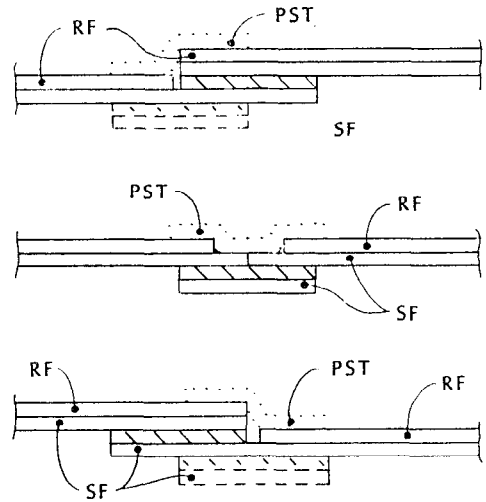
The approach implemented for the reflective membrane that was used on the prototype optical element was one that had already been successfully used at the 1.4- and 3.7-meter scale. This was to use aluminized, polyester film normally produced for food packaging, advertising products, and "space blankets." This film has a lower reflectivity than the ECP-305, but improved mechanical properties. We also had an established reliable seaming technique using a heat-activated, polyester-based adhesive. This material had previously been used only on membranes being operated indoors for measurement purposes. It is not expected to have good life outdoors where higher ultraviolet concentrations occur. To extend the outdoor operating life, the aluminized surface of the film would be on the front to help shield the polymer from the ultraviolet. The aluminum coating is so thin on these films that handling and very mild weathering tends to remove it in some areas.

The polyester film also tends to shrink when exposed to the adhesive activation heat. No method of avoiding the effect has been found. The result is that the seams in the finished membrane are slightly shorter than the panels. When the conic membrane is fixtured to the ring and before it is drawn all the way down to the metal membrane, the seams are higher than the panel areas. However, they do pull all the way down until they contact the metal membrane at a slightly increased vacuum.

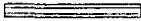

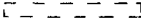
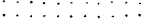
UN-LAMINATED REFLECTIVE FILM



LAMINATED REFLECTIVE FILM



SF - Substrate Film
 RF - Reflective Film
 PST - Pressure Sensitive Film

TFT - Transverse Fiber Tape 
 A - Adhesive 
 Alternate Construction 
 Post Fabrication Addition 

* Final Design

Figure 4.6 Diagrams of Seam Configurations Tested for Use in Reflective Polymer Membrane Fabrication.

4.2.3 Rear Membrane

The rear membrane forms one side of the vacuum plenum by draping across the rear set of spokes and sealing to the optical element ring. It is supported along 24 approximately radial lines by the rear spokes. It is pulled inwards toward the metal membrane between the spokes by the vacuum. It sags further between the spokes; therefore, the need for the rear membrane standoff rail around the membrane periphery. This additional space is provided to ensure the rear membrane will not sag as far as to touch the back of the metal membrane. Any contact prevents the differential pressure from operating across the metal membrane at that point and causes a local optical error.

The pressure differential across the rear membrane results in a tension in the membrane as it does for the front membranes. The theoretical tension in the back membrane is less uniform and more difficult to predict than for the parabolic front membranes. Added stress risers result where the rear membrane drapes over the rear-spokes-spring- assembly bodies and spoke attachments. There is also an area around the rear flange where the material drapes from the flange to the spokes. A very tough material was sought to withstand both the average and concentrated loads. The material also had to be readily fabricated, air tight, and possess excellent weathering properties. Such a material was found in architectural fabrics normally used for air-supported buildings, tension structures, and cargo covers. The selected material is a 10 oz/yd² polyester woven cloth, impregnated with PVC to a weight of 32 oz/yd². It has a tensile strength of over 800 lbs/in. (grab tensile Method 5100). It is fabricated with a combination of sewing and solvent welding. The net free shape of the fabricated membrane was a truncated cone with an additional hoop about the periphery. The peripheral edge was prepared with a rope sewn into the hem to assist in its fixturing to the optical element ring, as shown in Figure 4.7. Reinforcing rings were solvent welded to the membrane wherever penetrations through the membrane were made for vacuum connections and such.

4.3 RING AND MEMBRANE ATTACHMENTS

The optical element ring was fabricated from B500, 6 in. x 6 in. x 5/16 in. structural square steel tubing. It was rolled using an induction-heated hot rolling process. This provided major improvements in distortion, accuracy, and repeatability over the cold rolled process used on the tubing for the membrane forming tooling ring and previous heliostat tensioning tooling rings.

The ring was made in three segments that welded end-to-end. The ring segments were fixtured with the help of a rotating sweep arm mounted in the center of the ring. The sweep arm has a pair of dial indicators on the outer end of a rotating arm to measure planarity and concentricity of the ring. Where the ring segments were not quite the correct radius, they were aligned as well as possible to produce a minimal average error. The three butt joints were welded per the AWS Structural Welding Code.

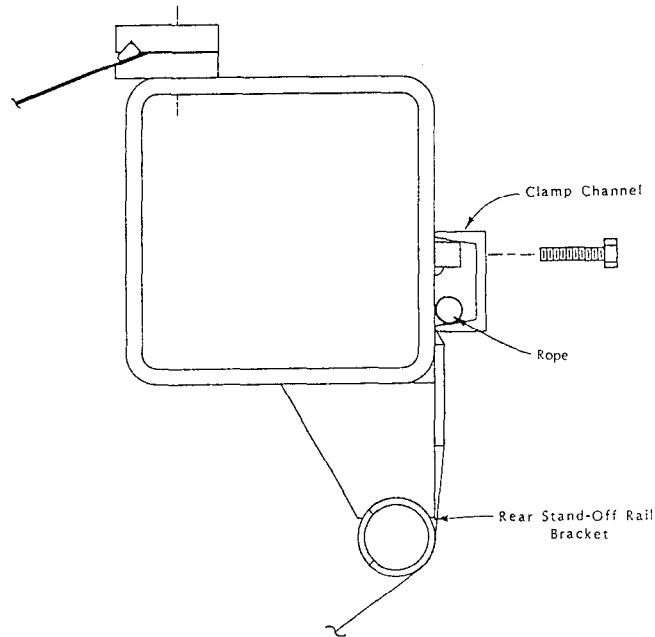


Figure 4.7 Cross Section of Dish Ring Showing Rear Membrane Clamping Arrangement.

After the ring was welded, a second rolled bar was fastened to it to form a more accurate "departure" bar for the membrane attachment. This bar has a machined bevel along the inside radius, as shown in Figure 4.8, for the formed membrane to lie against. The bar also had a series of holes along its length for fastening to the main ring. Each bar was individually set to have the correct radius, and the holes matched, drilled, and tapped into the main ring. Clamps were used to adjust the departure bar radius at the individual bolt locations before it was drilled. At each location, the elevation of the departure bar was also measured, and it was shimmed as required to keep it planar.

A curved bar was used to clamp the membrane against the departure bar. Clearance holes were made in both the clamp bar and the departure bar, and the ring was drilled and tapped for the clamping bolts.

These clamp-bolt holes were used to fixture the membranes to the ring. For forming, the flat-metal membrane was rolled out on the tooling. Weights were hung from the periphery of the membrane, as shown in Figure 4.8, at about 20 inch centers. This effectively tensioned the membrane to hold it flat during fixturing. A hole in the membrane was punched at each clamp-bolt hole location. Next, a rolled bar with matching clamp-bolt hole locations was set on top of the metal membrane and bolted to it. This held the membrane periphery during forming. Three-inch centers were used on this clamp bar to ensure sufficient clamp force to resist the loads of forming.

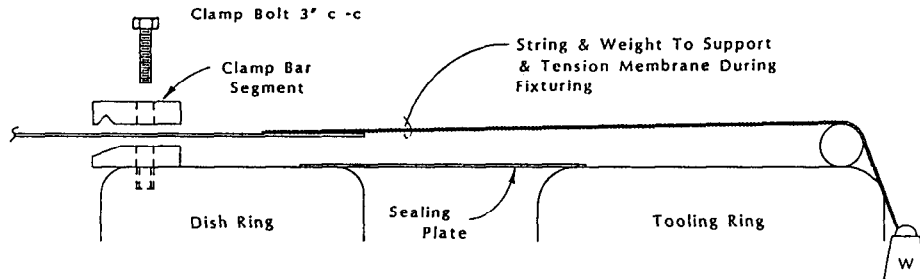


Figure 4.8 Cross Section of Dish Ring Positioned in Tooling for Forming Operation. Also Shown are Metal Membrane, Membrane Tensioning Weight, and Tooling Sealing Plate.

After the membrane was formed, the weights used to hold it in tension were reattached while the membrane outer material was cut off. The cut was made just at the top of the bevel of the departure bar. This would allow the membrane to roll onto the contoured mandrel for storing and shipping. Flat material left around the membrane periphery would not roll smoothly onto the contoured mandrel.

When the membrane was rolled back off the shipping mandrel onto the ring for assembly in the field, the weights were again used to support it. The beveled area around the departure bar matched the angle of the outer edge of the formed membrane. During field assembly, the outermost edge of the membrane was tack welded to the departure bar to hold it in place. Tack welding was done with a small hand-held capacitive discharge resistance welder.

Once the metal membrane was secured, the polymer membrane could be installed. A careful cleaning operation took place first, using alcohol spray and lint-free rags, followed by dusting with tack cloths. The polymer membrane was unrolled next. It was secured about the edge with masking tape to the optical element ring. Once it was properly aligned, holes were punched in the polymer membrane at each clamp-bolt hole location and the clamp bars reinstalled. This time, a section of O-ring cord was set in the groove around the inner radius of the clamp bars, as shown in Figure 4.9. This cord is slightly too large to fit in the groove when the clamp bar is tightened to the departure bar. Therefore, it presses on the polymer membrane and indirectly on the

metal membrane beneath. The clamping force was designed and tested to be great enough to restrain the membranes against the forces created by the membranes by the stabilization vacuum. The tack welds that attach the membrane to the departure bar are not necessary to withstand the working design loads.

The rear membrane is attached to the ring along the outer diameter. This permits the rear membrane to wrap around the rear spokes and the standoff rail described previously. The outer edge of the rear membrane has a rope sewn into its hem. A steel channel, rolled legs in, is fastened to the ring so that this rope was captured, as shown in Figure 4.7. The tension in the rear membrane is transferred by the rope to the rearward leg of the channel as the membrane tries to pull the hem out. A square bar welded to the ring outside diameter restrains the channel from slipping under this pull. The channel, which was made in 24 segments, was held to the outer diameter of the ring with three bolts per segment. These bolts prevent the channel from lifting away from the ring and allowing the membrane hem to escape. The clamp channels are cut away by the thickness of the strong back where the membrane is wrapped around the strong back at the spoke bracket on the outside of the ring, . This ensures that the membrane material is clamped continuously and equally in all areas.

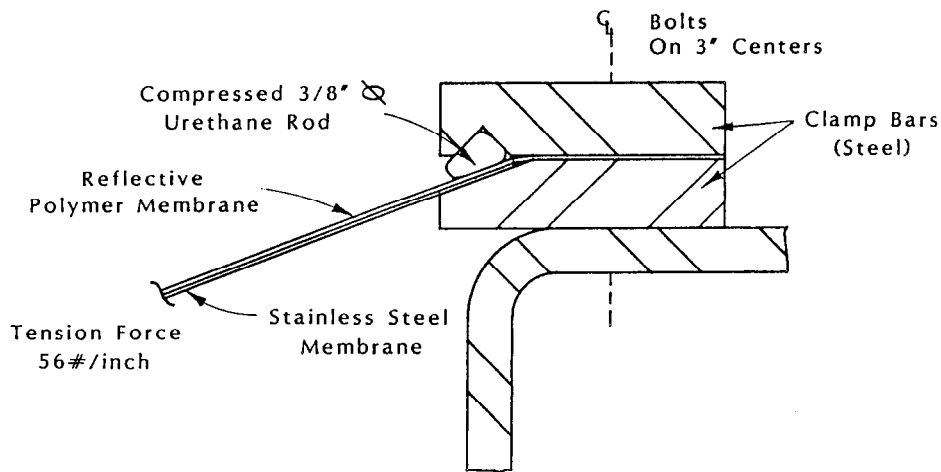


Figure 4.9 Cross Section of Formed Membrane Departure Bar on Optical Element Ring Showing Final Assembly Membrane Clamping Arrangement.

4.4 HUB AND SPOKES

The hub, spokes, and ring combine to provide the light weight and high stiffness structure of a spoked wheel. The vacuum acting on the rear membrane, and therefore, the rear spokes, adds additional loads to the structure. The tension in the rear spokes is reduced, as described in Section 2.0, by allowing some controlled extension and deflection of the rear spokes. This extension is allowed by including a spring element in series with the rear spokes. A pretension is applied to these spring elements during assembly to ensure a stable structure when the vacuum is removed. The elements have built-in adjustable stops that prevent additional spring extension after a set extension has occurred. A very high spring rate and small extension required for this design made use of a coil spring impractical. A Belleville spring stack loaded in compression was used, as shown in Figure 4.10. This allowed a compact design with off-the-shelf springs and simple assembly and adjustment of spring gap. The parts were nickel plated to prevent corrosion and assure free movement.

The hub is simply a structural tube, hot dip galvanized for corrosion resistance. The flange design was dictated by the clearance required for spoke attachment. The flange also has a collar that serves as a socket for the hub. Set screws in this collar allow the hub to be captured, so the flange can be used to lift the hub during assembly of the dish. The collar also reduces stress concentrations on the hub ends during assembly, spoke tensioning, and operation.

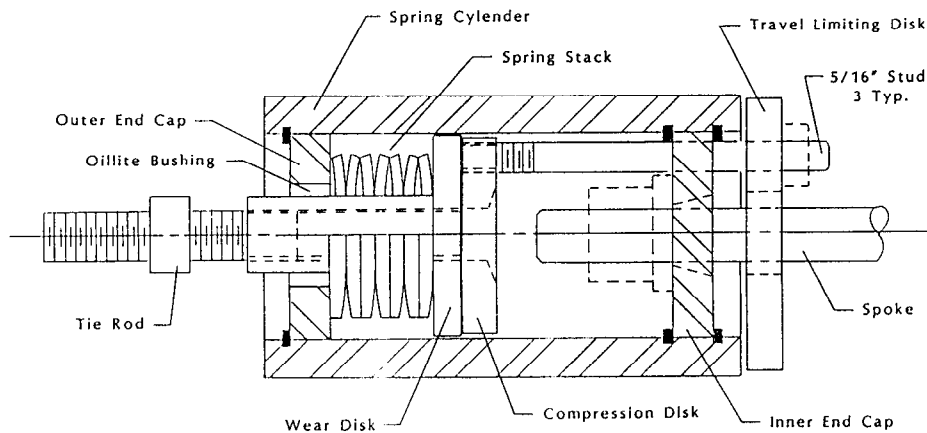


Figure 4.10 Detailed Cross Section of Rear Spoke Spring Assembly.

The spokes will experience high tensions when operating wind loads are combined with vacuum loads. The front spokes need to have as small a cross section as possible to reduce shadowing of the collector surface. These opposing requirements led to use of a high-strength steel alloy for the spokes. Half-hard 4130 steel rod was used with rolled threads to ensure reliability. The rear spokes were made from the same material to simplify fabrication, although they did not have the same shadowing concerns.

Spoke attachments to the flanges were designed to allow simple alignment during assembly. Welding this highly critical joint was specifically avoided. The design permitted simple machining and fabricating operations with no compound angle drilling or counter boring. Each spoke has a high-strength clevis threaded onto the inner end and secured with a jam nut. The clevis pinned to an ear with a round base. The ears are inserted into counter bored holes in the flange and secured by a grade 8 screw from the opposite side of the flange. An inner and outer circle of holes fitted the right-hand and left-hand spokes. Every other ear was tall to avoid interference of the spokes, as shown in Figure 4.11.

The outer ends of the spokes are different for the front and rear spokes, because the rear spokes need to accommodate the spring assemblies and the rear membrane standoff rail, as shown in Figure 4.12. The front spoke outer attachment was kept as simple as possible. A bracket was provided with a hole for the spoke to pass through. On the outside of the bracket, a spherical washer set was used to compensate for any angular misalignment of the spoke.

For the rear spokes, the spring assembly is located at the outer end of the spoke to provide clearance for the rear membrane. The rear membrane wraps around the outer end of the spoke and bracket. This bracket has to blend well with the standoff rail to avoid imposing stress concentrations on the rear membrane. A spherical rod end was selected as the rear spoke terminating element because it would meet several special requirements for the joint.

As the spoke deflects under stabilization vacuum load, the rod end permits angular movement of the spoke without imposing a bending load.

The rod end allows the static angular misalignment of the spokes resulting from their left- and right-hand positioning relative to the hub mounting flange.

The rod end can be obtained with a left-hand thread for use as part of a turnbuckle arrangement for preloading the spring assemblies.

The spoke-to-ring bracket is a simple weldment. A single strong back was used to attach the upper and lower spoke mounting brackets so the spokes pulled against each other. Welding was minimized to reduce cost and increase reliability. Gusseting was provided to reduce bending loads in the brackets. The portion of the bracket that wraps around the ring is flat to permit simple attachment of the rear membrane. The weldment is a low accuracy assembly. It was also hot dip galvanized for corrosion protection.

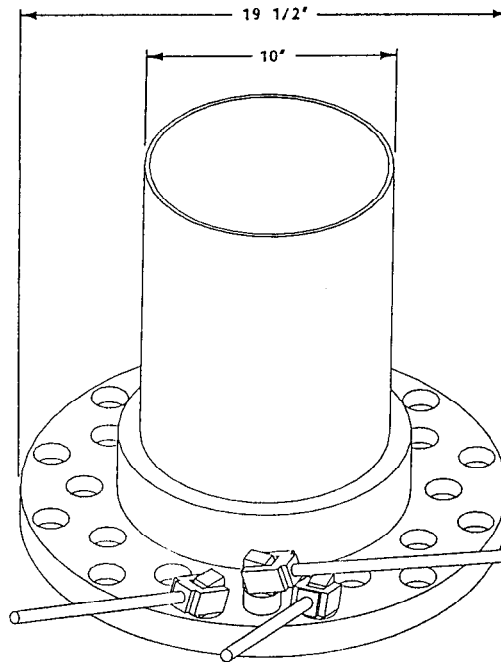


Figure 4.11 Diagram of Hub Flange with Inner Spoke End Connection Details Shown.

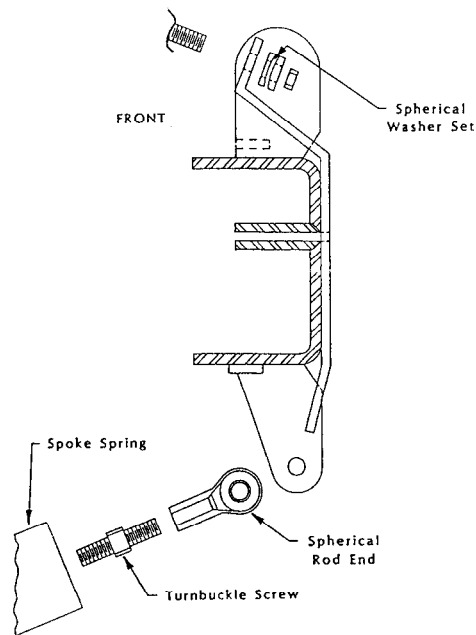


Figure 4.12 Cross Section of Dish Ring Showing Details of Outer Spoke End Attachment Bracket.

4.5 FILTER ASSEMBLY

Work in previous phases of this contract has revealed the importance of preventing dust and dirt from getting in between the formed metal membrane and the reflective polymer membrane. Dirt in this space "prints through" the polymer membrane when vacuum was applied. Local specular errors occur where the membrane "draped" over the dust particle. The magnitude of such errors was not determined, but if dust accumulates over the lifetime of the optical membrane or if large amounts are present, this would be a severe problem. One method of controlling the problem is through improved cleaning techniques during the assembly of the optical element.

Operation of the optical element in Dallas showed that improved cleaning did help reduce the dust. However, as the vacuum was turned off and on during testing, the quantity of dirt printing through increased. We concluded that the dirt was "inhaled" as the polymer membrane separated from the metal membrane under the influence of its own elasticity when the vacuum was reduced. A plan to add a filter to clean the air was implemented during final assembly at Sandia.

The filter was installed inside the rear plenum of the optical element, as shown in Figure 4.13. It consists of a cage secured to the rear part of the hub. The cage is sealed to the hub at the rear end. Its body is wrapped with filter media as used in HVAC systems. The front end is open and connected to the metal membrane with a flexible sleeve. The metal membrane has a collar to secure the forward end of the sleeve. The collar and sleeve are large enough to clear the bellows for sealing the polymer membrane. The filter medium is replaceable; access to it is difficult and would require removal of the back membrane.

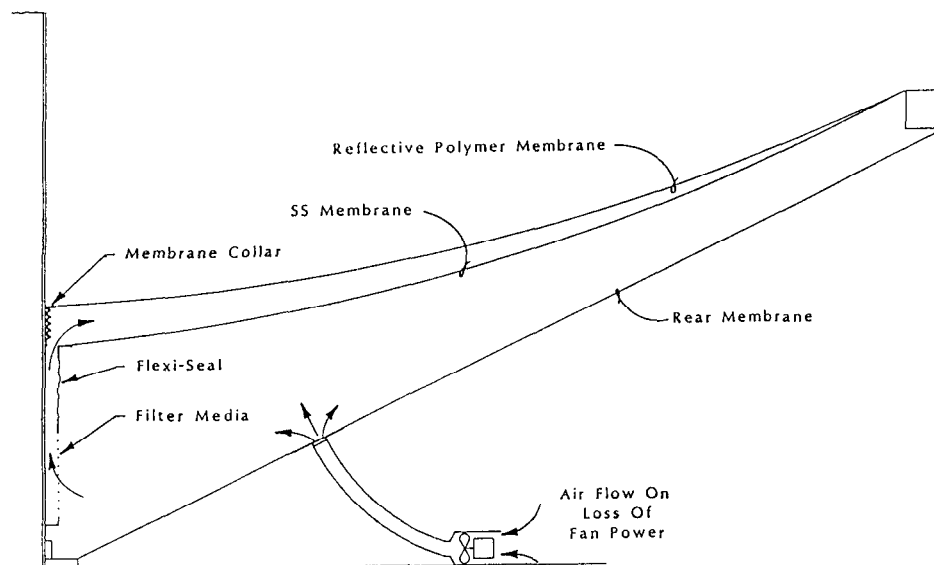


Figure 4.13 Cross Section of Assembled Dish Showing Vacuum Source Connection, Internal Filter Assembly, Membranes, and Polymer Membrane Central Bellows Seal.

4.6 VACUUM CONTROLS

The stabilization pressure is significantly higher than the dynamic pressure of the wind, therefore, no active control of the vacuum level is required. The vacuum control schematic is shown in Figure 4.14.

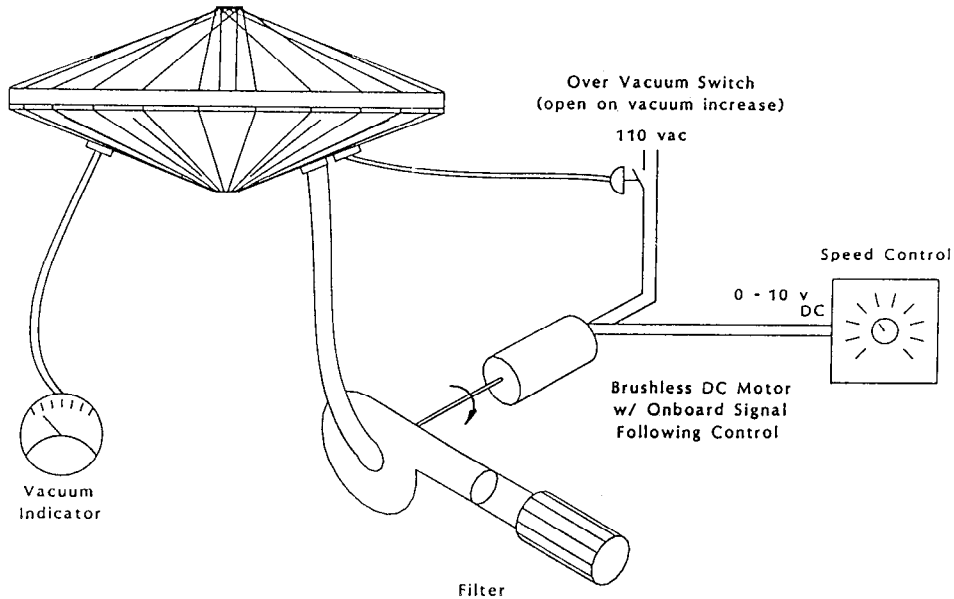


Figure 4.14 Schematic Diagram of Control System for Membrane Stabilization.

The vacuum blowers are driven by brushless DC motors. These motors have onboard circuitry to generate the DC power from AC line power and can follow a 0-10 vdc signal proportioning their speed to match the signal. The controller, therefore, consists only of an AC on/off relay and a variable DC power supply. An additional vacuum operated switch (open on vacuum increase) serves as a safety switch to prevent excess vacuum from damaging the optical element.

It was initially unknown just what volume of leakage the optical element would have, and therefore, what volume capacity the vacuum blowers should have. The blowers were sized conservatively. Two blowers were used operating in parallel (both electrically and flow). Each blower is capable of moving over 85 CFM at 7 inches water column at full speed. Tests show that they need only run at about 35 percent speed to

maintain 7 inches water column. Initial Sandia measurements of the flux distribution on the target plane suggest that the performance is slightly better at 3.5 inches water column than at 7 inches water column. Power usage at 3.5 inches water column is about 123 watts.

During assembly, considerable attention was paid to sealing potential leaks. The peripheral hem of the rear membrane was installed over a strip of 1/4-inch closed-cell PVC foam tape. The clamping channel pressed the membrane down on the foam to create the seal. The polymer membrane has to be both sealed where the hub penetrates its center and be free to move as the vacuum pulls it down to the metal membrane. This was done with a bellows seal, as shown in Figure 4.15. The bellows is a molded unit made of Hypalon for good weather resistance and flexibility at any ambient temperature. The ring-to-drive adapter links penetrated the rear membrane. A seal was maintained here with a length of flexible tubing clamped to a flange on the membrane at one end and a collar on the link itself at the other.

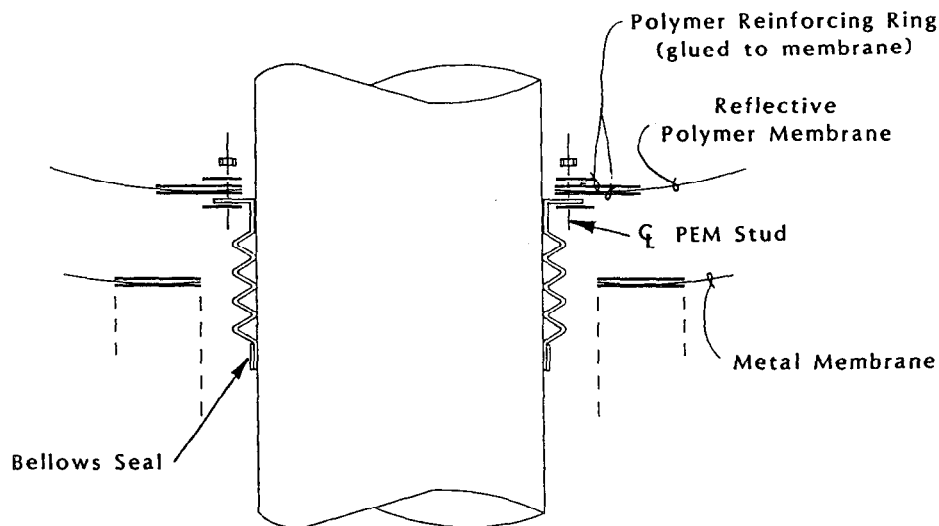


Figure 4.15 Detail of Reflective Polymer Membrane Central Seal.

4.7 POWER CONVERSION ASSEMBLY SUPPORT ARRANGEMENT

Sizing of the power conversion assembly (PCA) support components is discussed in Section 2.0 of this report. The detail design was conceived to carry the loads into the ring in the same manner as originally modeled. A spherical rod end at the end of each support leg eliminates the transfer of bending loads to the leg or the optical element ring. The bracket is dimensioned so that the leg effectively acts through the centroid of the optical element ring to eliminate rolling moments, as well.

The brackets were bolted with the same bolts that hold the ring/drive adapter brackets. In this way, the receiver loads are carried directly to the drive adapter with minimal effect on the ring at the lower two struts. All receiver mount and bracket components are hot dip galvanized for corrosion protection.

The receiver support at the focal plane is a rolled ring with an inside diameter of 33 inches. It has three axially oriented, adjustable threaded rods to support the target or calorimeter for testing purposes. Approximately +/- 6 inches of travel are permitted axially and +/-3 inches travel radially. The support was designed for a 500-pound load to accommodate the SNL cold water cavity calorimeter.

4.8 DRIVE ATTACHMENTS

The dish attachment to the drive was designed to transmit the gravity and wind loads from the optical element in a similar manner as the innovative drive proposed for the full-sized dish. It is supported at the rear central flange with a ball joint that is restrained from rotation about the optical element axis. Two additional supports at the base of the lower two receiver support legs resist loads perpendicular to the ring plane.

The central ball joint was fabricated using a large spherical rod end, as shown in Figure 4.16. The actual angular travel required is insignificant. The spherical bearing simply serves to eliminate the transfer of bending loads to the optical element hub. It effectively resists both axial and transverse loads. Its capacity for angular misalignment simplifies optical element installation and reduces the tolerances required on the drive adapter fabrication.

Since the ball joint cannot restrain the optical element from rotating about its axis, an additional torque restraint arm is bolted to the rear flange. This arm is linked by two tangentially opposed rods to brackets on the drive adapter. These rods anchor the torque restraint arm against rotation about the optical element axis.

The ring-to-drive adapter linkage, as shown in Figure 4.17, was originally designed with a spherical rod end at both ends. The rotation of the optical element and all side loads (forces acting parallel to the plane of the ring) and all central axial forces are resisted by the torque restraint and central ball joint respectively. Therefore, the ring/adapter links only need to resist overturning moments on the dish (moment load about the elevation axis). This results in pure tension or compression forces at this linkage.

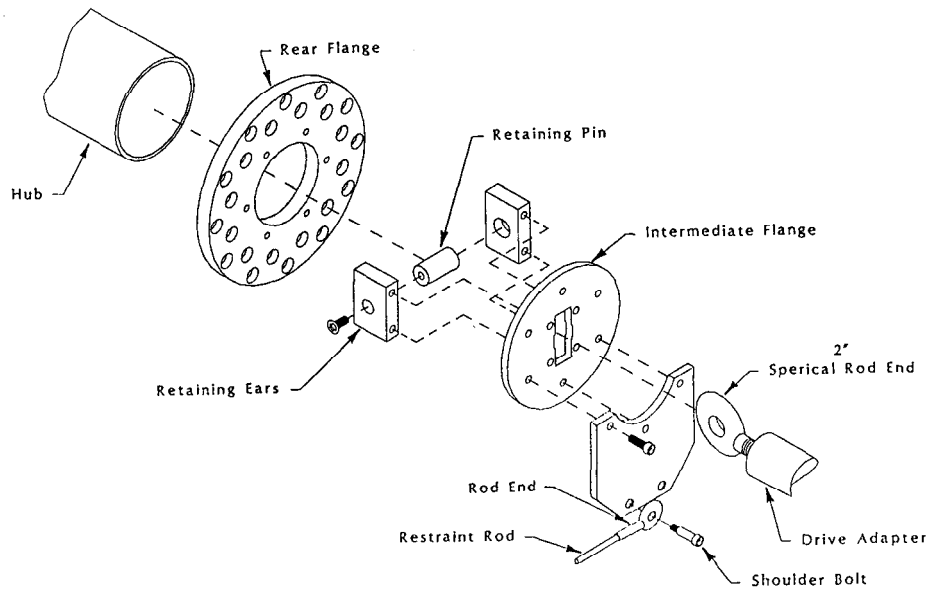


Figure 4.16 Exploded View Showing Components of the Rear Central Hub Drive Attachment.

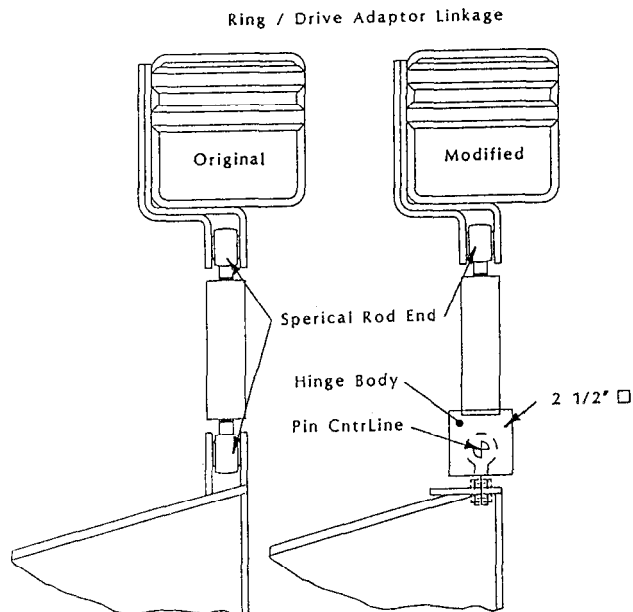


Figure 4.17 Cross Section of Dish Ring Showing Original and Modified Ring to Drive Adapter Attachment Components.

In practice, this approach was inadequate because of a misalignment in the mounting locations for the linkages in the drive adapter. Because the linkages were canted to mate with the drive adapter, the compression forces acting through the link resulted in lateral force in the plane of the ring. This tended to push the ring connection point one way and the drive adapter arm the opposite. The result is a relative circumferential displacement (rotation) between these two parts as the drive adapter arms were pushed to one side and twisted. The displacement was great enough that the rod ends bound between their mounting ears.

This problem was alleviated by changing the rear rod end to a hinge element, as shown in Figure 4.17. The hinge pins of each linkage are along a common line. By eliminating one degree of freedom in this way, the couple described above was eliminated. The tendency for the ring to translate relative to the drive adapter arm was eliminated.

4.9 SITE ASSEMBLY

The actual steps performed as part of the site assembly are outlined in Section 4.1 Work Plan. What is important to note is what was not involved in the site assembly.

Most important, no major tooling transportation and setup was required. The critical task of accurately forming a parabolic membrane on substantial, fine tolerance tooling was performed at the factory and the formed membrane shipped to the site.

Next in importance is that after the optical element was assembled, it was rigged as a single operational unit to the drive. The vacuum connections were made permanently, and it was ready to operate. The tracking controls would have to be aligned with actual sun position, as with any new drive. However, no multiple facet alignment is required. A single one-time adjustment of target to actual focal point position, if required, can be readily accomplished at the receiver support ring. Also no individual facet focus adjustment is required.

The fixturing, tools, and equipment required for assembly of the optical element are six simple support pylons with jackscrews, handtools, welder, and one pair of lightweight mandrel rails. All of this equipment fits in a single 14 foot box truck.

The prototype assembly at the DRTF proceeded as outlined in Appendix B. No significant problems were encountered, and the work was completed within the 4 weeks scheduled by a crew of 4 technicians and one engineer. This was the second time the entire optical element had been assembled (once previously in Dallas). It was the third time a formed membrane had been fixtured to the departure bar. This prior experience, along with careful preparation, contributed greatly to the field operations.

The field assembly of the optical element varied slightly from future ones in two aspects. The dish ring was assembled in Dallas and the departure bar installed before being cut in two for shipping. At Sandia, the two halves of the departure bar were fixtured and welded back together. Only two sections of the departure bar were reinstalled and reshimmed where they bridged the splice. Future optical elements would be assembled

for the first time on site. The main ring could probably be delivered in two pieces to reduce field welding. (The prototype ring was fabricated from three sections in Dallas.) The departure bar, with its 270 match drilled and tapped holes, would still have to be installed in the field. While this would increase field labor, the resulting ring would be more accurate (in planarity and concentricity) than the prototype that suffered being cut in two and rewelded again after the careful truing of the departure bar.

For future optical elements, the membranes will be formed on tooling with a known departure bar radius. The optical elements must be fabricated to duplicate precisely this radius to ensure an accurate formed membrane fit. The alignment of the membrane to the optical element departure bar will be more difficult without match marks, as was possible with the prototype. This difficulty is surmountable. The disadvantage of lacking match marks is far outweighed by the advantages of not having to move the forming tooling from one site to another.

The following figures show a sequence of assembly for the 7-m prototype.

Figures 4.18 through 4.27 show the sequence of assembly for the 7-m prototype. The formed membrane is shown in the forming tool at Dallas in Figure 4.18. The parallel rails of the penta-prism measuring system can be seen on the left side of the membrane. A steel beam spans the membrane and supports the rails near the center. The membranes were rolled onto contoured mandrels as shown in Figure 4.19. A wand was used to help the membrane onto the mandrel without buckling.

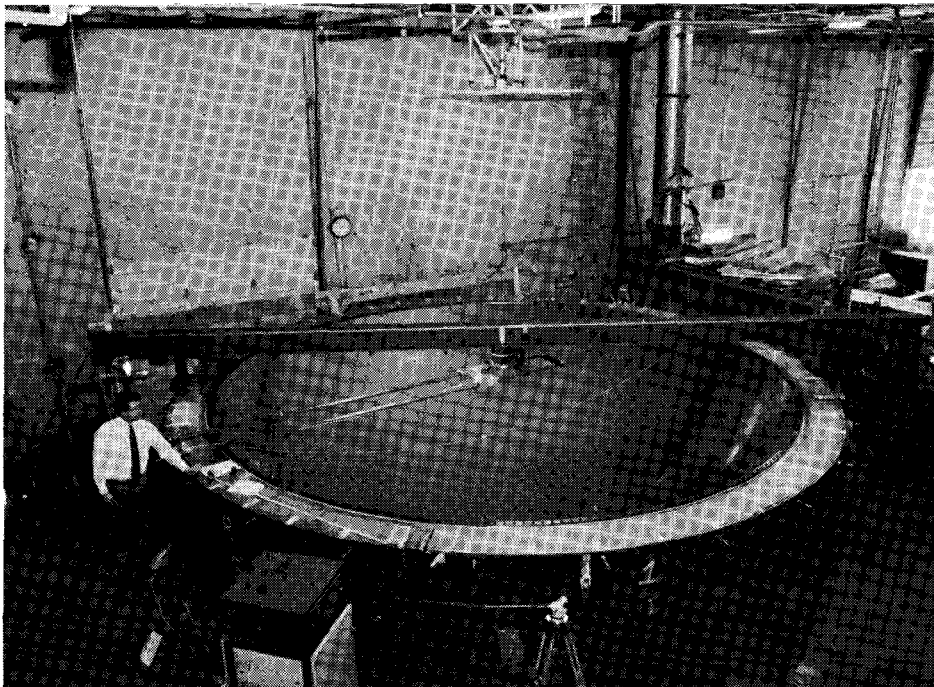


Figure 4.18 7-M Tooling Ring with Formed Membrane in Place.

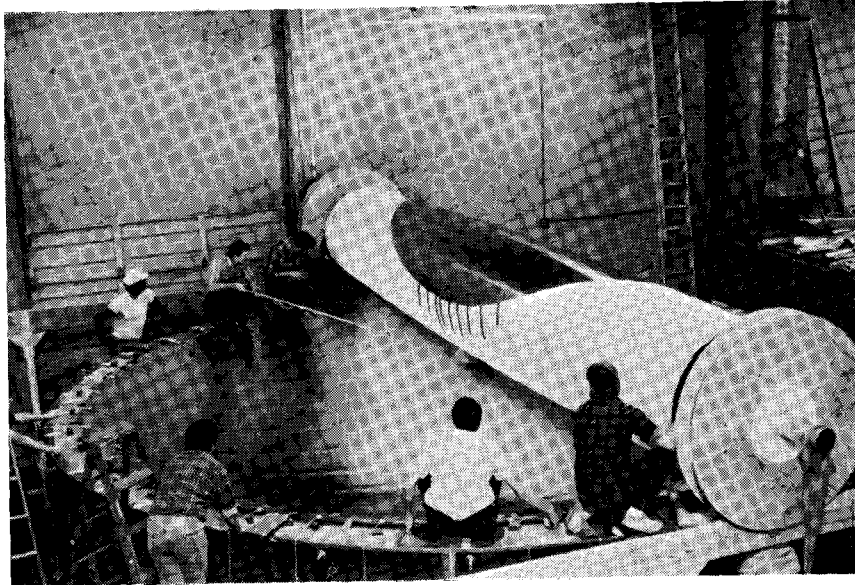


Figure 4.19 7-M Formed Membrane Being Rolled onto a Contoured Mandrel.

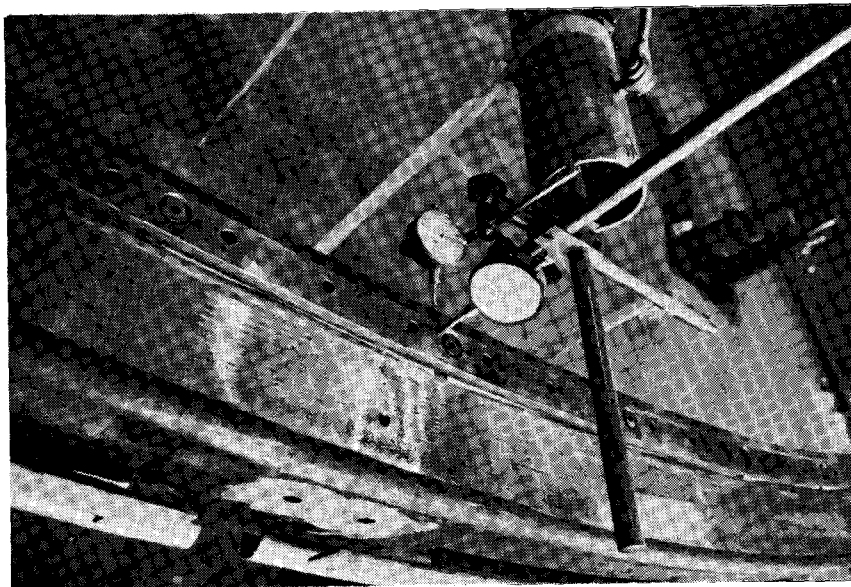


Figure 4.20 Final Assembly of Dish Ring Being Checked for Planarity and Concentricity with Dial Indicators Mounted on a Revolving Sweep Arm.

The ring was disassembled, cut into two pieces, and reassembled in Albuquerque. Planarity and concentricity of the ring were carefully checked (Figure 4.20). The membrane was unrolled in approximately the reverse steps as it was rolled (Figure 4.21, 4.22 and 4.23).

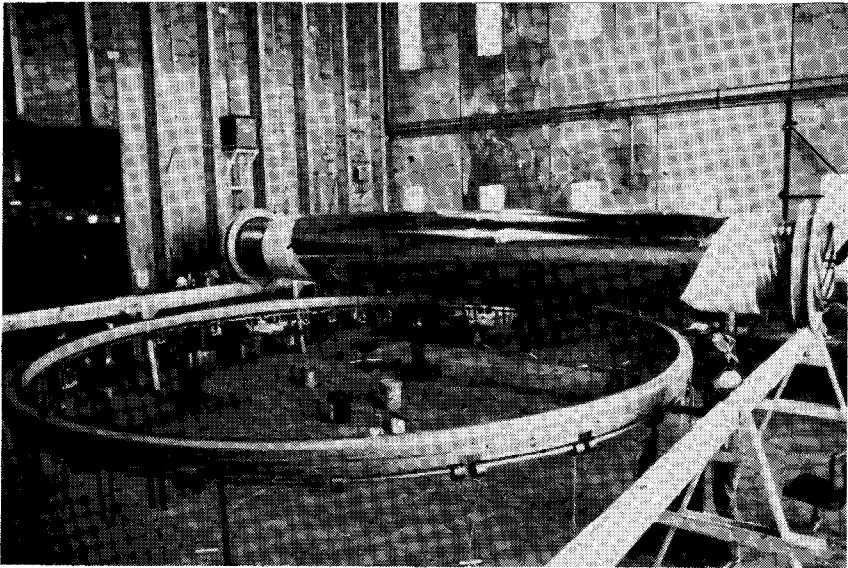


Figure 4.21 Assembled Dish Ring Supported in Field Tooling and Ready for Membrane Unrolling.

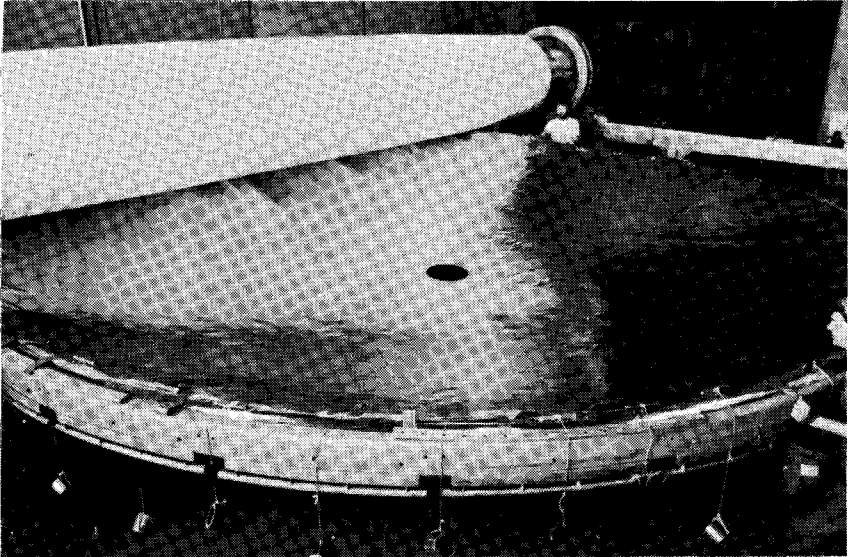


Figure 4.22 7-M Membrane Being Unrolled onto Dish Ring During Final Field Assembly.

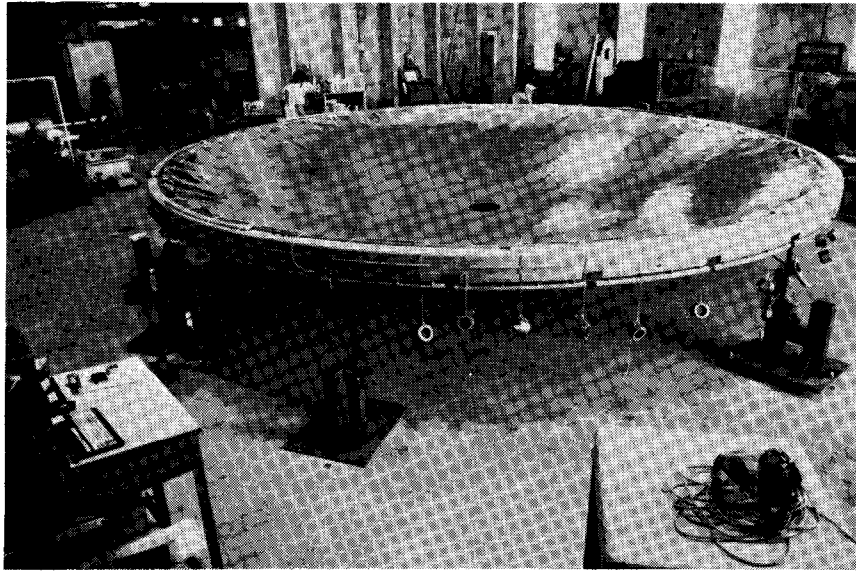


Figure 4.23 7-M Membrane Unrolled onto Dish Ring During Final Field Assembly.

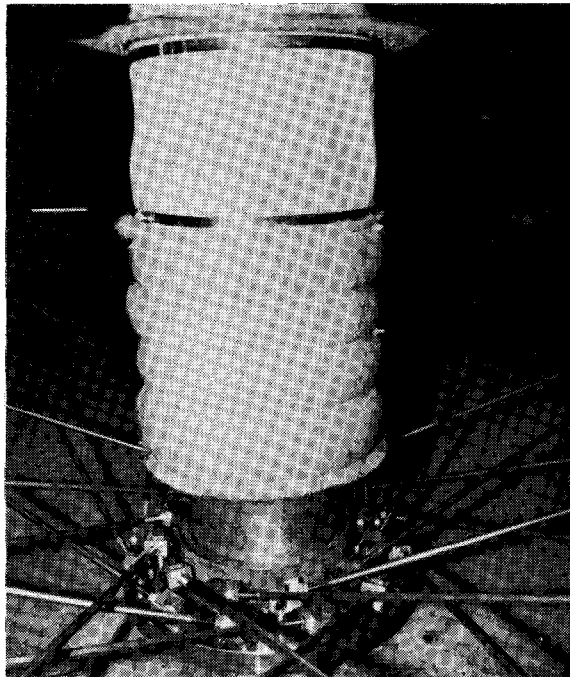


Figure 4.24 Rear Flange, Hub, Rear Spokes, and Internal Filter Assembly During Final Field Assembly. Rear Membrane is Not Yet Installed at This Time.

Refer to section 5 for details of membrane handling. After the membrane was installed on the ring, the hub was positioned in the center and the spokes were attached. The hub and filter element can be seen in Figure 4.24. the metal membrane is visible in the top quarter of the figure. Figure 4.25 shows the completed optical element with the reflective and rear membranes in place and with stabilization vacuum applied. The optical element was mounted on Sandia's pedestal and drive adaptor as shown in Figure 4.26. The PCA tripod was attached after the optical element was installed. The complete unit is shown in Figure 4.27.

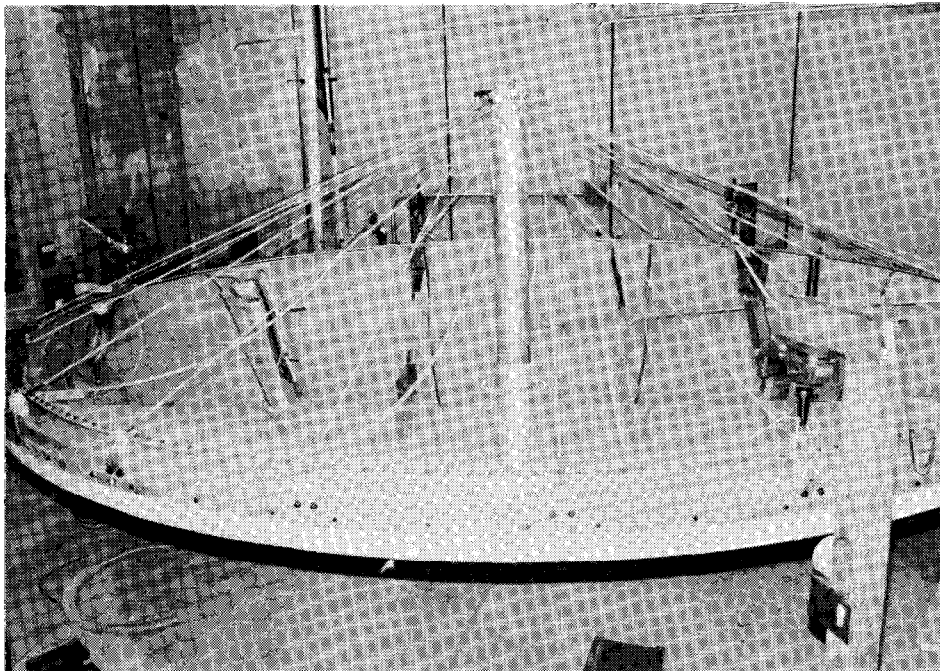


Figure 4.25 Completed 7-M Optical Element Supported from Upper Half of Field Tooling.

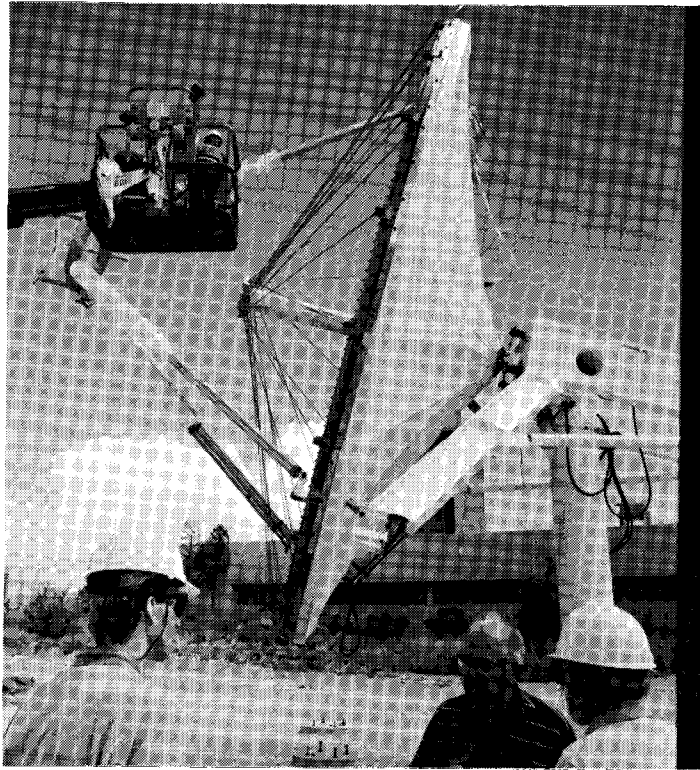


Figure 4.26 7-M Optical Element Mounted to Drive Adapter at SNLA.

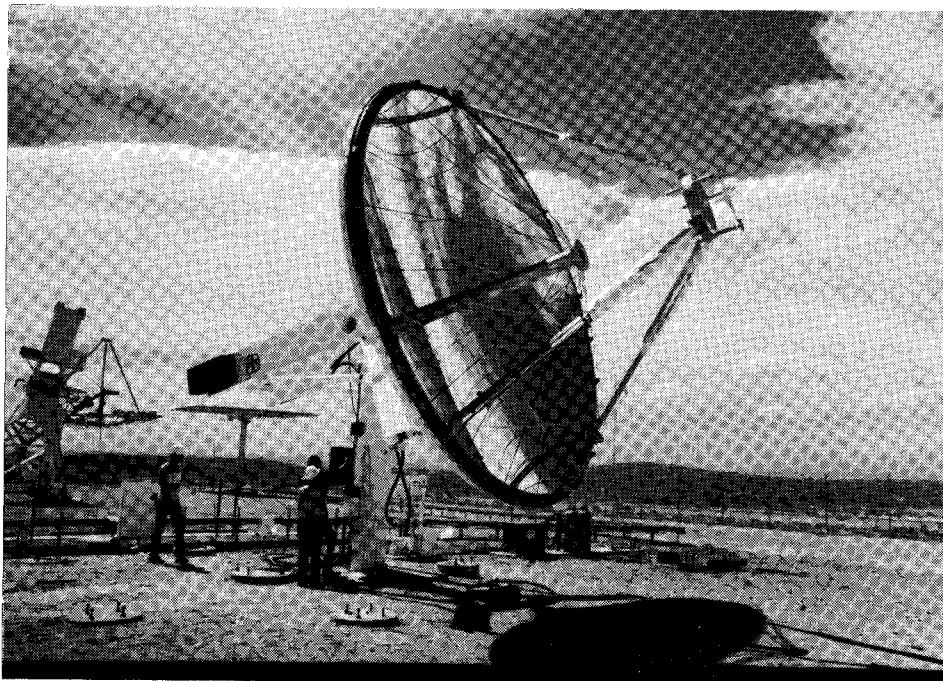


Figure 4.27 Completed 7-M Optical Element Mounted on Drive Adapter at SNLA.

5.0 MEMBRANE ROLLING AND TRANSPORTATION

5.1 INTRODUCTION

When we started this work, we expected that the metal membrane forming operation would be performed on-site where the dish was to be erected. The formed membrane was thought to be too large and too easily damaged to be shipped. The forming tooling would have to be substantial enough to support the weight of the forming water and withstand the forming vacuum. The tooling could then double as an assembly fixture after the membrane was formed.

Several concepts were explored for forming tooling although each had certain inherent disadvantages. The requirements of the tooling were that it be shippable by common means and be readily set-up in the field with as little site preparation as possible. The tooling would have to be safe and practical to erect and operate. The bulk of the tooling would probably be as important as its initial cost since it would have to be shipped from one dish site to the next.

One concept that we considered was to reinforce the dish ring and rear membrane structure during forming to serve as the forming vacuum plenum. Some separate additional ring support tooling also would be required. Another potential concept was to assemble a ring from separate shippable segments and install a liner similar to an above ground swimming pool. The segments would support the weight of the ring and the forming water. The liner would be filled partially with water to hold it down when a vacuum was drawn inside the tooling ring.

For the prototype, the problems were somewhat less than for a larger full-scale dish. The tooling SKI designed was made in four segments to ensure that it could be shipped. To minimize engineering effort at this phase of development and ensure safety and reliability, a simple rolled-and-welded steel tooling ring was built. To enclose the bottom of the tooling, a steel cable was reinforced and an engineering fabric membrane was used. This was described in Section 3.0.

We recognized that there were shortcomings to the stretched-membrane dish concept resulting from the problems associated with forming the membrane on-site. Many early-market dish applications are likely to be in remote areas where there is no utility power. These areas are also likely not to have easy access for bringing in heavy sections of tooling. Setting up the tooling and adjusting it to required tolerances of planarity and roundness will require skilled technicians to remain on-site for set-up and fabrication. For a full-scale dish, a source of up to 14000 gallons of water will be required for forming the membrane. Storage and transfer capability may also be needed if multiple dishes are being installed. These factors add to the cost and complexity of the on-site operations.

With the support of the SNL contract manager, the subject of transporting a pre-formed membrane was investigated further. The goal for this investigation was to develop a

method of shipping formed membranes to the dish-erection site. This also required development of a method for accurately and reliably fixturing the membrane to the dish ring in the field. Previous experience with field installation of flat membranes on large heliostats suggested that a membrane rolled onto a mandrel could be safely shipped and readily redeployed on-site. This was selected as the first direction to be investigated.

5.2 EXPERIMENTATION

Experimentation began at the 0.5-m diameter scale to reduce the cost of each iteration. A method for quickly forming 0.5-m diameter membranes had been developed under an on-going contract to NASA. A disk of membrane material was clamped between a flat plate and a 0.5-m inside diameter ring. Pressurized air was introduced through the plate between the flat membrane and the plate until the membrane material yielded. Center displacement was monitored during forming to achieve a desired f/D ratio. For initial investigations, this uniform pressure forming method produced membranes with a shape close enough to parabolic to allow qualitative evaluation of possible membrane handling techniques. The same ratio of membrane thickness to membrane diameter, as planned for the 7-m prototype, could not be used for the 0.5-m tests due to material availability. Initial experiments were conducted with 2-mil, dead soft aluminum.

Several membranes were formed and manually rolled with and without a center mandrel. As expected, they could not be rolled on a cylindrical mandrel without damage. However, with care, they could be rolled unsupported with very little evidence of damage. The roll of material was greater in diameter in the center than at the two ends. The ratio of the rolled material center diameter to the membrane diameter did not seem to be a critical value. However, it was difficult to do this without introducing local buckling in the membrane wherever even light pressure was misapplied. A concept was developed to roll the membrane onto a specially contoured mandrel. (See Figure 5.1)

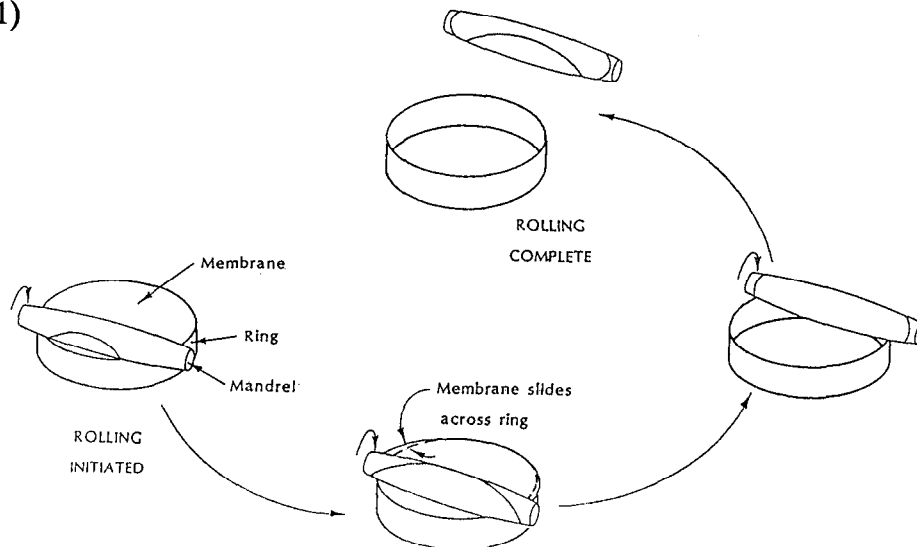


Figure 5.1 Schematic Diagram of Parabolic Membrane Rolling Procedure.

To test this concept required a mandrel with the same contour that the rolled membranes naturally assumed. This was fabricated by rolling a formed membrane and then filling its hollow center with room-temperature cure foam material. This mandrel was very resistant to major deformations, although it could be "dinged" by point contact with hard objects. Several other formed membranes were rolled about this mandrel with encouraging results. A rolled membrane was also unrolled and refixed to the ring it was formed on. Qualitative observations were again encouraging.

Experimental investigations continued at the 1.4-m scale because tooling for forming this size membrane existed from previous Phase I work on this project. A mandrel was constructed using the same method as at 0.5-m scale. The rolling technique was improved by mounting the mandrel on a shaft that was supported at either end on two parallel rails. This permitted improved control during the rolling operation. Rolling was begun by positioning the mandrel over the membrane with its axis tangent to the membrane edge. The edge was taped to the mandrel, and the mandrel rolled along the rails picking up the membrane as it rolled. Care was required in how quickly the mandrel advanced, so as not to wrap too quickly and put too much tension into the membrane or too slowly so as to allow too much slack. As the membrane is rolled, its center displacement is reduced because the curvature of the mandrel (parallel to its axis) is less than that of the membrane. As the membrane flattens, its outside diameter effectively increases, so its rolled length along the mandrel is greater than its original free diameter.

Again, a rolled membrane was unrolled and refixed to the forming tooling. Care was taken to refix it just as it had originally been fastened to the tooling. When a stabilization vacuum was reapplied, the membrane contour appeared unaffected by the rolling operation. Local dings and buckles from handling largely disappeared under vacuum. The membrane thickness at this scale was still not in the correct ratio to the diameter of the membrane. The results were judged to be sufficiently representative and positive to justify continued investigation along these lines.

The next larger forming tooling available was 3.7-m diameter. At this scale, the membrane material could not be rolled without the support of a mandrel. Therefore, a mandrel would have to be fabricated to theoretical contour prior to any rolling. This contour was first predicted by scaling physical measurements from the .5-m and 1.4-m experiments. Agreement in scaled dimensions from each mandrel was fair, but a more exact solution was sought. Work was initiated on mathematically determining the correct contour for the rolling mandrel. A solution was derived relating mandrel diameter as a function of axial position to membrane diameter and f/D ratio.

The 3.7-m mandrel was fabricated using 6-inch O.D. by 0.060-inch wall aluminum tubing as a core. Rings of expanded polystyrene foam were cut to tapered contours and assembled onto the core to approximate the desired overall mandrel contour, as shown in Figure 5.2. Foam cutting was done on a hot wire lathe jig built for this purpose. Tolerances of about ± 0.030 inches could be maintained. The remainder of the set-up appeared as shown in Figure 5.3.

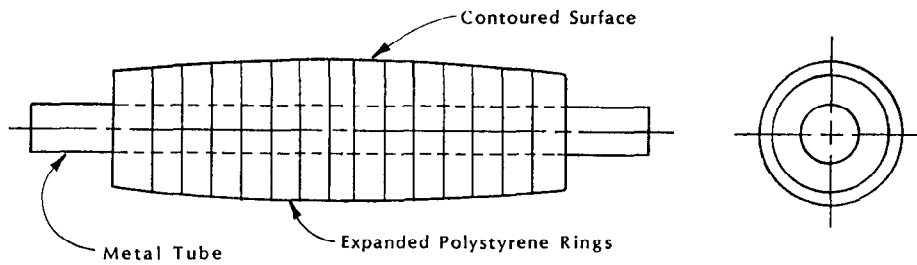


Figure 5.2 Contoured Mandrel Fabrication Details.

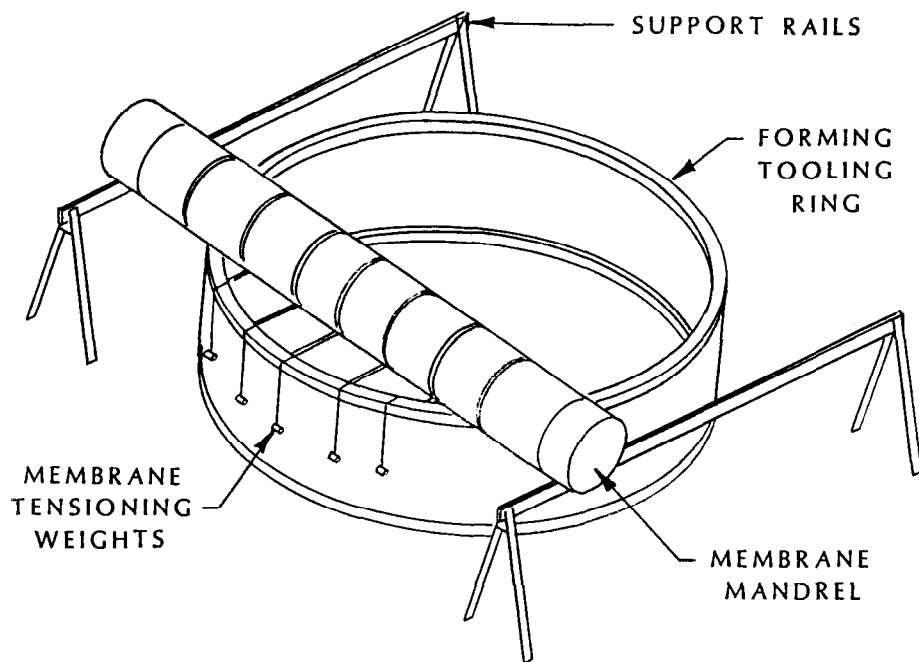


Figure 5.3 Set-up for Formed Membrane Rolling.

All tests up to this point had been done with aluminum membranes because the stainless steel had too high a yield stress to form easily on the small diameter tooling. At 3.7 m, stainless steel was used to be more representative of the 7-m and 14-m membranes. It was very easy to get buckles in the formed membrane while rolling at the larger scale. We found that maintaining correct tension in the membrane was critical to smooth rolling.

A method of keeping tension in the membrane was developed using multiple weights hung on strings attached to the periphery of the membrane. This can be seen in Figure 5.4. The weights were sufficient to balance the entire membrane so it could be completely unclamped from the tooling prior to rolling. This was important because the membrane periphery had to be free to slide over the tooling edge as the membrane flattened onto the mandrel. As the membrane was rolled onto the mandrel, weights were detached just ahead of the mandrel. Unrolling the membrane proceeded in reverse order. Tension was also controlled by the rate of travel of the mandrel on the rails. If it turned too many revolutions as it traversed, it tended to wind the membrane too quickly and pull wrinkles into it. For the 3.7-m mandrel, it was light enough for a person to lift one end and wind or unwind membrane material without traversing the mandrel, and by that, control tension.

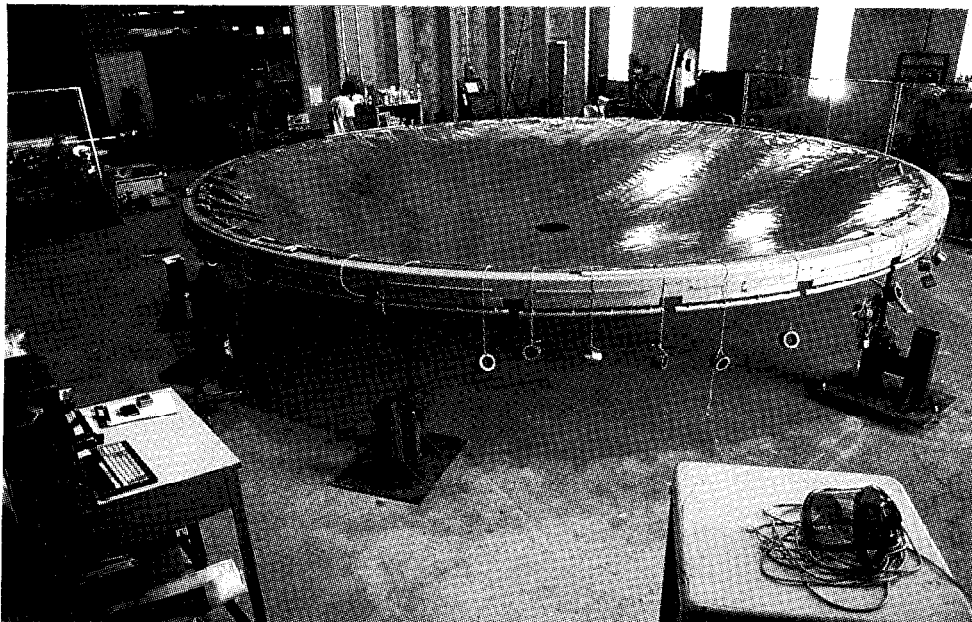


Figure 5.4 7-M Formed Membrane Unrolled onto Final Optical Element Ring Prior to Field Assembly.

When the mandrel was heavier and could not be manually "slipped", as is true for the 7-m mandrel, the diameter of the mandrel where it sat on the rails had to be correct so that the distance traversed by the mandrel was correct for the amount of membrane wound onto it. This was accomplished by mounting separate wheels on the mandrel core where it sat on the rails.

The first 3.7-m membrane was rolled and unrolled at the 3.7-m scale multiple times. Two separate mandrels were built with slightly varying contours. The second one was modified further. After positive results were achieved with the first membrane and mandrel, a fresh membrane was formed and a third mandrel fabricated. This membrane was rolled and unrolled with some wrinkling still occurring in the center and at the extreme edges from manual handling and tensioning weight attachment. When stabilization vacuum was reapplied, the wrinkles improved significantly, but still appeared to have a measurable impact. Additional improvements in weight attachment and handling were planned.

5.3 IMPLEMENTATION AT 7-M DIAMETER OPTICAL ELEMENT

The task of fabricating an accurately stiff, contoured mandrel 7 m long and 1.2 m in diameter was considered next. The first such mandrel used 6-inch diameter aluminum tubing as a core. Foam disks were cut and stacked on the core to define the contour. Six steel tie rods were then run parallel to the axis through all the foam disks and through a pressure plate at each end. After tightening, they acted to preload the entire assembly in compression to stiffen it. New rails were built to support this mandrel over the higher 7-m forming tooling.

When we decided to implement membrane rolling for the 7-m prototype, the stainless steel membrane mounting hardware on the optical element ring had to be redesigned to permit fixturing of a preformed membrane. It had become apparent in early rolling experiments that the membrane had to retain its formed contour all the way to the very edge in order to smoothly roll over itself. It was not possible to leave a flat perimeter edge for easy clamping to the ring. The design of the departure bar shown in Section 4.4 permitted this refixturing. An inclined inner edge was provided on the departure bar having the same angle as the formed membrane. When the membrane is unrolled onto the ring, it is first aligned and then tack welded to the departure bar for temporary fixturing during assembly.

Another critical issue for successful unrolling and refixturing of the membrane to the dish ring is the alignment of the membrane to the departure bar. The membrane must be reattached so its periphery is in the same position as it was when originally formed to ensure repetition of the desired formed shape. A fixture that held a fine point drafting pen containing indelible ink was designed to rest on the membrane clamp bar and reference off the outer side of the departure bar. The entire membrane periphery was marked with this device immediately after forming. Four radial marks were also made to permit rotational realignment. When the membrane was unrolled and still supported by the tensioning weights, it could be manually adjusted to realign the four radial marks. The marking fixture pen was then replaced with a pointer, and the

membrane circumferential line was aligned with the pointer as it was tacked in place. The membrane was tacked first at the four compass points, then the eighth points, then sixteenths, and so on to ensure an even fit up. This method is successful only when the departure bar is reassembled precisely in its original position during field assembly operations.

The first 7-m membrane was rolled successfully and then unrolled and refixtures to the ring. The penta-prism measuring system was reinstalled, and the membrane scanned along two radial lines to measure the effects of rolling. There was a concern that wrapping the membrane about a mandrel with a longer radius of curvature than the formed membrane would yield it parallel to the mandrel axis, but this effect was not evident. Figure 5.5 shows how little the slope changed. Note that scans are compared on two different radii. This was done because the area scanned before rolling was locally damaged in a handling mishap during rolling. The error prior to rolling was measured to be 3.4 mrad. After rolling, the measured error was 3.9 mrad.

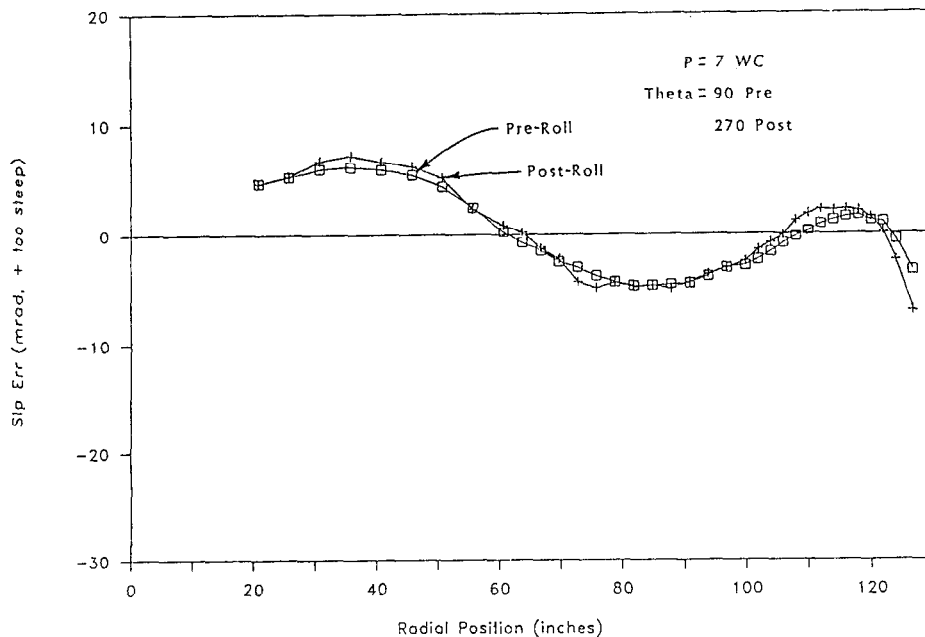


Figure 5.5 Plot of Radial Slope Error on First 7-M Membrane Before and After Membrane was Rolled onto Contoured Mandrel.

The membrane was rolled again to gain experience at the 7-m scale. Some minor changes were made to the procedure that yielded poorer results. The difficulties experienced caused some buckling of the membrane along one edge. Once buckles exist, in subsequent rolling operations, buckles would almost always reoccur in the same location. At this time, the mandrel developed a sag as the foam disks yielded in creep under the tie rod preload and the bending stresses from gravity loads. The membrane was rolled and scrapped and a new membrane mounted to the fixture for forming.

Before continuing rolling experiments, we designed and built a stiffer mandrel. A steel tube 3 feet in diameter was used as the core. Additional stiffeners were welded inside the core in the form of eight longitudinal stringers plus five circular bulkheads. Foam rings were again used to define the contour of the membrane. An optical machinists level was used to ensure assembly to the desired contour in spite of some initial curvature in the core material.

The next membrane was rolled smoothly and stored as a spare membrane for final assembly. After a third membrane was formed, the entire dish was assembled and tested and then disassembled before rolling the membrane. This meant that the membrane already had a hole in the center with reinforcing rings welded to it there. This did not affect the rolling. The membrane also had some very minor buckling from previous too rapid changes in stabilization pressure while the polymer membrane was installed. These buckles did not cause a major problem during rolling, although extra care was required to prevent buckling from reoccurring at these locations. Precautions involved careful control of local tension approaching the buckles and use of a long padded wand to push out any initial signs of buckling. This membrane was stored for eventual use in the field during final assembly of the optical element at Sandia.

5.4 FUTURE WORK

Additional work on membrane rolling could yield more efficient space utilization for shipping. It was not attempted to minimize the mandrel diameter in this work. Additional improvements in membrane handling during rolling and unrolling will reduce the labor effort for these tasks. Most of this work will involve the design and perfection of improved tensioning hardware and mandrel traversing and rolling equipment.

6.0 SUMMARY

The objective of Task 2 of this project was to demonstrate a large-scale stretched-membrane solar concentrator optical element. This was to include design procedures, membrane forming procedures, structural mechanical details, and field assembly procedures. Tests indicate successful achievement of these goals. In addition to the original goals, it was realized during this contract that a method for easily transporting formed membranes from a factory to the dish assembly site was of critical importance to marketability of a dish. A practical technique for rolling a formed membrane was developed and demonstrated as part of the subject work.

Success was achieved in five major areas of development.

The technique of large-scale membrane forming was shown to be predictable, accurate, and repeatable. Three 7-m membranes were formed, and all three had acceptable slope error, indicating the repeatability and control of the forming process.

The tensioned spoke, hub, and ring structure was demonstrated to be practical to fabricate and provide sufficient stiffness. Efficiency of field assembly was also demonstrated.

A technique was demonstrated for rolling a formed stainless steel membrane on a contoured mandrel. This will facilitate shipping of formed membranes from a factory, thus avoiding forming operations in the field.

A practical method for mechanically securing a replaceable polymer reflective membrane to the front of the dish was developed and utilized on the prototype.

A method for design of the optical element was developed that can be used for larger dishes. This includes models to predict the load and deformation response of the rear membrane/spoke combination and the reaction of the ring to loading.

Measurement of the shape of the assembled optical element showed a low slope error of 3.6 mrad. The shape was shown not to be significantly influenced by internal stabilization vacuum, optical element orientation, or loads imposed on the optical element by the power conversion assembly.

After the 7-m prototype optical element was fabricated and tested at SKI's facility, it was disassembled and reassembled at the Sandia National Laboratories' Solar Thermal Test Facility in Albuquerque, New Mexico. It was mounted on a pedestal and drive provided and instrumented by SNL.

Our development effort indicates that the stretched-membrane dish concept is a promising approach to building a concentrating collector. High optical accuracy is obtainable with a forming technique that should be very cost-effective in production. The ring, hub, and spoke structure provides efficient use of materials to support the reflective surface. The use of a readily replaceable reflective polymer membrane promises a cost-effective combination of low initial cost and practical optical surface replacement when degradation takes place from weathering. The ability to form the metal membrane in a factory without moving bulky, high-accuracy tooling from site to site helps to minimize installed costs.

We recognize the need for follow-on development efforts in several areas. Results from on-sun testing being conducted presently may suggest other areas for improvement. Existing areas requiring more work are

- 1) Selection or development of a ductile, cost-effective, and long-lived reflective polymer membrane material or the replacement of the polymer membrane with glass reflectors.
- 2) Increase the size of the optical element and optimization of its components for 25 KWe generation. This size will be compatible with heat engines currently being developed and is judged to have more commercial potential than the 7-m unit.
- 3) Design and demonstration of a support and tracking unit expressly for the stretched-membrane optical element.
- 4) Refinement of formed membrane handling techniques for membrane rolling and unrolling. Additional jigging and fixturing could reduce this effort significantly.

7.0 REFERENCES

1. Development of a Stretched-Membrane Dish-Phase I, SAND88-7035 (Solar Kinetics, Inc., Dallas, Texas), Albuquerque, NM: Sandia National Laboratories, March 1989.
2. Development of a Stretched-Membrane Dish, SAND88-7031 (Solar Kinetics, Inc., Dallas, Texas), Albuquerque, NM: Sandia National Laboratories, October 1989.
3. "Collector Subsystem Requirements," A10722, Issue F, Albuquerque, NM: Sandia National Laboratories, February 1985.
4. Peterka, J. A., Z. Tan, B. Bienkiewicz and J. E. Cermak. Wind Loads on Heliostats and Parabolic Dish Collectors. SERI/STR-253-3431. Golden, CO: Solar Energy Research Institute, November 1988.
5. C. Kutscher, Solar Energy Research Institute, "Calculation of Rear Cable Deflection for Dish," inter-office memorandum, September 11, 1987.
6. Manual of Steel Construction, 8th ed., Chicago: American Institute of Steel Construction, Inc., 1980.
7. Compilation of Wind Tunnel Coefficients for Parabolic Reflectors, JPL Publication 78-16, Pasadena, CA: Jet Propulsion Laboratory.
8. Ferdinand P. Beer and E. Russell Johnston, Jr., Mechanics of Materials, New York: McGraw-Hill, 1981.
9. L. M. Murphy and C. Tuan, The Formation of Optical Membrane Reflector Surfaces Using Uniform Pressure Loading, SERI/TR-253-3025, Golden, CO: Solar Energy Research Institute, August 1987.

Appendix A

Procedure for Use of the Forming Tool.

1. Assemble tooling
 - a. leave doors off
 - b. leave bottom membrane off, and
 - c. install 48 support brackets.
2. Install sweep template jig in center of tooling ring
 - a. adjust fixture concentricity and level.
3. Fixture main dish ring segments to tooling
 - a. support on brackets
 - b. shim to level, and
 - c. set concentricity with sweep template.
4. Weld ring segments.
5. Install membrane departure bar
 - a. ensure concentricity during drilling and tapping with sweep fixture, and
 - b. ensure planarity by shimming under departure bar.
6. Prepare tooling
 - a. link dish ring to tooling at 24 positions
 - b. install sealing plates in outer annulus between dish ring O.D. and Tooling I.D.
 - c. remove sweep fixture
 - d. install bottom tooling sealing membrane
 - e. install tooling doors, and
 - f. connect tooling vacuum system in reverse to pressurize tooling.
7. Position mandrel support rails.
8. Set flat membrane mandrel on rails.
9. Lay out membrane
 - a. turn on pressurization blowers
 - b. unroll membrane
 - c. attach edge tensioning weights to membrane edge as it is unrolled, and
 - d. with membrane supported by peripheral weights and air pressure, align membrane on dish ring and mark.
10. Attach membrane to ring
 - a. mark departure bar hole locations in membrane periphery with rubber hammer
 - b. punch clamp bolt holes in membrane periphery at marked locations with circle punch, hammer, and soft aluminum backing plate
 - c. recheck membrane alignment
 - d. tack weld membrane to outer edge of departure bar with hand held capacitive discharge indirect spot welder, and
 - e. bolt clamp bar to departure bar, capturing membrane periphery.

11. Prepare for forming
 - a. install bridge beam across tooling ring (This serves as vertical reference for interim membrane deflection and slope measurements during forming.)
 - b. install water handling equipment
 - c. connect vacuum blowers for negative pressure
 - d. cover membrane with water liner, and
 - e. remove mandrel support rails.
12. Form Membrane
 - a. form membrane with vacuum and water while monitoring membrane center displacement and slope at 4 points along a diameter.
13. Secure from forming
 - a. remove water handling equipment, and
 - b. remove membrane liner.
14. Tune membrane shape
 - a. install laser and penta-prism membrane measuring system
 - b. set up video laser strike data recording system
 - c. measure membrane shape, and
 - d. reform membrane, if necessary, using vacuum only.
15. Mark membrane for reinstallation alignment
 - a. use custom jig and ink pen to mark circumferential line set distance from departure bar O.D., and
 - b. make four radial marks at 0, 90, 180, & 270 degree positions.
16. Roll membrane
 - a. set up rails
 - b. set contoured shipping and storage mandrel on rails (Axis perpendicular to welded membrane seams.)
 - c. attach tensioning weights
 - d. remove clamp bars
 - e. cut membrane circumferentially along upper inclined edge of departure bar, and
 - f. roll membrane onto contoured mandrel
remove tensioning weights just ahead of mandrel as it advances
insure against buckles in membrane material.

Appendix B

Procedure for use of the Field Assembly Tooling.

1. Anchor every other tooling pylon to floor
 - a. do not install upper pylon portions.
2. Support ring segments on lower jackscrews.
3. Install sweep template jig in center of tooling
 - a. adjust fixture concentricity and level.
4. Join ring segments
 - a. adjust ring segment positions concentrically and for planarity
 - b. bolt on ring butt joint splice fixtures
 - c. pull open side of ring segments in to correct diameter with cable pullers
 - d. weld butt joint, and
 - e. fit departure bar segments to ring adjust radially with clamps while bolting adjust planarity with shims check with sweep template jig.
5. Fixture membranes to ring
 - a. set up membrane mandrel support rails
 - b. unroll formed stainless steel membrane onto ring attach tensioning weights
 - c. align membrane use match marks for rotational position use moveable alignment jig which references off departure bar O.D. for circumferential position
 - d. tack weld membrane periphery to departure bar start at quarter points proceed to halfway in between initial tacks continue halfway in between previous tacks complete on 1.5 inch centers
 - e. set up polymer membrane mandrel
 - f. unroll reflective membrane fixture with tape
 - g. align membrane use match marks for rotational position use center deflection for radial position, and
 - h. Install clamp bars use urethane cord for sealing and grip surface start at quarter points proceed to halfway in-between initial tacks continue halfway in-between previous tacks.
6. Install spoke brackets.
7. Refixture ring support
 - a. install support pylon upper portions
 - b. lower upper jackscrews
 - c. rig jackscrews to spoke brackets, and
 - d. lift ring with upper jack screws to assembly height.
8. Assemble optical element.
9. Remove optical element from tooling
 - a. connect temporary vacuum source to optical element
 - b. attach crane to front hub of optical element
 - c. lift optical element 2 inches
 - d. detach support pylons from ring
 - e. remove upper portions of support pylons, and
 - f. lift optical element clear of tooling.

**UNLIMITED DISTRIBUTION
INITIAL DISTRIBUTION
REVISION 4/2/91/trm**

U.S. Department of Energy (5)
Forrestal Building
Code CE-314
1000 Independence Avenue, SW
Washington, DC 20585
Attn: M. Scheve
S. Gronich

U.S. Department of Energy (2)
Forrestal Building
Code CE-33
1000 Independence Avenue, SW
Washington, DC 20585
Attn: B. Annan

U.S. Department of Energy (3)
Albuquerque Operations Office
P.O. Box 5400
Albuquerque, NM 87115
Attn: C. Garcia
G. Tennyson
N. Lackey

U.S. Department of Energy
San Francisco Operations Office
1333 Broadway
Oakland, CA 94612
Attn: R. Hughey

AAI Corporation
P. O. Box 6787
Baltimore, MD 21204

Acurex Corporation (2)
555 Clyde Avenue
Mountain View, CA 94039
Attn: J. Schaefer
H. Dehne

Advanced Thermal Systems
7600 East Arapahoe
Suite 319
Englewood, CO 80112
Attn: D. Gorman

Arizona Public Service Company
P.O. Box 21666
Phoenix, AZ 85036
Attn: J. McGuirk

Arizona Solar Energy Office
Dept. of Commerce
1700 W. Washington, 5th Floor
Phoenix, AZ 85007
Attn: F. Mancini

Australian National University
Department of Engineering Physics
P. O. Box 4
Canberra ACT 2600 AUSTRALIA
Attn: S. Kaneff

Barber-Nichols Engineering
6325 West 55th Avenue
Arvada, CO 80002
Attn: R. Barber

Battelle Pacific Northwest
Laboratory (2)
P.O. Box 999
Richland, WA 99352
Attn: T. A. Williams
D. Brown

BDM Coporation
1801 Randolph Street
Albuquerque, NM 87106
Attn: W. Schwinkendorf

Bechtel National, Inc.
50 Beale Street
50/15 D8
P. O. Box 3965
San Francisco, CA 94106
Attn: P. DeLaquil

Black & Veatch Consulting
Engineers
P.O. Box 8405
Kansas City, MO 64114
Attn: J. C. Grosskreutz

Tom Brumleve
1512 Northgate Road
Walnut Creek, CA 94598

California Energy Commission
1516 Ninth Street, M-S 43
Sacramento, CA 95814
Attn: A. Jenkins

California Polytechnic University
Dept. of Mechanical Engineering
Pomona, CA 91768
Attn: W. Stine

California Public Utilities Com.
Resource Branch, Room 5198
455 Golden Gate Avenue
San Francisco, CA 94102
Attn: T. Thompson

Cummins Engine Co.
MC 60125
P. O. Box 3005
Columbus, IN 47202-3005
Attn: R. Kubo

Dan Ka
3905 South Mariposa
Englewood, CO 80110
Attn: D. Sallis

DLR
Pfaffenwaldring 38-40
7000 Stuttgart 80 WEST GERMANY
Attn: R. Buck

DSET
P. O. Box 1850
Black Canyon Stage I
Phoenix, AZ 85029
Attn: G. Zerlaut

Electric Power Research
Institute
P.O. Box 10412
Palo Alto, CA 94303
Attn: J. Schaeffer

Engineering Perspectives
20 19th Avenue
San Francisco, CA 94121
Attn: John Doyle

Energy Technology Engr. Center
Rockwell International Corp.
P. O. Box 1449
Canoga Park, CA 91304
Attn: W. Bigelow

ENTECH, Inc.
P. O. Box 612246
DFW Airport, TX 75261
Attn: R. Walters

Florida Solar Energy Center
300 State Road 401
Cape Canaveral, FL 32920
Attn: Library

Ford Aerospace
Ford Road
Newport Beach, CA 92663
Attn: R. Babbe

Foster Wheeler Solar Development
Corporation (2)
12 Peach Tree Hill Road
Livingston, NJ 07039
Attn: M. Garber
R. Zoschak

Garrett Turbine Engine Co.
111 South 34th Street
P. O. Box 5217
Phoenix, AZ 85010
Attn: E. Strain

Georgia Power (2)
7 Solar Circle
Shenandoah, GA 30265
Attn: W. King

Harris Corporation (2)
Government and Aerospace
Systems Division
P. O. Box 9400
Melbourne, FL 32902
Attn: K. Schumacher

Industrial Solar Technologies
5775 West 52nd Avenue
Denver, CO 80212
Attn: R. Gee

Institute of Gas Technology
34245 State Street
Chicago, IL 60616
Attn: Library

ISEIR
951 Pershing Drive
Silver Spring, MD 20910
Attn: A. Frank

Jet Propulsion Laboratory
4800 Oak Grove Drive
Pasadena, CA 91109
Attn: M. Alper

LaJet Energy Company
P. O. Box 3599
Abilene, TX 79604
Attn: M. McGlaun

L'Garde, Inc. (2)
1555 Placentia Avenue
Newport Beach, CA 92663
Attn: M. Thomas
J. Williams

Lawrence Berkeley Laboratory
MS 90-2024
One Cyclotron Road
Berkeley, CA 94720
Attn: A. Hunt

Luz International (2)
924 Westwood Blvd.
Los Angeles, CA 90024
Attn: D. Kearney

3M-Energy Control Products (2)
207-1W 3M Center
St. Paul, MN 55144
Attn: R. Dahlen

Mechanical Technology, Inc. (2)
968 Albany Shaker Road
Latham, NY 12110
Attn: G. Dochat
J. Wagner

Meridian Corporation
4300 King Street
Alexandria, VA 22302
Attn: D. Kumar

NASA Lewis Research Center (4)
21000 Brook Park Road
Cleveland, OH 44135
Attn: R. Beremand 500-215
R. Evans 500-210
J. Savino 301-5
R. Corrigan 500-316

Nevada Power Co.
P. O. Box 230
Las Vegas, NV 89151
Attn: Mark Shank

Pacific Gas and Electric Company (2)
3400 Crow Canyon Road
San Ramon, CA 94526
Attn: G. Braun
J. Iannucci

Polydyne, Inc.
1900 S. Norfolk Street, Suite 209
San Mateo, CA 94403
Attn: P. Bos

Power Kinetics, Inc.
415 River Street
Troy, NY 12180
Attn: W. Rogers

Renewable Energy Institute
1001 Connecticut Ave. NW
Suite 719
Washington, DC 20036
Attn: K. Porter

Rocketdyne Division
6633 Canoga Park Ave.
Canoga Park, CA 91304
Attn: W. Marlatt

San Diego Gas and Electric Company
P.O. Box 1831
San Diego, CA 92112
Attn: R. Figueroa

SCE
P. O. Box 800
Rosemead, CA 91770
Attn: P. Skvarna

Schlaich, Bergemann & Partner
Hohenzollernstr. 1
D - 7000 Stuttgart 1
West Germany
Attn: W. Schiel

Sci-Tech International
Advanced Alternative Energy
Solutions
5673 W. Las Positas Boulevard
Suite 205
P.O. Box 5246
Pleasanton, CA 84566
Attn: U. Ortabasi

Science Applications International
Corporation (2)
10343 Roselle Street, Suite G
San Diego, CA 92121
Attn: K. Beninga

Solar Energy Research Institute (5)
1617 Cole Boulevard
Golden, CO 80401
Attn: B. Gupta
L. M. Murphy
G. Jorgensen
T. Wendelin
A. Lewandowski

Solar Kinetics, Inc. (2)
P.O. Box 540636
Dallas, TX 75354-0636
Attn: J. A. Hutchison
P. Schertz
D. Konnerth

Solar Power Engineering Company
P.O. Box 91
Morrison, CO 80465
Attn: H. Wroton

Solar Steam
P. O. Box 32
Fox Island, WA 98333
Attn: D. Wood

SPECO
P. O. Box 91
Morrison, CO 80465
Attn: W. Hart

SRS Technologies
990 Explorer Blvd., NW
Huntsville, AL 35806
Attn: R. Bradford

Stearns Catalytic Corporation
P.O. Box 5888
Denver, CO 80217
Attn: T. E. Olson

Stirling Thermal Motors
2841 Boardwalk
Ann Arbor, MI 48104
Attn: B. Ziph

Sun Power, Inc.
6 Byard Street
Athens, OH 45701
Attn: W. Beale

Tom Tracey
6922 South Adams Way
Littleton, CO 80122

United Solar Tech, Inc.
3434 Martin Way
Olympia, WA 98506
Attn: R. Kelley

University of Chicago
Enrico Fermi Institute
5640 Ellis Avenue
Chicago, IL 60637
Attn: J. O'Gallagher

University of Houston
Solar Energy Laboratory
4800 Calhoun
Houston, TX 77704
Attn: L. Vant-Hull

University of Utah
Mechanical and Industrial
Engineering
Salt Lake City, UT 84112
Attn: B. Boehm

Eric Weber
302 Caribbean Lane
Phoenix, AZ 85022

WG Associates
6607 Stonebrook Circle
Dallas, TX 75240
Attn: V. Goldberg

1840 R. E. Loehman
1846 D. H. Doughty
1846 C. S. Ashley
3145 Document Processing for
DOE/OSTI (8)
3151 G. C. Claycomb (3)
4051 Disclosure Division (3)
6000 V. L. Dugan
6200 B. W. Marshall
6210 J. T. Holmes
6215 C. P. Cameron
6215 R. M. Houser
6216 C. E. Tyner
6216 D. J. Alpert
6216 J. W. Grossman
6216 T. R. Mancini (30)
6216 J. E. Pacheco
6217 P. C. Klimas
6217 R. B. Diver
6220 D. G. Schueler
6223 G. J. Jones
6224 D. E. Hasti
7470 J. L. Ledman
7476 F. P. Gerstle
7476 S. T. Reed
8523 R. C. Christman